AD-A096 801 AUBURN UNIV ALA ENGINEERING EXPERIMENT STATION F/G 19/7
LAUNCHERS AS PASSIVE CONTROLLERS.(U)
DEC 80 J E COCHRAN DAAH01-80-C-0523
UNCLASSIFIED DRSMI/RL-CR-81-2 NL

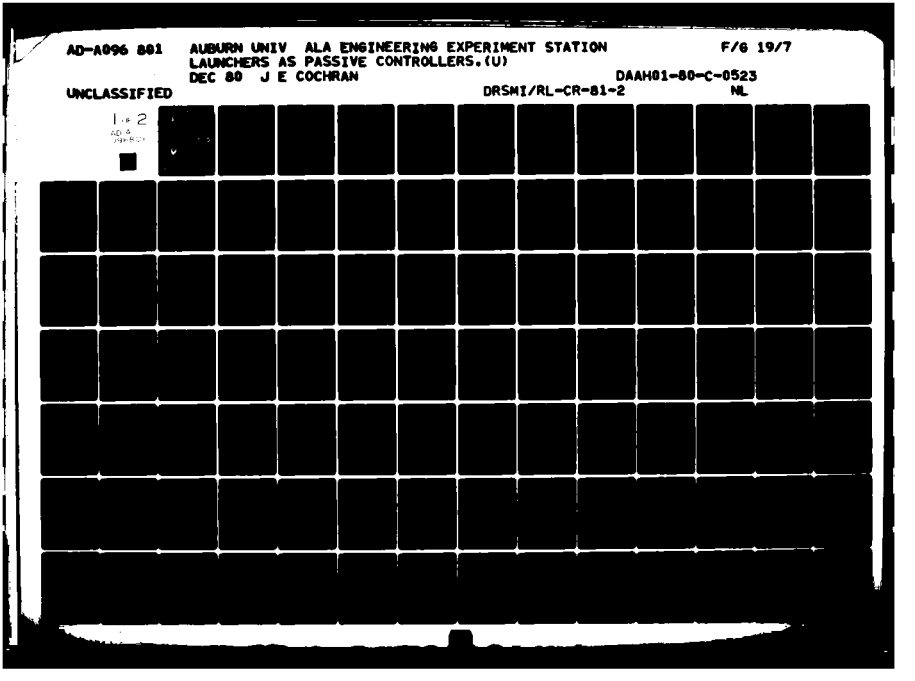

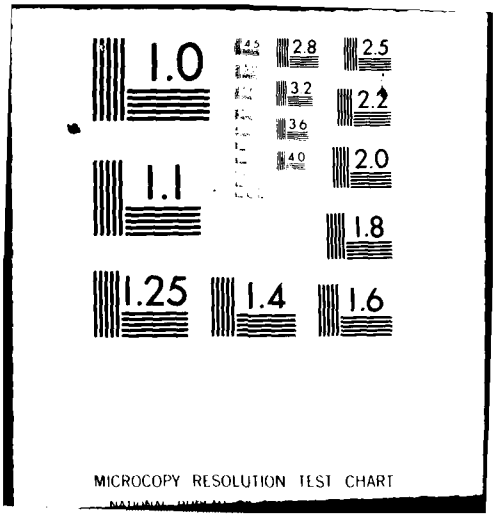
1.0
2.8
2.5
3.2
2.2
3.6
4.0
2.0
1.1
1.8
1.25
1.4
1.6
MICROCOPY RESOLUTION TEST CHART

(2) LEVEL III

TECHNICAL REPORT RL-CR-81-2

LAUNCHERS AS PASSIVE CONTROLLERS

by

John E. Cochran, Jr.
Aerospace Engineering Department
Auburn University, Alabama 36849

INTERIM REPORT
under
Contract DAAH01-80-C-0523

administered through

Engineering Experiment Station
Auburn University, Alabama 36849

U.S. ARMY MISSILE COMMAND
Redstone Arsenal, Alabama 35898

31 December 1980

Approved for Public Release
Distribution Unlimited

DISPOSITION INSTRUCTIONS

DESTROY THIS REPORT WHEN IT IS NO LONGER NEEDED. DO NOT RETURN IT TO THE ORIGINATOR.

DISCLAIMER

THE FINDINGS IN THIS REPORT ARE NOT TO BE CONSTRUED AS AN OFFICIAL DEPARTMENT OF THE ARMY POSITION UNLESS SO DESIGNATED BY OTHER AUTHORIZED DOCUMENTS.

TRADE NAMES

USE OF TRADE NAMES OR MANUFACTURERS IN THIS REPORT DOES NOT CONSTITUTE AN OFFICIAL INDORSEMENT OR APPROVAL OF THE USE OF SUCH COMMERCIAL HARDWARE OR SOFTWARE.

UNCLASSIFIED

SECURITY CLASSIFICATION OF THIS PAGE *(When Data Entered)*

REPORT DOCUMENTATION PAGE	READ INSTRUCTIONS BEFORE COMPLETING FORM
1. REPORT NUMBER: TR-RL-CR-81-2	2. GOVT ACCESSION NO.: AD-A096 801
	3. RECIPIENT'S CATALOG NUMBER
4. TITLE *(and Subtitle)*: LAUNCHERS AS PASSIVE CONTROLLERS	5. TYPE OF REPORT & PERIOD COVERED: Technical Report, Interim 27 Feb. 1980-31 Dec. 1980
	6. PERFORMING ORG. REPORT NUMBER
7. AUTHOR(s): John E. Cochran, Jr.	8. CONTRACT OR GRANT NUMBER(s): DAAH01-80-C-0523
9. PERFORMING ORGANIZATION NAME AND ADDRESS: Engineering Experiment Station, Auburn University, AL 36849	10. PROGRAM ELEMENT, PROJECT, TASK AREA & WORK UNIT NUMBERS
11. CONTROLLING OFFICE NAME AND ADDRESS: Commander, U.S. Army Missile Command, Attn. DRSMI-RPT, Redstone Arsenal, AL 35898	12. REPORT DATE: December 31, 1980
	13. NUMBER OF PAGES: 104
14. MONITORING AGENCY NAME & ADDRESS *(if different from Controlling Office)*: Commander, U.S. Army Missile Command, Attn. DRSMI-RLH, Redstone Arsenal, AL 35898	15. SECURITY CLASS. *(of this report)*: UNCLASSIFIED
	15a. DECLASSIFICATION/DOWNGRADING SCHEDULE

16. DISTRIBUTION STATEMENT *(of this Report)*

Approved for public release; distribution unlimited

17. DISTRIBUTION STATEMENT *(of the abstract entered in Block 20, if different from Report)*

18. SUPPLEMENTARY NOTES

19. KEY WORDS *(Continue on reverse side if necessary and identify by block number)*

Free-Flight Rockets
Rocket Launcher Dynamics
Passive Control
Dispersion
Launcher Frequency Response
Thrust Misalignment
Dynamic Mass Imbalance

20. ABSTRACT *(Continue on reverse side if necessary and identify by block number)*

Results are reported of an investigation into the passive control capability of launchers for free-flight rockets. Causes of free-flight rocket dispersion (principally thrust misalignment), the general concept of passive control and the potential of launchers as passive controllers are discussed. Control of important free flight rockets by altering launch conditions is treated as a preliminary step. Next, launcher

DD FORM 1 JAN 73 1473 EDITION OF 1 NOV 65 IS OBSOLETE
S/N 0102-LF-014-6601

UNCLASSIFIED
SECURITY CLASSIFICATION OF THIS PAGE *(When Data Entered)*

conditions caused by rocket imperfections are considered. The concept of "nonlinear frequency response" of a launcher/rocket system is used to define frequency bands which result in favorable launch conditions. Although only limited numerical results are obtained, they indicate that for a non-tip-off, light-weight (as compared to the rocket) launcher, or sub-launcher, of the type considered there are two frequency bands, one very high and one fairly low, within which the launcher is very effective as a passive controller of rocket dispersion. For a tip-off launcher, the results are similar, but operation within a low frequency band produces better control. Theoretically, dispersion can be reduced to less than fifty percent of the "rigid launcher" value.

PREFACE

This report contains interim results obtained during an investigation of the passive control capabilities of launchers for free-flight rockets, under U.S. Army Contract DAAH01-80-C-0523, for the U.S. Army Missile Command, Redstone Arsenal, Alabama. The Contracting Officer's Technical Representative is Mr. Dean E. Christensen. His advice and support have been greatly appreciated.

Several students assisted in the research reported herein and/or in the preparation of this report. Mr. Grant A. Castleberry, a graduate research assistant until November 1980, helped in modifying and writing computer codes. Since September 1980, Mr. David M. Smith has worked in a similar capacity and also helped prepare this report. Mr. Russell L. Keller worked during the summer of 1980 as an undergraduate research assistant. Mr. Ted W. Warnock and Mr. Richard T. Gunnels, undergraduate research assistants, helped in report preparation.

Mrs. Marjorie McGee deserves special thanks for her expert typing of the manuscript.

John E. Cochran, Jr.
Project Leader

TABLE OF CONTENTS

TABLE OF CONTENTS (CONTINUED)

LIST OF FIGURES

LIST OF FIGURES (CONTINUED)

LIST OF FIGURES (CONTINUED)

LIST OF TABLES

SECTION 1. INTRODUCTION

1.1 Some Causes of Free-Flight Rocket Dispersion

As their designation implies, free-flight rockets are not guided after they are launched. Hence, their flight paths are altered by random disturbing forces and moments which act during free-flight. Two of the more important of the random disturbing moments are those due to thrust misalignment and dynamic mass imbalance.[1] For a spinning rocket, the observed effects of these two types of moments are similar during the thrusting portion of flight; they both lead to random deviations of rocket flight paths which are categorized as "dispersion."

Another cause of dispersion can be the motion of the launcher during the guidance phase, since such motion determines the initial conditions for the free-flight phase of the rocket's total trajectory. However, motion of the launcher (except during pointing) is caused only by the rocket(s) fired from it. Thus, except for random imperfections in the rocket(s), motion of the launcher should be essentially deterministic. It also follows that the random motion of a free-flight rocket after it is launched and the random motion of the system of rocket-plus-launcher during guidance are intimately connected since they arise, at least partially,† from the same source(s).

Previously, the connection between the random motion of a launcher and that of a rocket fired from it has, for the most part, been disregarded

† Other random imperfections in the rocket - for example, misaligned fins - cause random motion of the rocket, but not the launcher.

There are at least two reasons for this. First, because launchers are often fairly massive (as compared to the rocket(s)) and the random disturbing moments are small in magnitude, the random part of the launcher motion caused by rocket imperfections is often very small. Second, because mathematical "simulation" of the flight of all sorts of vehicles is very widespread, while simulation of launcher/rocket systems is not, the only option an analyst has may be to treat the random parts of rocket and launcher motions as independent. Still, because rocket imperfections cause launcher motions, one may logically inquire if these motions are always detrimental or may, by proper launcher design, be used to decrease dispersion.

1.2 General Concept of Passive Control

The idea of designing a launcher to compensate for rocket imperfection lead to the PADA[2] concept of compensating for dynamic mass imbalance by allowing an unbalanced, spinning rocket to spin about its principal axis of least inertia on the launcher. This concept has been noted in a later design handbook.[3] Apparently little has been done to utilize it, although interest has not entirely died out.[4] The work reported in Ref. 5 should also be mentioned. During that analysis, Christensen noted that for certain launcher natural frequencies, the launcher motion partially compensated for post-launch effects of rocket imperfections.

The PADA concept can be categorized as passive control. That is, "control" over the motion of the rocket at end of guidance (EOG)[†] results

[†]"End of guidance," as used herein, is the time at which physical contact between launcher and rocket ends. It is assumed that no motion of the rocket is caused by motion of the launcher after this time. This assumption does not entirely preclude the presence of aerodynamic interference effects. but does require that they be the same regardless of the launcher's motion.

in a smaller deviation from the flight path it would have flown had there been no disturbance (the nominal flight path), than there would have been if the launcher did not respond at all. The control action is passive as opposed to active since no energy from outside the system, only energy inherent in the system, is used to implement control. Passive control has been used effectively to stabilize spacecraft.[6] Another example is controls-fixed stability of aircraft.[7]

1.3 Potential of Launchers as Passive Controllers

An effective control system (passive or active) must sense random disturbances and reduce the undesirable effects of the disturbances. Hence, the system of launcher-plus-rocket must meet two basic requirements for passive control to be possible: (1) The launcher must respond to disturbances arising from random imperfections of the rocket. (2) The launcher's response must be such that the flight path of the rocket is "nearer" the nominal (ideal) flight path than it would be if the launcher had not responded. "Nearness" to the nominal flight path at impact is the most obvious measure of performance of such a system. However, if the perturbed position and velocity of the rocket, at a time after burnout sufficiently long for a basically steady-state to have been achieved, are nearer their nominal values than they would be if the launcher had been non-moving, then the launcher has been successful.

Consider as a specific example, a launcher/rocket system wherein the rocket has a misaligned thrust vector and is spinning (but not spin-stabilized) at EOG. To act as a passive controller, the launcher must respond to the thrust misalignment during the usually very brief period of time (say, 80 milliseconds) encompassing the detent and guidance

(including any tip-off) phases. Hence, a very short response time is mandatory. Short response times of oscillatory systems are only achieved if the natural frequencies of the system are high.

Secondly, the response of the launcher must be favorable. The principal way in which thrust misalignment of a spinning rocket causes dispersion is that the torque due to thrust misalignment produces a very slow precession of the rocket's longitudinal axis (see Appendix D), and since the thrust acts primarily along this axis, the rocket is driven in the direction it is pointed until burnout. Aerodynamic torques on a stable rocket reduce the rate of precession, but these torques are very small at EOG. The rate of precession of the rocket can be reduced by imparting a suitable angular velocity to the rocket while it is on the launcher. If, in responding to the thrust misalignment, the launcher has such an angular velocity, its response is favorable.

As to the potential of launchers to act as passive controllers, one should first consider, in light of the above, the physical characteristics of existing launchers.† In doing this, some sort of classification of launchers is required. For the present, launchers are classified as light or heavy as compared to the rocket. That is, the mass of a heavy launcher and its moments of inertia are much greater than those of the corresponding rocket, while the mass and moments of inertia of a light launcher are of the same order of magnitude (or less) than those of the rocket launched from it.

---

†One must also, at some point, consider the fact that some launchers are mounted on vehicles. However, for the purposes of this report, the motion of such vehicles is not considered.

If a launcher is heavy, even though it is supported with stiff springs, its natural frequencies will be rather low, say 1 to 10 Hz. Furthermore, the angular accelerations caused by the thrust misalignment will be very small. Thus, unless some part of the launcher (a launch tube, for example) can move relative to the main part of the launcher, or the rocket itself can rotate, little passive control is foreseeable. However, if rotation of a relatively small portion of the launcher with the rocket is provided for, there is good reason to believe passive control can be achieved with heavy launchers.

Imperfections in the rocket should produce enough motion of light launchers for control to be implemented if the launchers are not very firmly attached to the ground or to a substantially rigid body. In the case of shoulder-fired launcher/rocket systems, the natural frequencies of the launcher motion may be fairly low, so that large enough angular rates are not produced by the imperfections; however, angular rotations of several milliradians can be expected. Theoretically, these aim changes can be used to reduce dispersion.

From the above reasoning, it is clear that some passive control potential exists for suitably designed launcher/rocket systems. The aim of this research effort is to determine qualitatively the degree of this potential.

1.4 Scope of This Effort

As indicated, the objective of this research is not to design a rocket/launcher system which is optimal in the sense that the dispersion due to all random imperfections is minimized, but rather to determine the extent to which such an ambitious task may be successful. To achieve

this objective, the following steps have been taken: (1) Mathematical models of launcher/rocket systems ranging from very simple to fairly general have been developed or taken from previous work.[8,9] (2) Digital computer codes incorporating some of the models have been written and codes incorporating the other models have been modified. (3) The effects of rocket imperfections, principally thrust misalignment, on the trajectories of rockets, have been studied to determine the magnitude and nature of the control required to reduce dispersion to a very low level. (4) Methods of producing the required control have been developed. For the most part, these involve choosing favorable launcher physical characteristics. (5) Typical numerical results have been generated which illustrate that, at least theoretically, dispersion can be reduced.

In Section 2, ideal control of rocket flight paths by choosing launch conditions - i.e., the state of the rocket at EOG - is considered. Launch conditions which are produced by rocket imperfections are studied in Section 3 by using several launcher models, but no concerted attempt is made to obtain "favorable" conditions. The production of favorable launch conditions is treated in Section 4. The "tuning" of the launcher, or a sub-launcher, so that it responds to produce favorable launch conditions, is treated in detail in Section 4, using the concept of "nonlinear frequency response" of a launcher/rocket system. Conclusions are stated in Section 5. Mathematical details are covered in the appendices.

SECTION 2. IDEAL CONTROL VIA LAUNCH CONDITIONS

2.1 Introductory Comments

It is obvious that the only control a launcher can exercise is over the rocket's state at EOG. The values of variables which collectively define this particular state are referred to here as the "launch conditions" and are linear velocity components, angular velocity components, attitude variables (Euler angles) and coordinates. At EOG an imperfect rocket generally has some non-zero transverse linear and angular velocities because certain imperfections have caused the launcher to move. These are in addition to the linear and angular velocities caused by non-rocket-specific random factors such as detent release. Random imperfections in the rocket also generally cause changes in its attitude and the position of its center of mass at EOG.

As stated in Section 1, the precessional part of the angular velocity* of a free-flight rocket which is produced by imperfections subsequent to EOG is a major cause of dispersion. Hence, the way the transverse angular velocity at EOG and that produced later by imperfections interact is of great importance. Because the dynamic pressure is relatively small at EOG a small transverse linear velocity at EOG has a much smaller effect on the rocket's trajectory than a corresponding angular velocity. Similarly, aim changes (angular rotation) may propogate into significant trajectory

*Nutational motion of a spinning rocket apparently has little effect on its trajectory as long as its frequency is much greater than the frequency of aerodynamically produced oscillations.

deviations; but, displacements of the rocket's center of mass at EOG are of little consequence.

In the following subsections, typical numerical results are presented and used to support the preceding statements. The results were obtained using a computer code incorporating the simple six-degree-of-freedom free-flight rocket model described in Appendix A. The data used, except for thrust misalignment and dynamic imbalance angles, is listed in Table 1.

Table 1. Data for Simple Six-Degree-of-Freedom Free-Flight Model

Mass (kg)	113.5
I_x (kg-m^2)	0.2712
I_T (kg-m^2)	94.313
F_T (Nt)	46720
S (M^2)	0.01929
d (m)	0.1567
ρ (kg/m^3)	0.00098
C_x	-0.4
C_{z_α}	-4.0
C_{m_α},$-C_{n_\beta}$	-0.5
C_{ℓ_p}	-0.5
C_{m_q},C_{n_r}	-2000.0
Initial Speed (m/sec)	61
Initial Spin Rate (rad/sec)	40

2.2 Free-Flight Motion with Thrust Misalignment

Regarding the effects of thrust misalignment on the free-flight motion of a rocket, two cases must be considered: (1) the rocket is essentially not spinning and (2) the rocket is spinning, but not "spin stabilized." In the first case, either the thrust misalignment must be very small in magnitude, or burnout must occur very shortly after EOG; otherwise, the angular rate acquired after EOG will not be compensated for during detent and guidance. In the second case, the transverse angular rate due to thrust misalignment which causes most of the dispersion is the precession rate. In Appendix D, a rather simple analysis is used as the basis for the conclusion that this precession rate is generated during the first quarter of a revolution of the rocket after EOG. Figures 1 and 2 show that this conclusion is valid even when aerodynamic reactions and gravitational forces are present. The flight path angle[†] time histories shown in Fig. 1, for $\alpha_y = 0.001$ rad and $\alpha_z = 0.0$ until burnout at t=1 sec (solid curves) and for $\alpha_y = 0.001$ only until the rocket has rolled through $\pi/2$ rad (dashed curves), clearly show that after the first quarter of a revolution of the rocket, very little additional precession rate is generated by the thrust misalignment. Figure 2 provides the lateral deviation time histories for both cases. They are very similar.

2.3 Free-Flight Motion with Dynamic Mass Imbalance

In this section, and in Appendix A, the very idealized case of constant mass imbalance, mass and moments of inertia is considered. This model may seem too idealized, but the results obtained are only used for quantitative purposes. In fact, since the largest parts of the trajectory

---

[†]Definitions of the flight path angles γ and ψ_w, as well as other variables, are given in Appendix A.

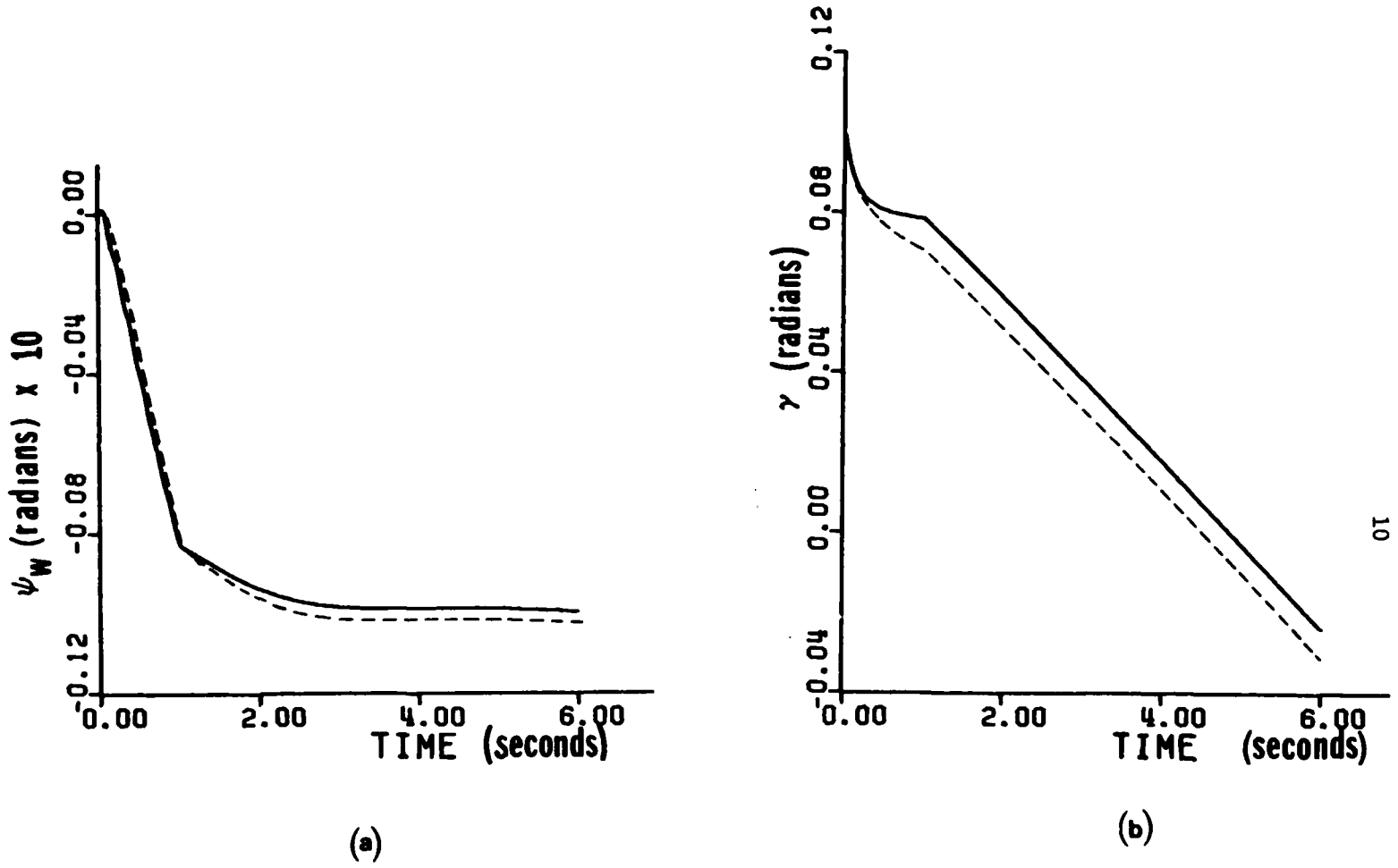

Fig. 1 Flight path angles for $\alpha_y = 0.001$; (a) velocity yaw angle, ψ_w; (b) velocity pitch angle, γ.

deviations occur during the first part of the trajectory, this idealized model is actually quite good as a quantitative one.

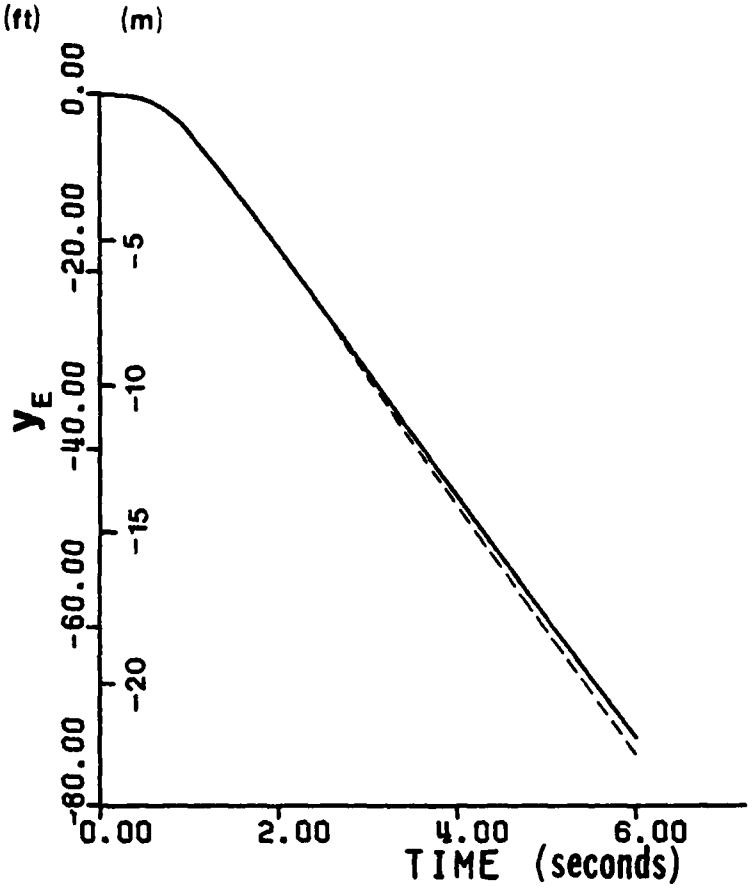

Fig. 2. Lateral deviation of rocket center of mass, y_E, for $\alpha_y = 0.001$.

The effects of dynamic mass imbalance on the trajectory of a free-flight rocket are similar to those of thrust misalignment. Both types of imperfection cause a precessional rate to arise very soon after EOG and because of this rate, the rocket is driven off course during the thrust period. Because of this similarity, results analogous to those already given for thrust misalignment are given with little comment.

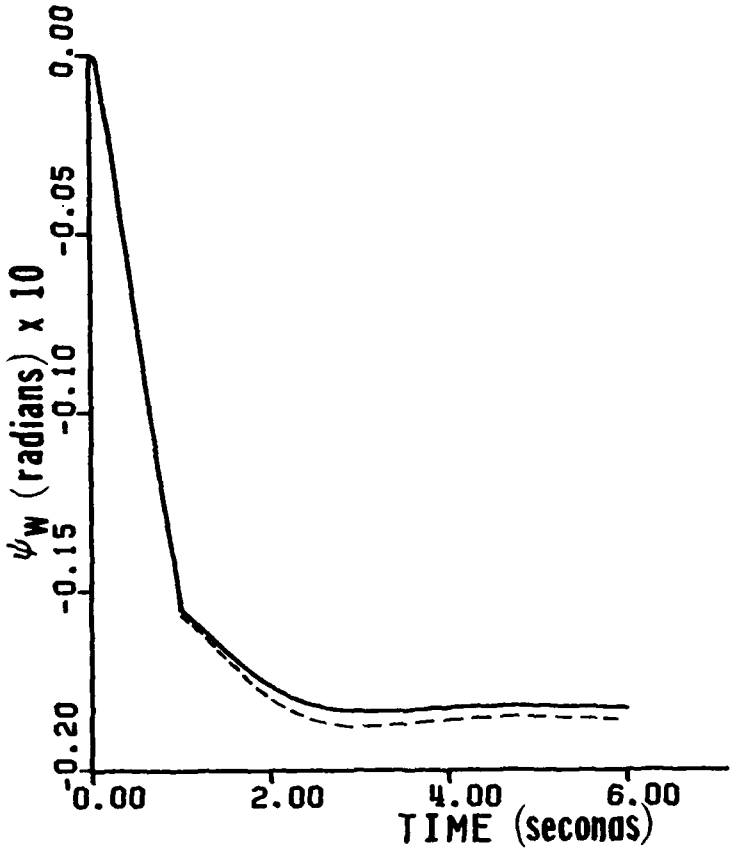

(a)

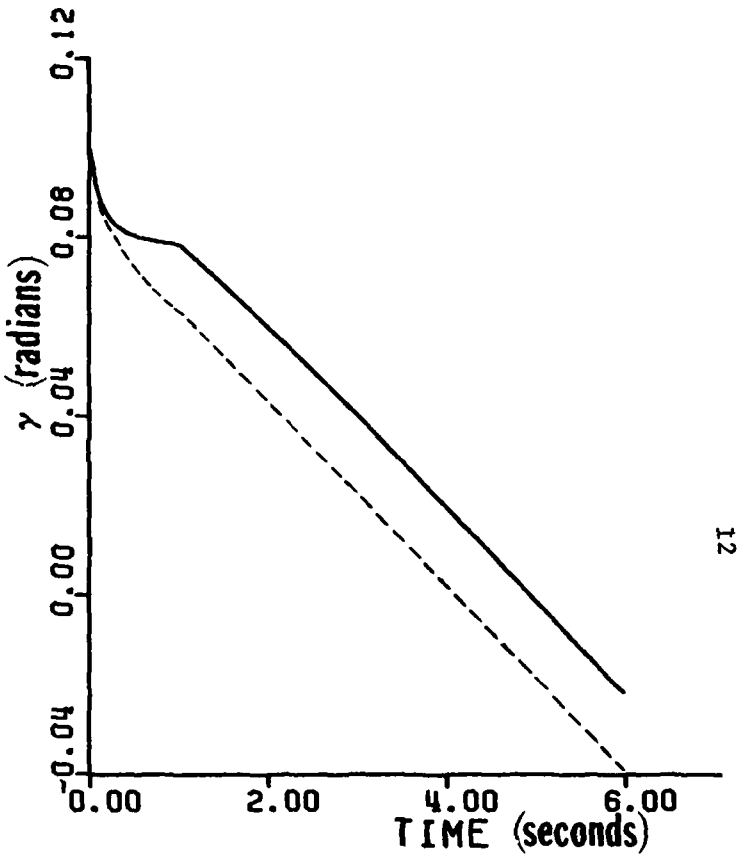

(b)

Fig. 3 Flight path angles for μ_2 = 0.001; (a) velocity yaw angle, ψ_w; (b) velocity pitch angle, γ.

For dynamic imbalance, as well as thrust misalignment, the precessional component of the rocket's transverse angular velocity is created during the first quarter revolution in spin of the affected rocket. The flight path angles shown in Fig. 3 were obtained by using a mass imbalance defined by $\mu_2 = 0.001$ and $\mu_3 = 0$.

To obtain the dashed curves, the mass imbalance was "magically" removed when the rocket had rolled through $\pi/2$ rad. These curves are qualitatively the same as those in Fig. 1. The lateral deviation curves shown in Fig. 4 are also qualitatively the same as those in Fig. 2.

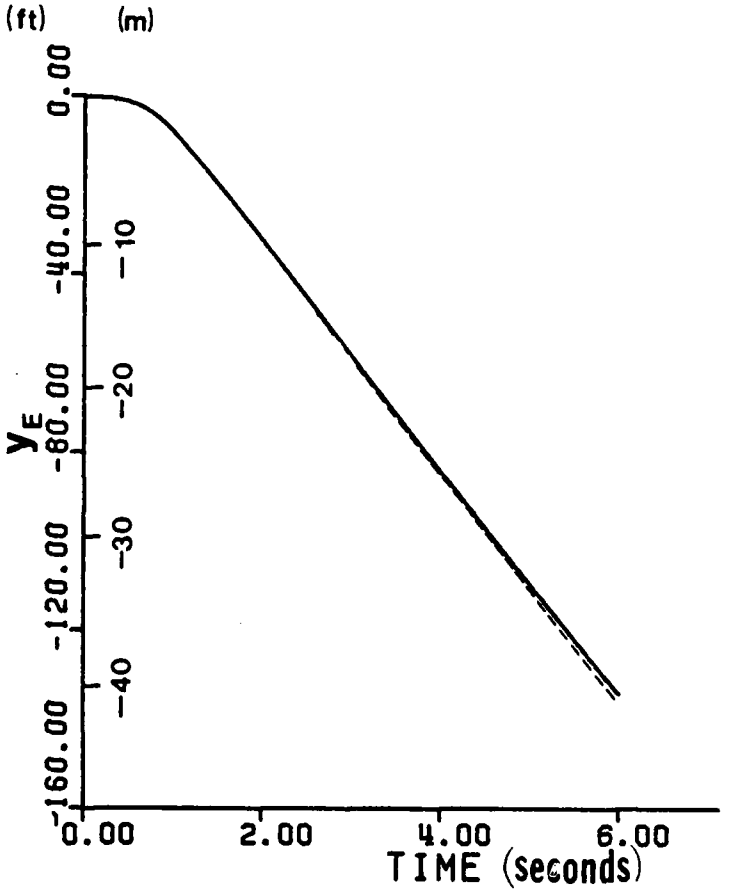

Fig. 4 Lateral deviation of rocket center of mass, y_E, for $\mu = 0.001$.

2.4 Reduction of Trajectory Deviations by Imposing Suitable Launch Conditions

By imposing suitable launch conditions, the values of the flight path angles well after burnout can be made essentially zero. The lateral and vertical deviations can also be reduced.

Generally, if transverse angular velocity exists at EOG, there will be some transverse linear velocity of the rocket's center of mass. However, this velocity will normally be small in magnitude. For example, if at EOG, the launcher/rocket system is rotating with an angular rate of 0.05 rad/sec about a point 10 ft. from the rocket's center of mass, then the transverse velocity will have a magnitude of only 0.5 ft/sec due to the rotation. Such small transverse linear velocities have little effect on the trajectory. It is also rather obvious that the displacement of the rocket's center of mass at EOG will not be large enough to produce any significant change in its point of impact.

Since one-half of the rocket's state has been effectively eliminated from consideration the remaining alternatives are to compensate by either an attitude change or a change in angular rate. That is, to either make the pitch and yaw angles at EOG as nearly equal to the negatives of the "final" values of deviation in flight path angles or impose an angular rate opposite in sign to that caused by thrust misalignment or dynamic imbalance. The attitude change required to make $\psi_w \simeq 0$ at burnout for the thrust misalignment example of subsection 2.2 is obviously $\Delta\psi \simeq 0.010$ rad. Alternatively, the required angular rate is approximately 0.024 rad/sec.

The time histories of ψ_w and y_E for the angular rate alternative are presented in Fig. 5. Comparison of these modified histories with the ones

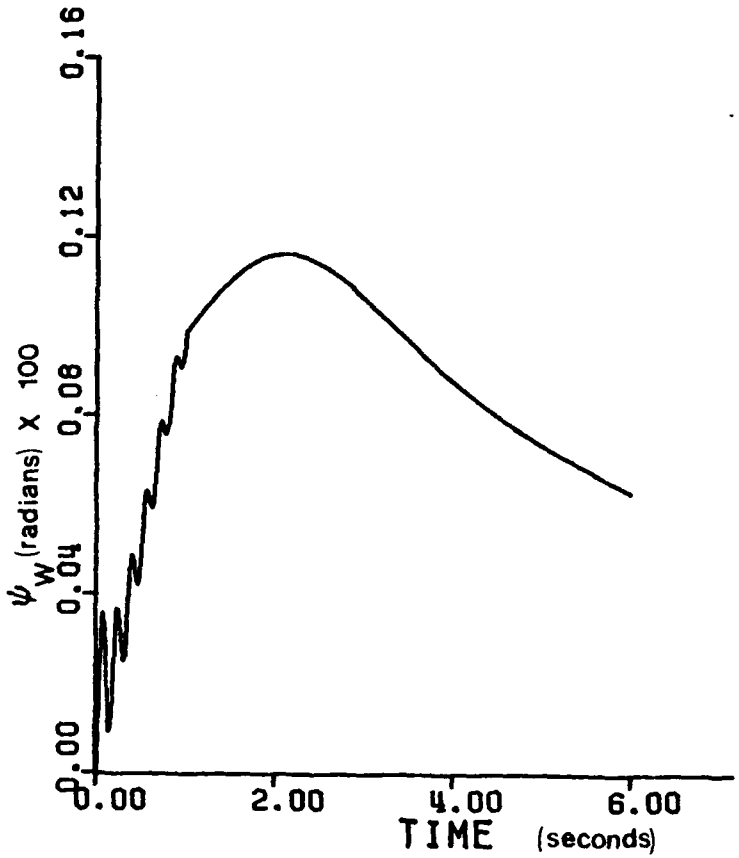

(a)

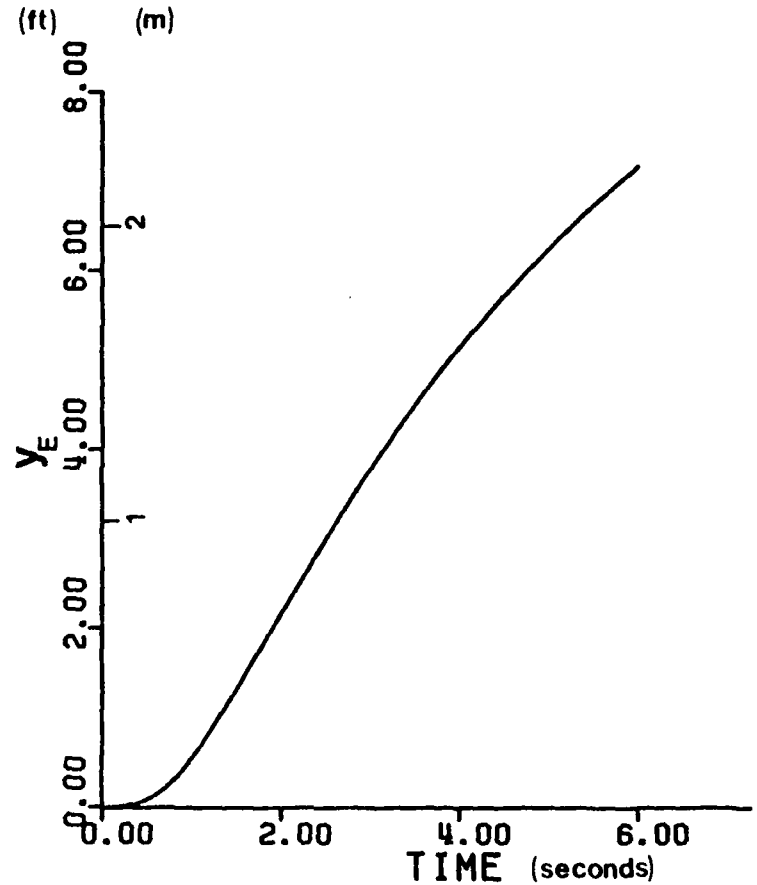

(b)

Fig. 5 Lateral deviations for ω_y = 0.001 and initial yaw rate of 0.024 rad/sec; (a) angular; (b) translational.

in Figs. 1 and 2 clearly shows that dispersion can be decreased if the required angular rates of the launcher, or sub-launcher, are produced by the imperfections. In the next section, the possibility of getting a launcher to respond significantly to the forces and moments caused by thrust misalignment is investigated.

SECTION 3. LAUNCH CONDITIONS CAUSED BY ROCKET IMPERFECTIONS

3.1 General Comments

It was hoped that results for dynamic mass imbalance of the rocket could be included in this report; however, such results are only now being obtained. Therefore, in this and following sections only thrust misalignment is considered as the "imperfection."

3.2 Idealized Launcher Model

The idealized launcher physical model used in this and later sections is shown in Fig. 6. There are several reasons this model was chosen. The first, and most obvious, reason is that it is geometrically simple. Second, although it is geometrically simple, the model is general enough that both pitch and yaw motions of the launcher are modeled. Third, because the center of mass of the launcher, C_L, lies at the pivot point, O, the bias effects of launcher mass are eliminated. Fourth, because the launch axis (x_L-axis) passes through the pivot point, the detent force does not affect the launcher motion. Fifth, by considering the equations of motion of the one-degree-of-freedom launcher/rocket system model in Appendix B, one finds that the "torque" on the system due to the Coriolis acceleration is destabilizing if the rocket is located behind the pivot point and stabilizing if forward of that point. Hence, the idealized model should be more sensitive to rocket imperfections. Therefore, the model minimizes, to some extent, biases and at the same time is general enough for use in this qualitative analysis of launcher motion caused by rocket imperfections.

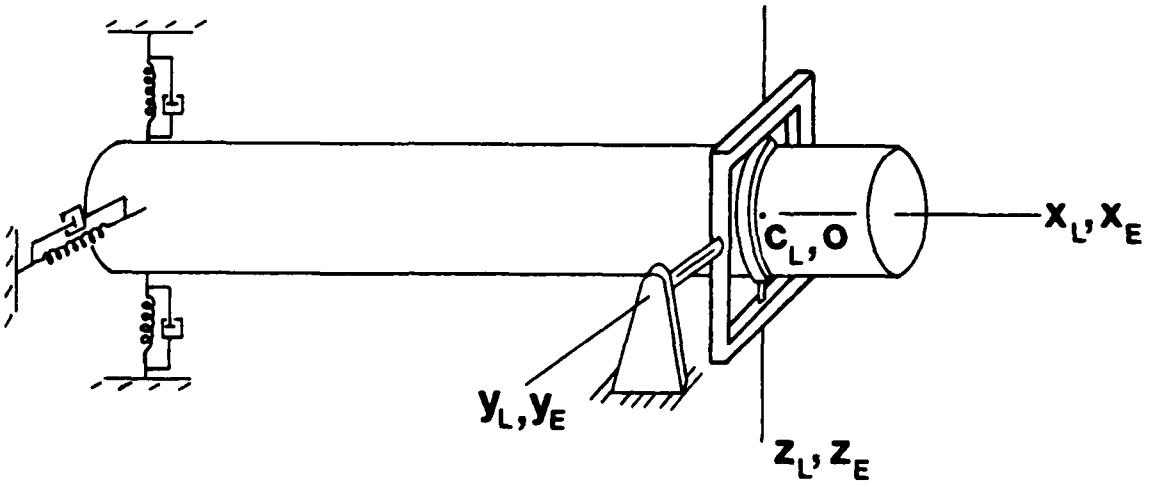

Fig. 6 Idealized launcher for nonlinear frequency response analysis. (Unloaded equilibrium position)

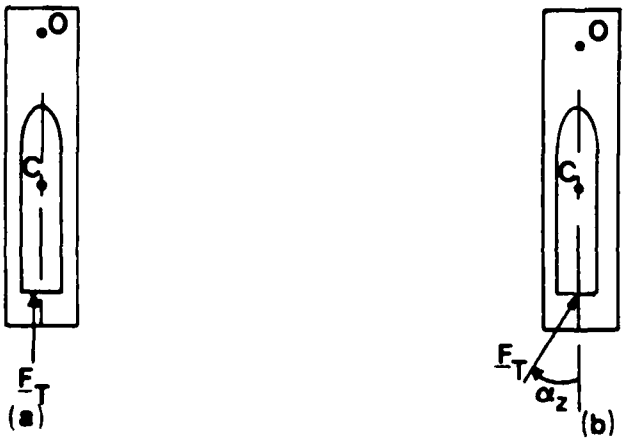

Fig. 7 Launcher with pivot point forward and non-spinning rocket; (a) linear thrust misalignment, (b) combination.

The launcher model is constrained so that it cannot roll about the x_L-axis. This constraint is imposed because of the desire to obtain a precise roll angle at EOG. It may also be constrained in either pitch or yaw, or both, thereby obtaining a single-degree-of-freedom launcher or a rigid one.

Mathematically, the springs and dashpots shown in Fig. 6 are replaced by torsional springs and dashpots at 0.

3.3 Effects of Thrust Misalignment

3.3.1 Non-spinning Rockets

If the rocket does not rotate while it is on the launcher, then the thrust misalignment (if constant in direction) will result in a torque of essentially constant direction about 0 and the launcher will respond by rotating about that direction until the restoring torque of magnitude exceeds the torque due to thrust misalignment are generated. The launcher will then "rebound." Whether or not the launcher should be rebounding at EOG is determined by whether the thrust misalignment causes the launcher to rotate adversely, or proversely, as far as the free-flight effects of thrust misalignment are concerned.

In Fig. 7(a), the rocket shown is acted upon by thrust misalignment which will initially cause positive yaw of the launcher. Following EOG, the rocket will also yaw positively. If the launcher rebounds prior to EOG, then some decrease in dispersion will be achieved. Figure 7(b) depicts a case in which the rocket's thrust vector misalignment is defined by the angle α_z. This case is representative of a misaligned rocket nozzle. The torque due to thrust misalignment will initially cause a negative

rotation of the launcher and, since the rocket will yaw negatively at EOG, the launcher should rebound if dispersion is to be decreased.

Rebound of the launcher during guidance requires it to be very stiff if the guidance period is short. If the launcher cannot be made stiff enough to rebound, an aft pivot point (see Fig. 8) will be worse if the thrust is misaligned in the manner shown in Fig. 8(a). However, if the misalignment is as shown in Fig. 8(b), then launcher motion due to thrust misalignment will be beneficial. The misalignment defined by α_z is, according to the definition of Ref. 1 (pages 28-29), a combination of linear and angular misalignment.

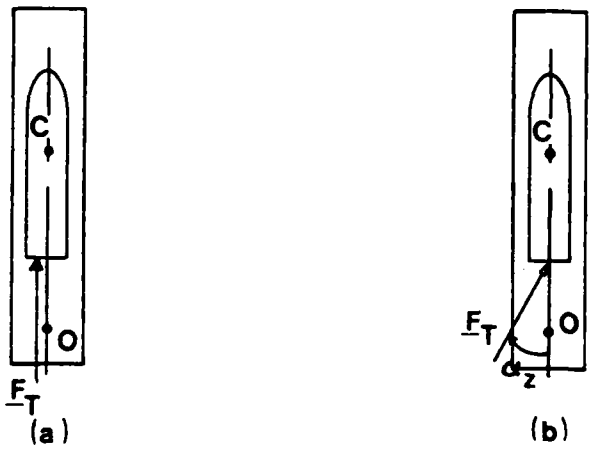

Fig. 8 Launcher with pivot point aft and non-spinning rocket; (a) linear thrust misalignment, (b) combination.

A mathematical model representative of launcher/rocket systems in which the rocket does not rotate on the launcher has been developed. However, the computer code which incorporates this model has not been checked out sufficiently to present results at this time, but they will be included in the final report.

3.3.2 Spinning Rocket

When the rocket rotates with respect to the launcher during guidance - for example, as it does if helical rails are used to impart spin - then the thrust misalignment will generally rotate with the rocket. It is assumed here that this is the case.

Assuming a forward pivot point for the launcher, Fig. 9 depicts the thrust misalignment force, $\underline{F}_{TM}$, and the thrust misalignment torque, $\underline{T}_{TM}$, due to a "combination" thrust misalignment defined by $\alpha_y \neq 0$, $\alpha_z = 0$. For a roll angle between 0 and $\pi/2$, there is a negative pitching moment about the y_E-axis. For roll angles between $\pi/2$ and π, the thrust misalignment generates a positive pitching moment. During the entire rotation from 0 to π, a negative yawing moment is generated. If EOG occurs when the roll angle (say Φ) is π, the rocket, according to the theory presented in Appendix D, will yaw positively due to the thrust misalignment. It follows, that if the launcher has a low enough frequency that no rebound occurs, or if it has a high enough frequency that more than one cycle is completed by EOG, some benefit should be derived from the launcher motion.

The more general model of a rocket/launcher system was used to generate some time histories of launcher motion. The launcher moments of inertia and launcher natural frequencies were varied to determine the effects of these parameters on launcher motion. The model of the rocket used is described in Appendix B. Physical data for the system is given in Table 2 and the aerodynamic data appears in Table 3. The model of the rocket has essentially the same characteristics as that used in Ref. 8, with the

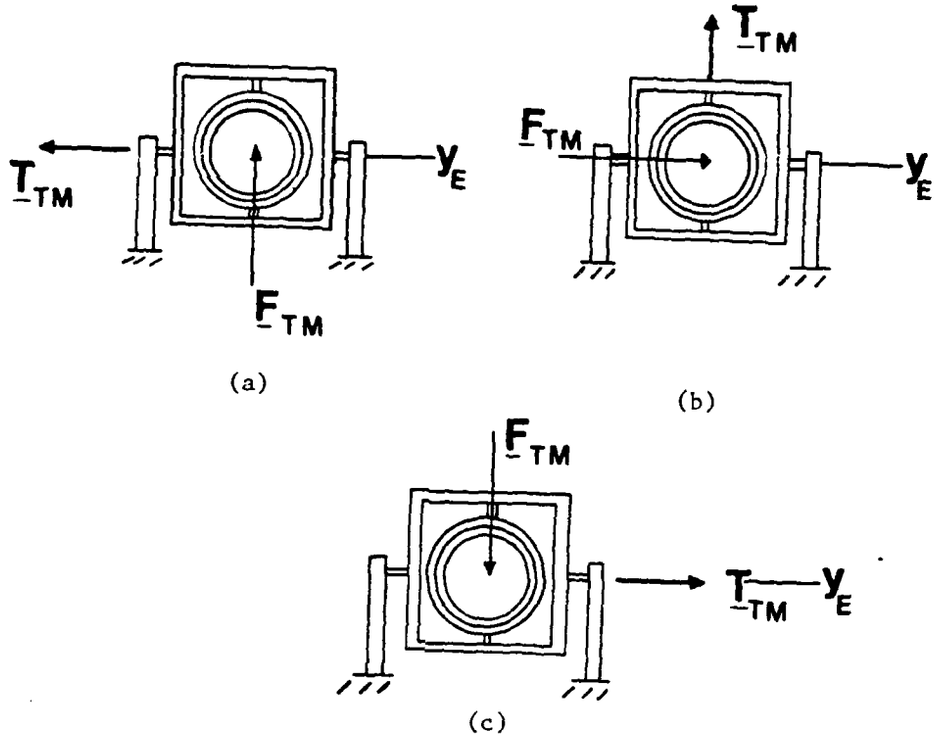

Fig. 9 Rotating rocket on launcher; (a) roll angle of 0; (b) roll angle of $\pi/2$ rad; (c) roll angle of π rad.

Table 2. Physical Characteristics of the More General Launcher/Rocket Model.

LAUNCHER

Mass (kg) 146.

Inertia Matrix ($kg\text{-}m^2$)

"small" inertia case

$$\begin{bmatrix} 0.542 & 0 & 0 \\ 0 & 54.24 & 0 \\ 0 & 0 & 54.24 \end{bmatrix}$$

"intermediate" inertia case

$$\begin{bmatrix} 0.542 & 0 & 0 \\ 0 & 108.48 & 0 \\ 0 & 0 & 108.48 \end{bmatrix}$$

"large" inertia case

$$\begin{bmatrix} 0.542 & 0 & 0 \\ 0 & 216.96 & 0 \\ 0 & 0 & 216.96 \end{bmatrix}$$

Damping Ratio 0.1 all axes

Detent Force (Nt) 817

ROCKET

Initial Mass (kg) 113.35

Initial C.G. (m from nose) 5.84

Burnout Mass (kg) 76.08

Burnout C.G. (m from nose) 3.48

Inertia Matrix ($kg\text{-}m^2$)

Initial

$$\begin{bmatrix} 0.40 & 0 & 0 \\ 0 & 93.12 & 0 \\ 0 & 0 & 93.12 \end{bmatrix}$$

At Burnout

$$\begin{bmatrix} 0.26 & 0 & 0 \\ 0 & 39.3 & 0 \\ 0 & 0 & 39.3 \end{bmatrix}$$

Thrust Time Variation

Time (sec)	Thrust (Nt)
0	0
0.05	0
0.0647	667.4
0.0794	6766.4
0.0912	7050.0
0.1147	6943.0
0.1400	6943.0
0.7014	12204.0
0.9585	11663.0
0.9944	267.0
1.1000	0

Table 3. Aerodynamic Data for the More General Rocket Model.

Reference Area (m^2) 0.01923 Reference Length (m) 0.157

Length (m) 3.5

Mach No.	C_N	C_{m_q}	x_{cp} (m from nose)
0.0	4.41	-1460	1.876
0.4	4.24	-1540	1.722
0.6	4.12	-1610	1.628
0.8	3.95	-1730	1.457
0.9	3.80	-1780	1.408
1.0	3.58	-1780	1.384
1.1	3.84	-1730	1.378
1.2	4.07	-1660	1.378
1.4	4.41	-1560	1.423
1.6	4.61	-1460	1.469
1.8	4.70	-1380	1.512
2.0	4.76	-1300	1.533
2.2	4.71	-1230	1.548
2.4	4.67	-1170	1.533
2.6	4.54	-1120	1.487
3.2	4.41	-1010	1.298

Mach No.	C_x
0.00	0.425
0.80	0.328
0.90	0.310
0.95	0.305
1.00	0.330
1.10	0.403
1.20	0.381
1.28	0.373
1.50	0.372
2.00	0.340
2.50	0.299
3.00	0.262
3.50	0.231
4.00	0.205

exception that the center of pressure position is moved aft to provide more static stability. The rocket is spun up using a helical rail so that for the non-tip-off cases $\Phi_{EOG} = \pi$. A spin rate of approximately 14 Hz is generated during a guidance length of 1.219 m.

The launcher motion time histories shown in Figs. 10 through 15 are actually perturbations in launcher motion due to thrust misalignment. To obtain them, two integrations were performed, one with no thrust misalignment and one with $\alpha_y = 0.01$ rad and $\alpha_z = 0$. In all cases, the rocket's center of mass is 1.323 m aft of the pivot point at ignition. The thrust is modeled as acting at a point 1.947 m aft of the initial center of mass. Hence, the initial moment arm for the thrust misalignment is 3.27 m.

Figures 10 through 15 are arraigned in three groups according to the value of ω_{Ln}. There are two figures in each group. In each figure, three curves are presented, one for each of the three moment of interia values used. For the "small" launcher case, the pitch and yaw moments of inertia of the launcher about 0 are 54.236 kg-m^2. For the "intermediate" and "large" inertia cases, the moments of inertia are respectively two and four times 54.236 kgm^2. For $\omega_{Ln} = 5$ Hz (Figs. 10 and 11), the launcher responds without rebounding. For the higher frequency values, $\omega_{Ln} = 20$ Hz (Figs. 12 and 13), $\omega_{Ln} = 30$ Hz (Figs. 14 and 15), the launcher always rebounds in pitch, but not necessarily in yaw. As expected, an increase in the inertia of the launcher results in a decrease in the magnitude of the corresponding response.

Notice that the magnitudes of the launcher rotations at EOG for $\omega_{Ln} = 5$ Hz are large. Also, the time rates of change of $\Delta\alpha_2$ and $\Delta\alpha_3$ are

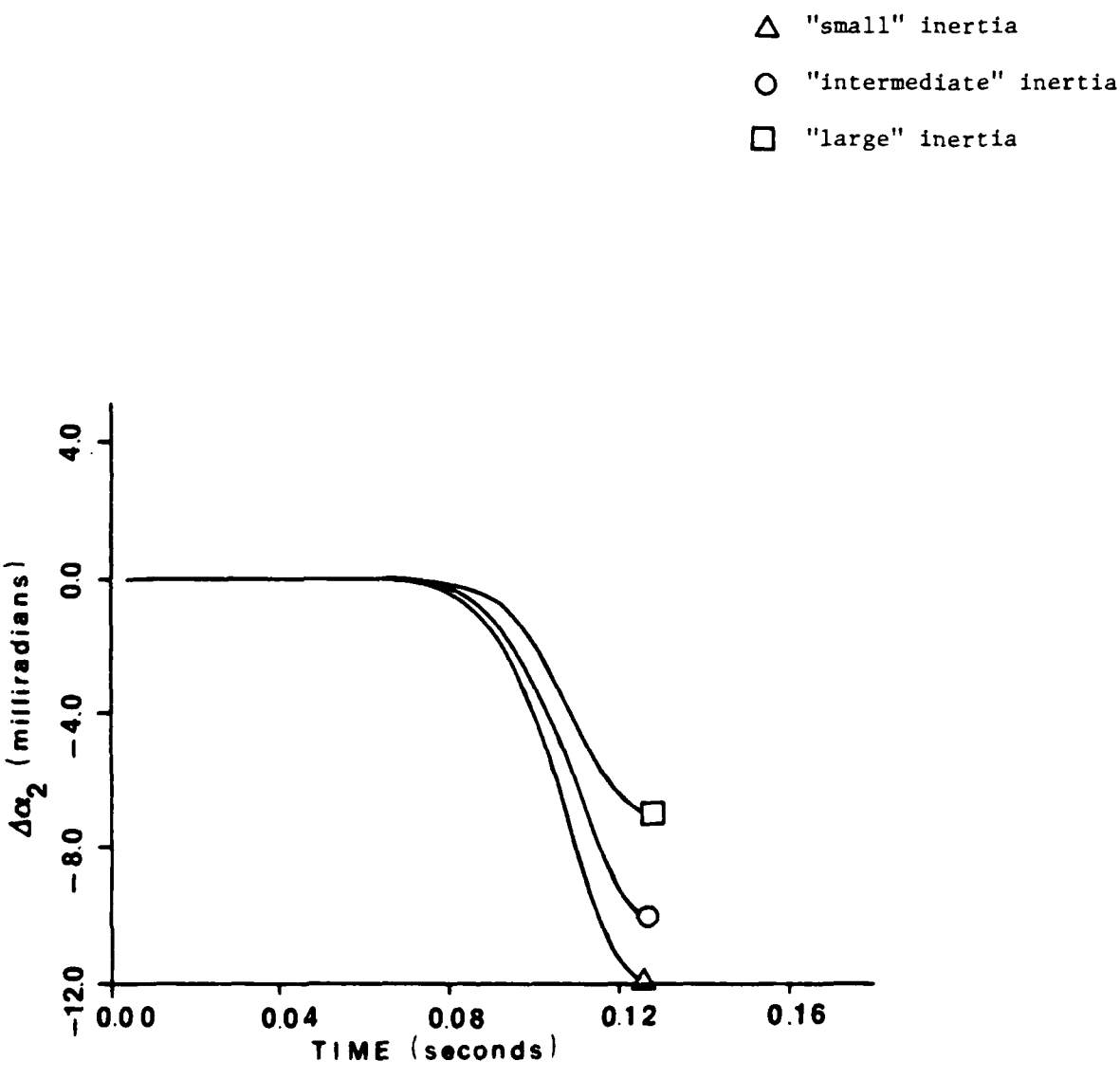

Fig. 10 Launcher pitch angle deviations for ω_{Ln} = 5 Hz.

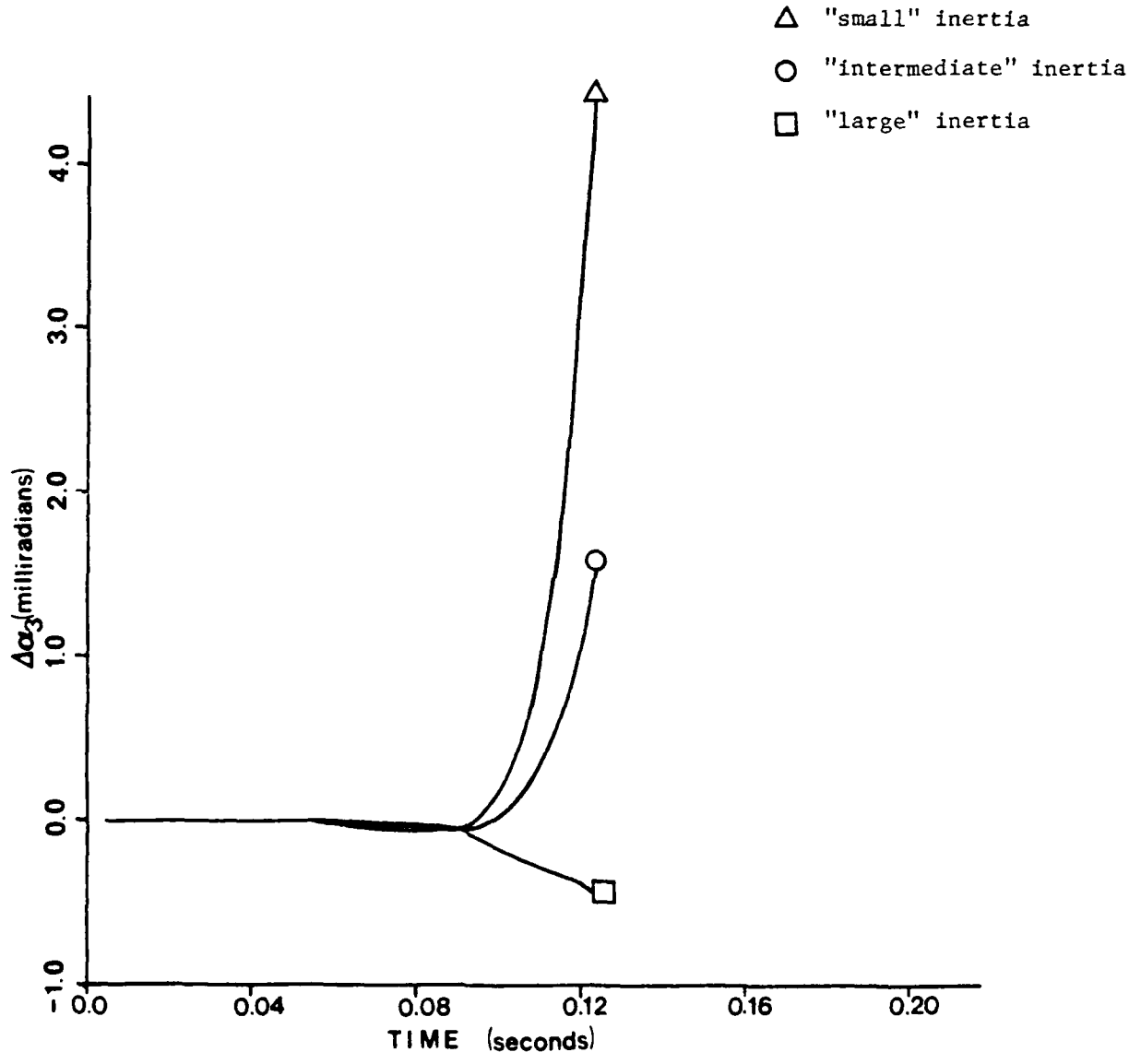

Fig. 11 Launcher yaw angle deviations for ω_{Ln} = 5 Hz.

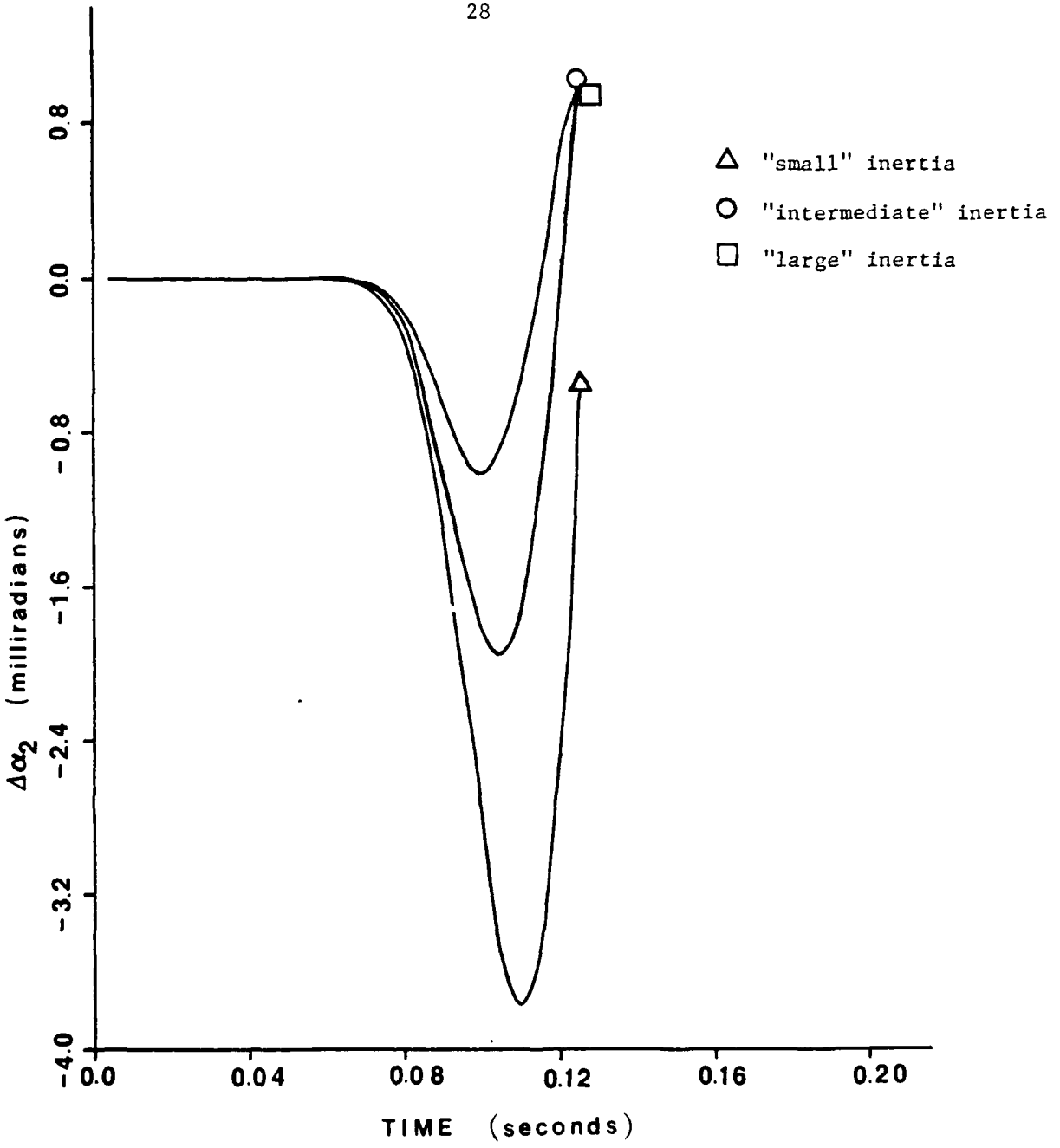

Fig. 12 Launcher pitch angle deviations for ω_{Ln} = 20 Hz.

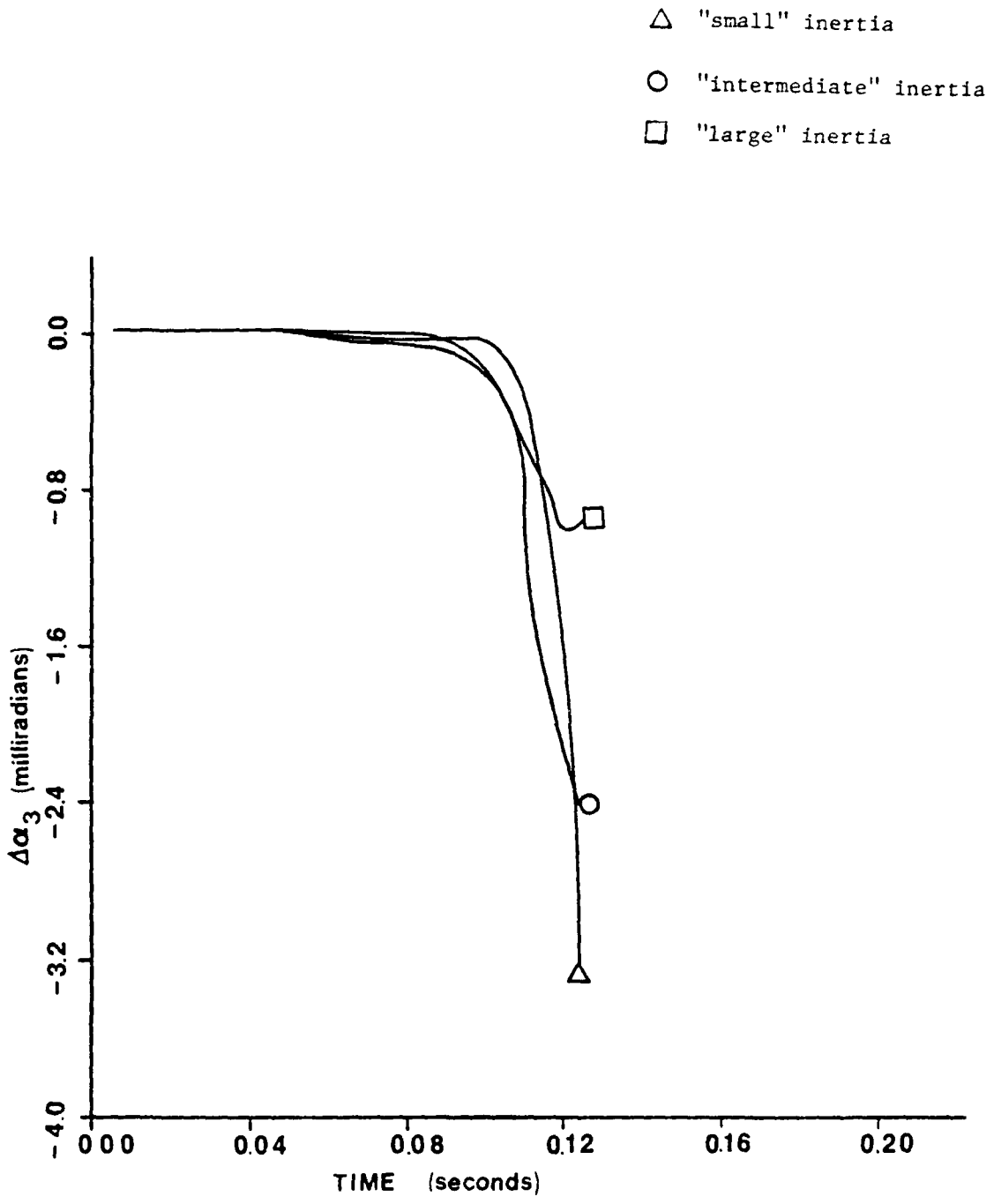

Fig. 13. Launcher yaw angle deviations for ω_{Ln} = 20 Hz.

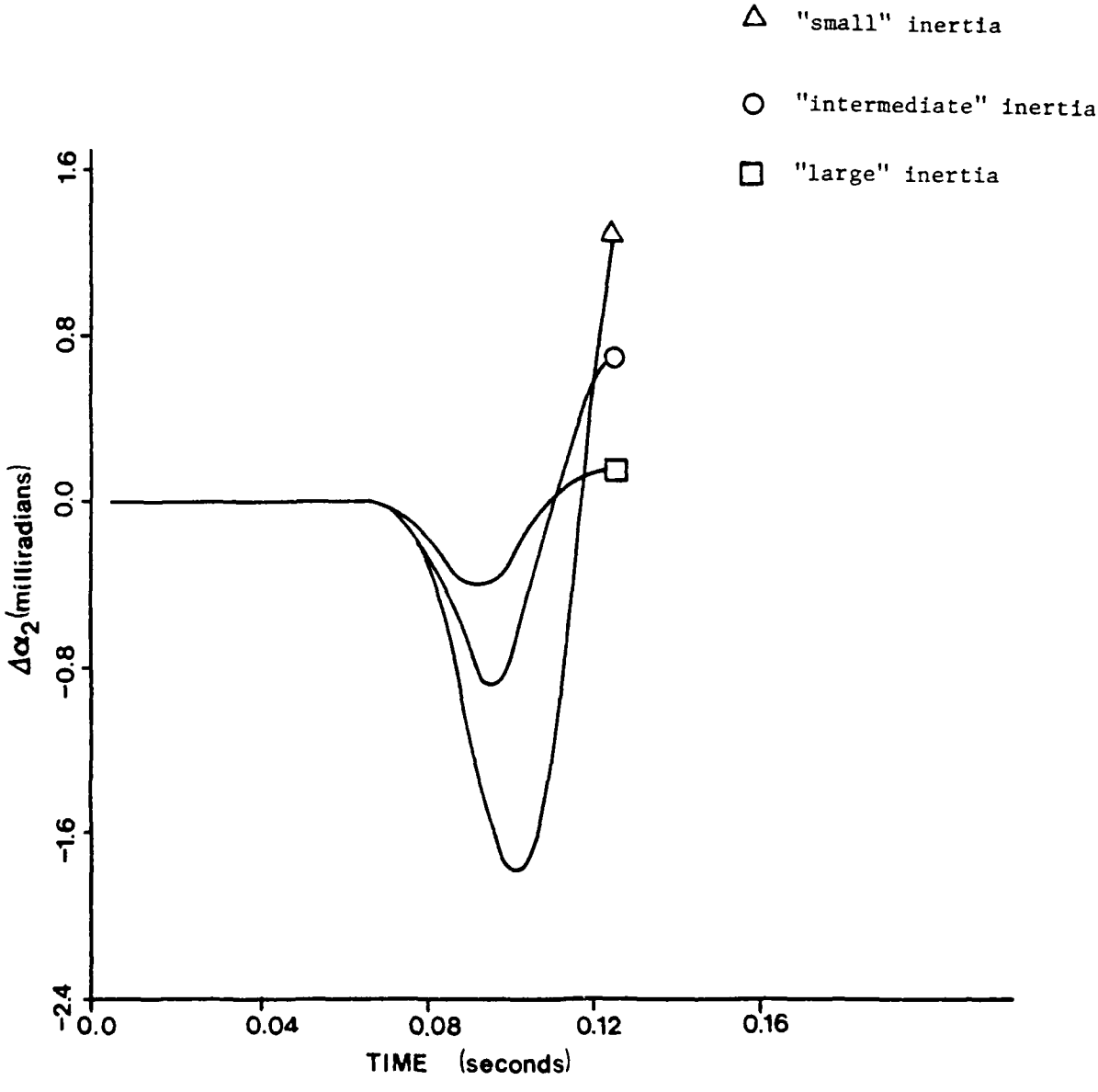

Fig. 14 Launcher pitch angle for deviations for ω_{Ln} = 30 Hz.

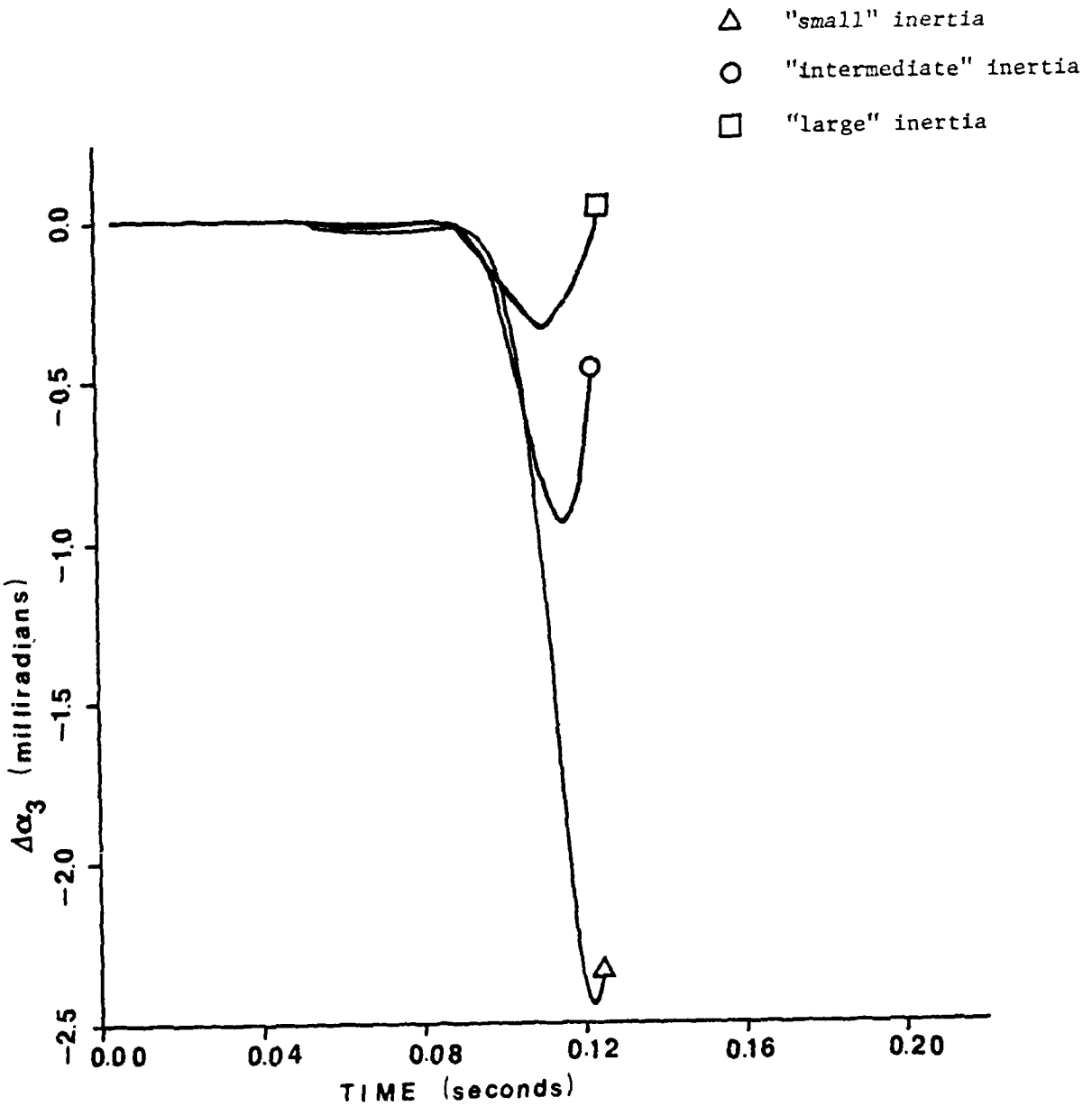

Fig. 15 Launcher yaw angle deviations for ω_{Ln} = 30 Hz.

SECTION 4. PRODUCTION OF FAVORABLE LAUNCH CONDITIONS

4.1 Present Approach - Nonlinear Frequency Response

The equations of motion of a launcher/rocket system are nonlinear. Under certain conditions, they may be approximated by linear equations with variable coefficients as is done in Appendix E. However, solutions to even such simplified equations can generally be obtained only by numerical methods. Furthermore, because nonlinear terms in the equations may possibly be as significant as those due to rocket imperfections, the safest approach is to numerically integrate the full nonlinear equations to obtain the dynamic response of the system.

Measures of how well the launcher acts as a passive controller are considered to be the lateral and negative vertical deviations of the rocket's center of mass and the flight path angles, γ and ψ_w, at a time after burnout when an essentially constant value of ψ_w has been achieved. The deviations, or perturbations, in these variables at this somewhat arbitrary time are ΔY_f, ΔZ_f, $\Delta\gamma_f$ and $\Delta\psi_{w_f}$. They are defined with respect to the nominal trajectory which the rocket flies when there is no thrust misalignment.

Results are given in the next two subsections for two launcher configurations, one non-tip-off and one tip-off. In all cases, the rocket was spun up via helical rails so that $\phi_{EOG} = \pi$ and the spin rate at EOG was 14 Hz. Furthermore, the "small" inertia case (see Table 2) was considered.

4.2 Non-Tip-Off Launcher Results

4.2.1 Nonlinear Frequency Responses

By varying the frequency of the unloaded launcher from 5 to 50 Hz, the frequency responses shown in Figs. 16 and 17 were obtained. The time at which the deviations were computed corresponds to a range of 2133 m and is about 1.8 sec after burnout (t_{BO} = 1.1 sec). For the frequency response computations $\alpha_y = 0.01$ and $\alpha_z = 0$. Note that α_y is fairly large. Effects of the randomness of actual thrust misalignment are considered shortly.

There are two frequency bands within which the launcher acts as a passive controller. These are centered about 5 and 36 Hz. The frequency band centered at approximately 36 Hz is theoretically the best, but would dictate a very stiff launcher. The responses at frequencies in the lower band, centered at about 6 Hz, are not as favorable, but still a reduction of $\sqrt{\Delta\gamma_f^2+\Delta\psi_w^2}$ by more than 50 percent from a rigid launcher value of 32.44×10^{-3} is possible. ΔY_f and ΔZ_f are also reduced significantly if the launcher frequency is 6 Hz.

4.2.2 Effect of Randomness of Thrust Misalignment

Because only a single thrust misalignment was used to obtain the above frequency responses, there is no guarantee that for a different misalignment passive control will be achieved at the same frequencies for an arbitrary thrust misalignment. To verify that the thrust misalignment direction has little impact on the effectiveness of the launcher, the thrust misalignment direction was varied to obtain Figs. 18 and 19. The launcher natural frequency of 36 Hz was used but the results are similar at other frequencies. The $\Delta\psi_{w_f}$ curve is essentially periodic in

δ, the thrust misalignment direction angle. The $\Delta\gamma_f$ curve is not as well-behaved because of gravity effects, but is basically periodic also. These results and those for the center of mass displacements indicate that regardless of the thrust misalignment, for certain launcher frequencies considerable passive control is achieved.

"Good" and "bad" case time histories of $\Delta\gamma$ and $\Delta\psi_w$ are shown in Figs. 20 through 27. Figs. 20 and 21 are for ω_{Ln} = 36 Hz and represent the "good" high-frequency case. These should be compared to Figs. 22 and 23 for ω_{Ln} = 30 Hz, which are representative of a "bad" high-frequency case. An order of magnitude reduction in the final flight path angle is evident. Some "good" low-frequency (ω_{Ln} = 5 Hz) results are presented in Figs 24 and 25. The reduction in $\Delta\psi_{w_f}$ from 32.44 x 10^{-3} rad to about 13 x 10^{-3} rad is certainly significant. Dynamic coupling results in a larger $\Delta\gamma_f$ than that for a rigid launch, but $\sqrt{\Delta\gamma_f^2 + \Delta\psi_{w_f}^2}$ is still reduced significantly. That the motion of the launcher in response to rocket imperfections can be detrimental is clearly shown in Figs. 26 and 27 for a "bad" low-frequency case (ω_{LN} = 10 Hz).

4.3 Tip-Off Launch Results

The tip-off launcher configuration is the same as the non-tip-off configuration except, after the 1.33 m of guidance on helical rails, 0.3048 m of guidance with tip-off is modeled. The nonlinear frequency response curves analogous to those in Figs. 16 and 17 are presented in Figs. 28 and 29. The tip-off launcher response curves are noticeably different from the non-tip-off curves. Some passive control effectiveness is present at high frequencies around 36 Hz. At lower frequencies near 6 Hz, the dispersion, as measured by the aforesaid deviations, is greatly reduced.

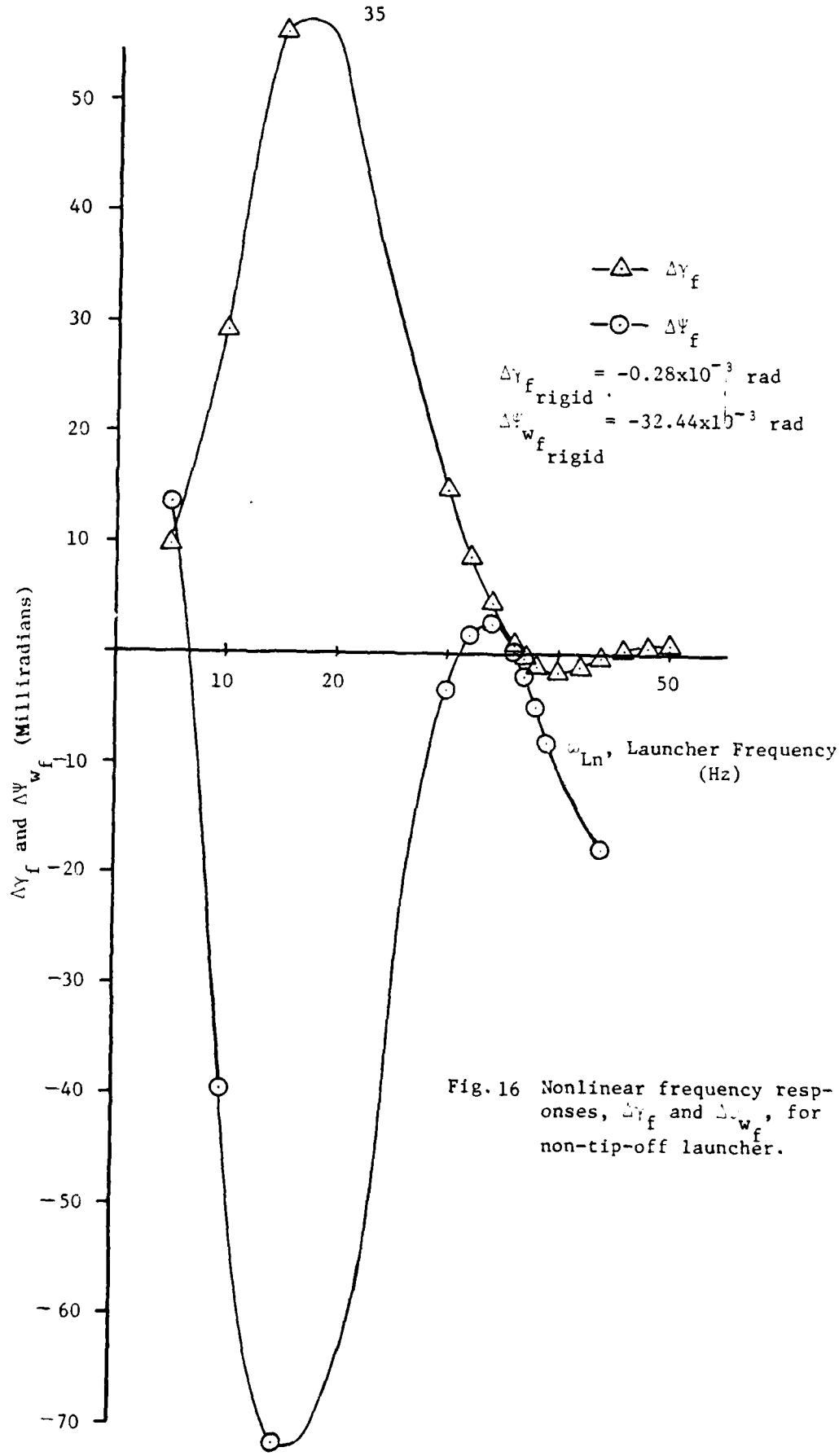

Fig. 16 Nonlinear frequency responses, $\Delta\gamma_f$ and $\Delta\Psi_{w_f}$, for non-tip-off launcher.

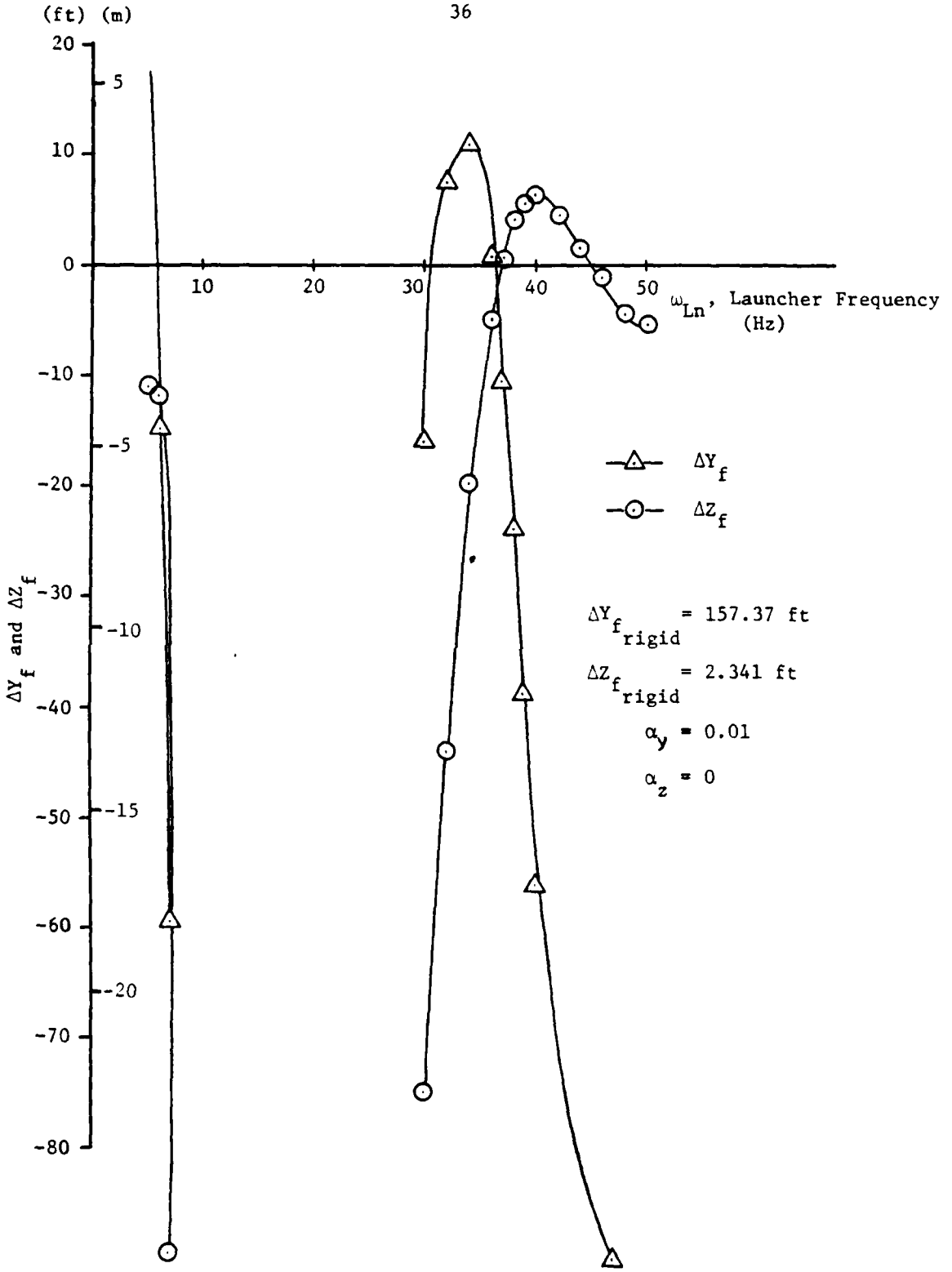

Fig.17 Nonlinear frequency responses, ΔY_f and ΔZ_f, for non-tip-off launcher.

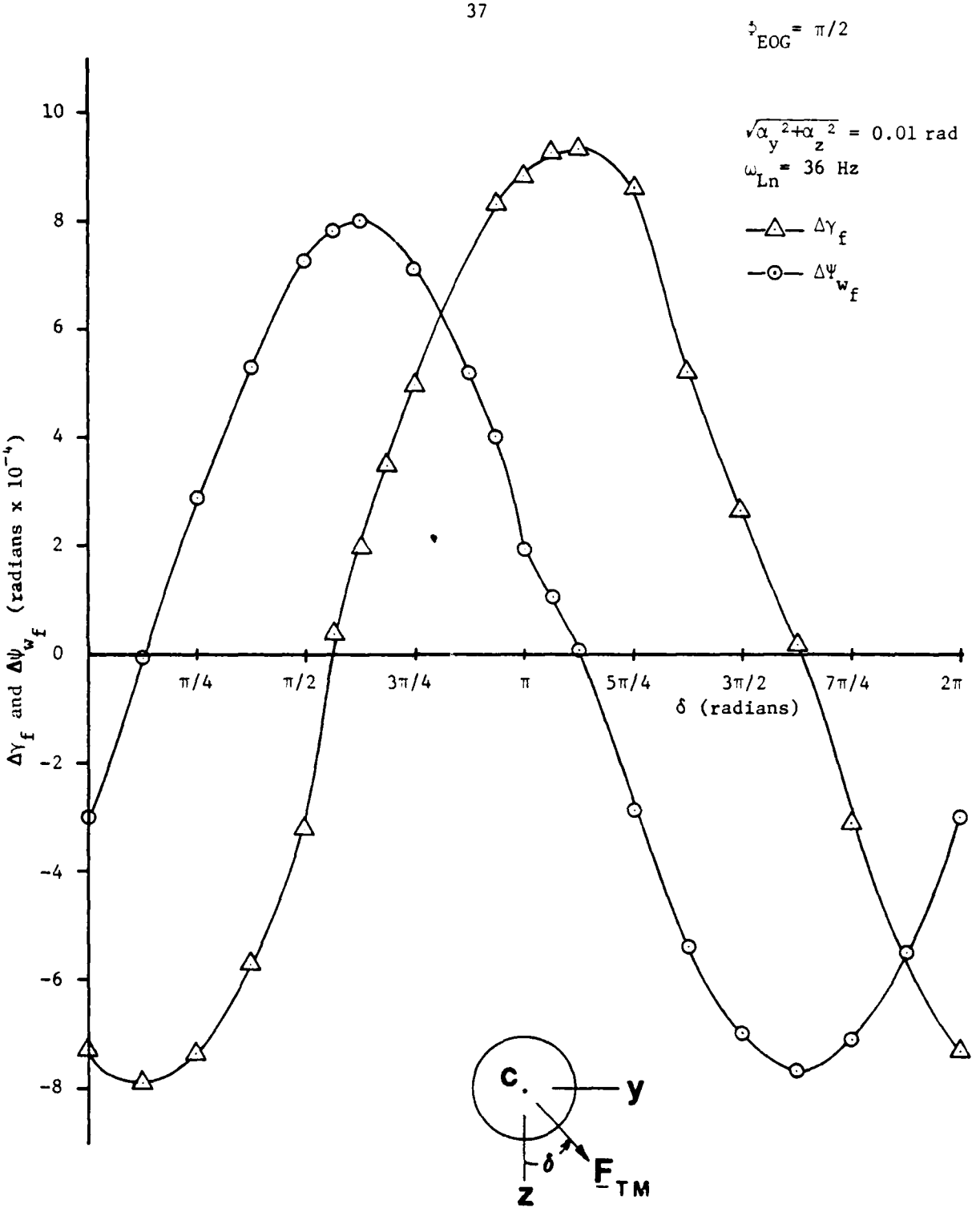

Fig. 18 Effect of direction of thrust misalignment, $\Delta\gamma_f$ and $\Delta\psi_{w_f}$.

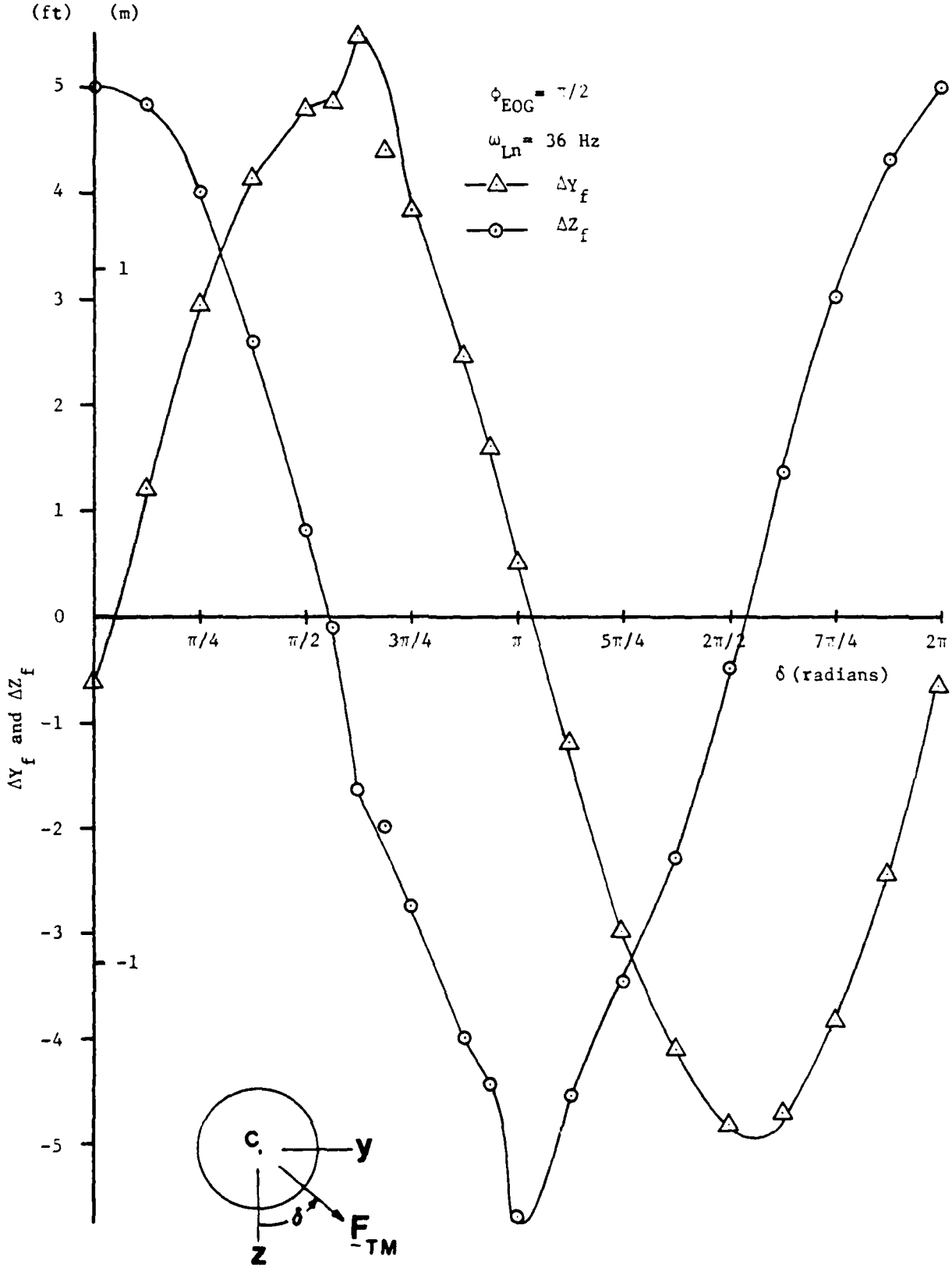

Fig. 19 Effect of direction of thrust misalignment, ΔY_f and ΔZ_f.

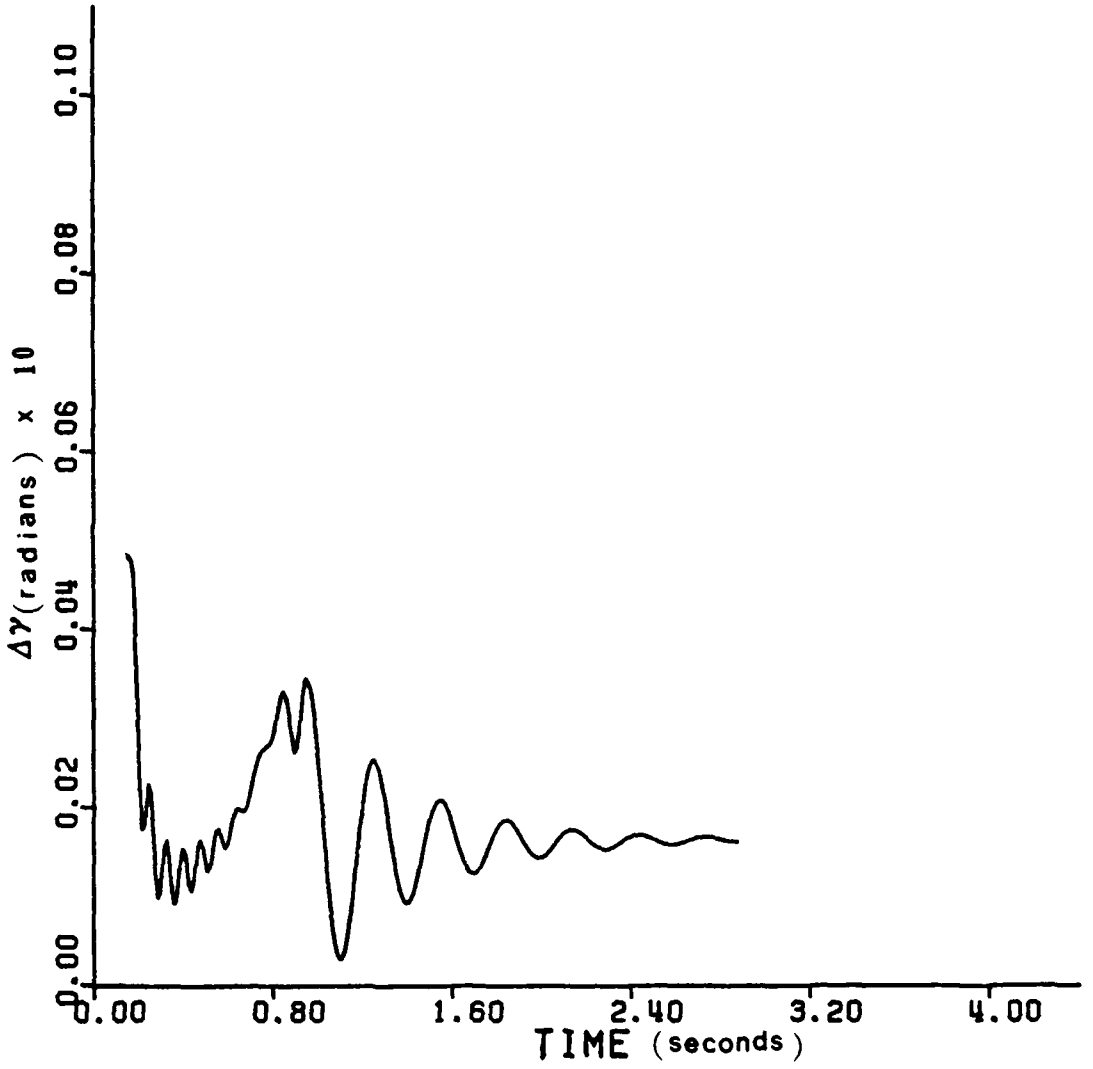

Fig. 20 Flight path angle deviation , $\Delta\gamma$, for non-tip-off launch – ω_{Ln} = 36 Hz.

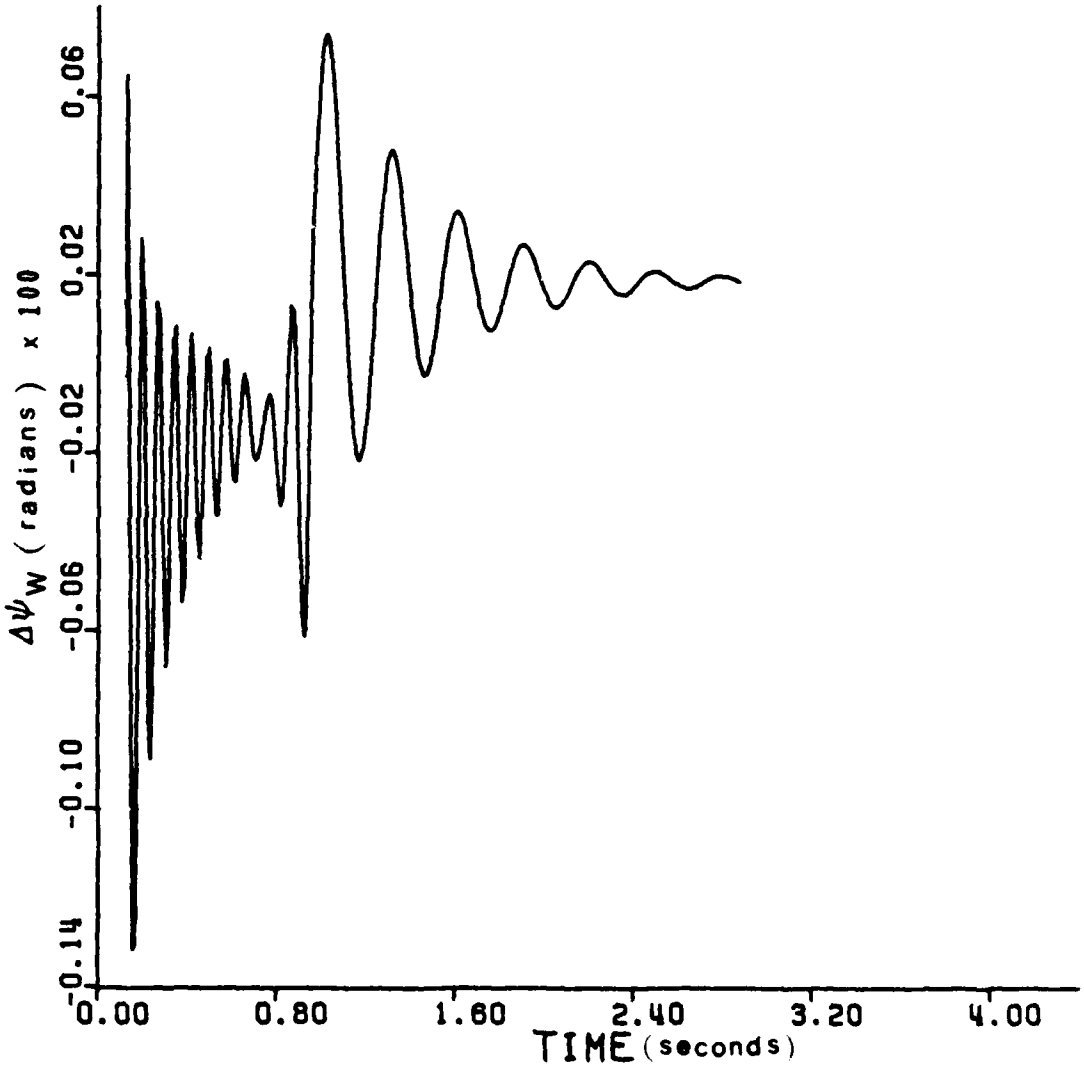

Fig. 21 Flight path angle deviation, $\Delta\psi_W$, for non-tip-off launch – ω_{Ln} = 36 Hz.

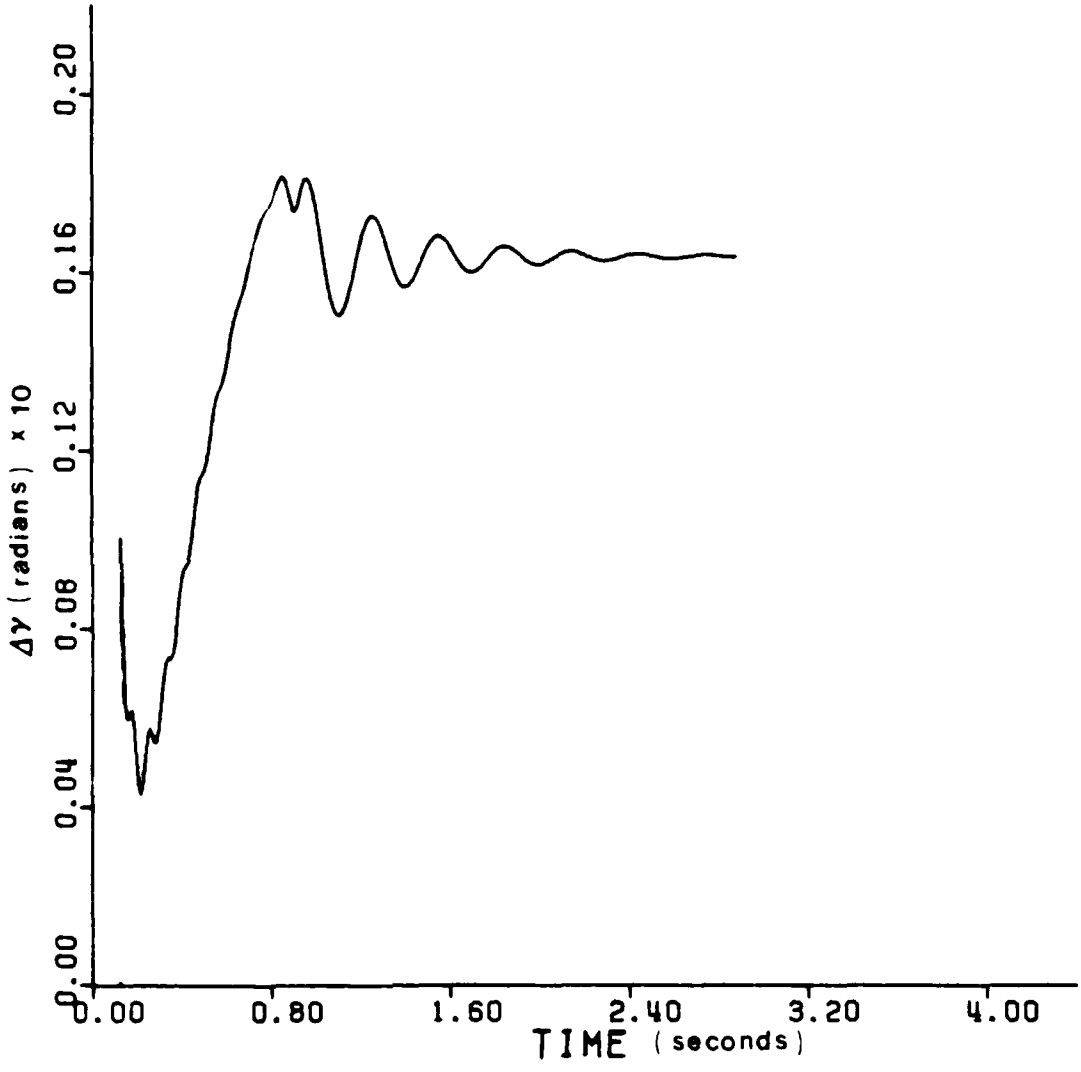

Fig. 22 Flight path deviation, , for non-tip-off launch - ω_{Ln} = 30 Hz.

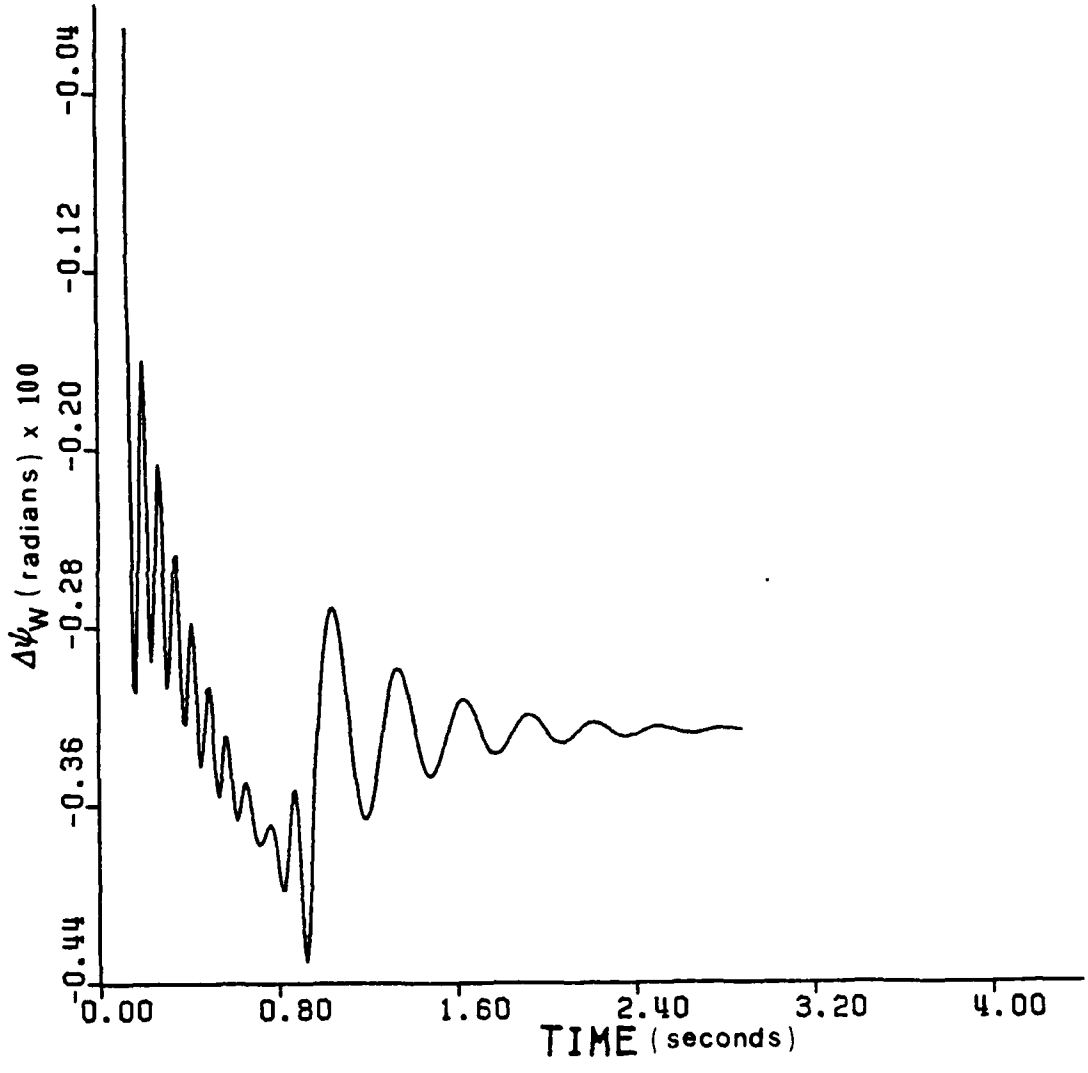

Fig. 23 Flight path angle deviation, $\Delta\psi_w$, for non-tip-off launch — ω_{Ln} = 30 Hz.

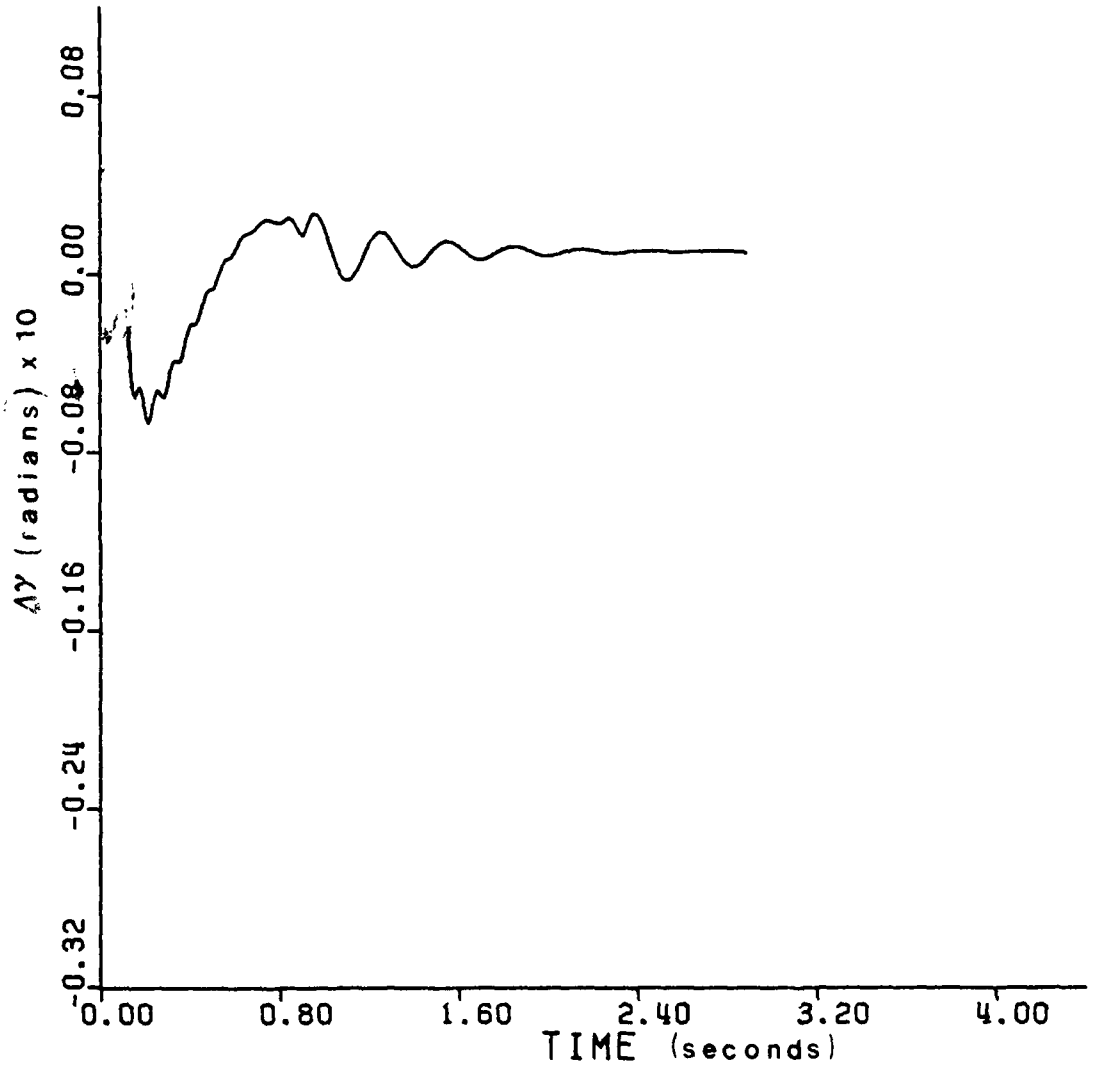

Fig. 24 Flight path angle deviation, $\Delta\gamma$, for non-tip-off launch – ω_{Ln} = 3 Hz.

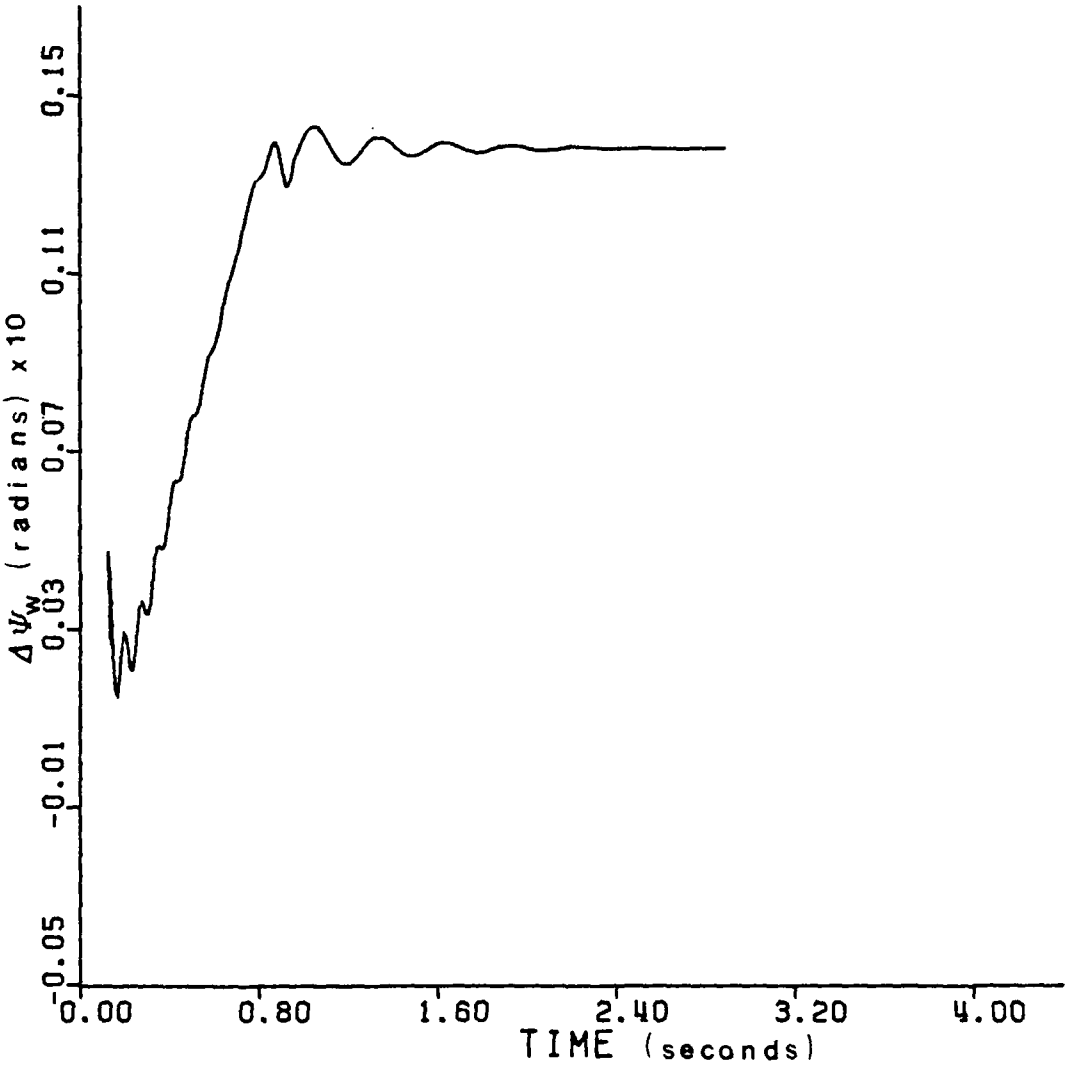

Fig. 25 Flight path angle deviation, $\Delta\psi_w$, for non-tip-off launch — ω_{Ln} = 5 Hz.

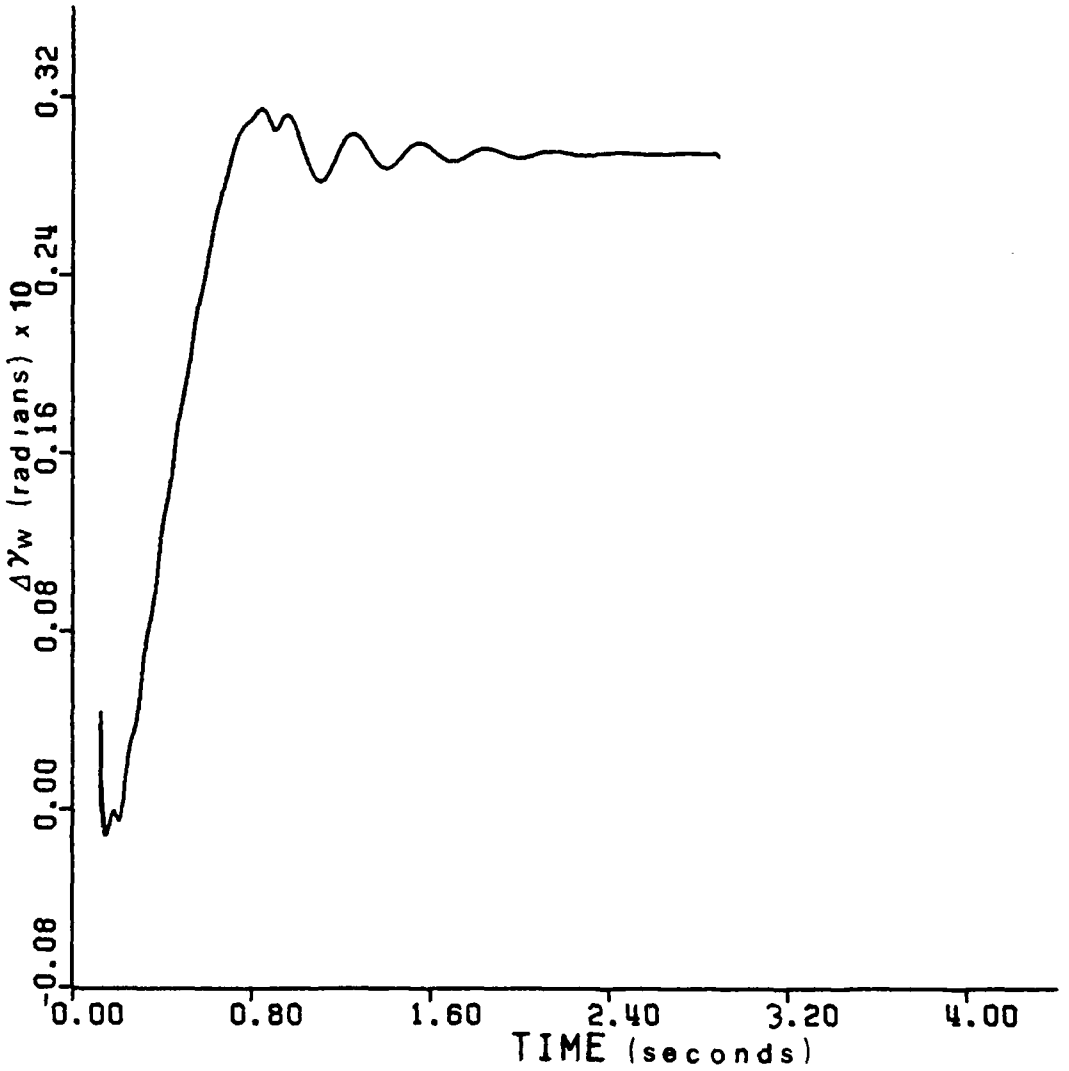

Fig. 26 Flight path angle deviation, $\Delta\gamma$, for non-tip-off launch — ω_{Ln} = 10 Hz.

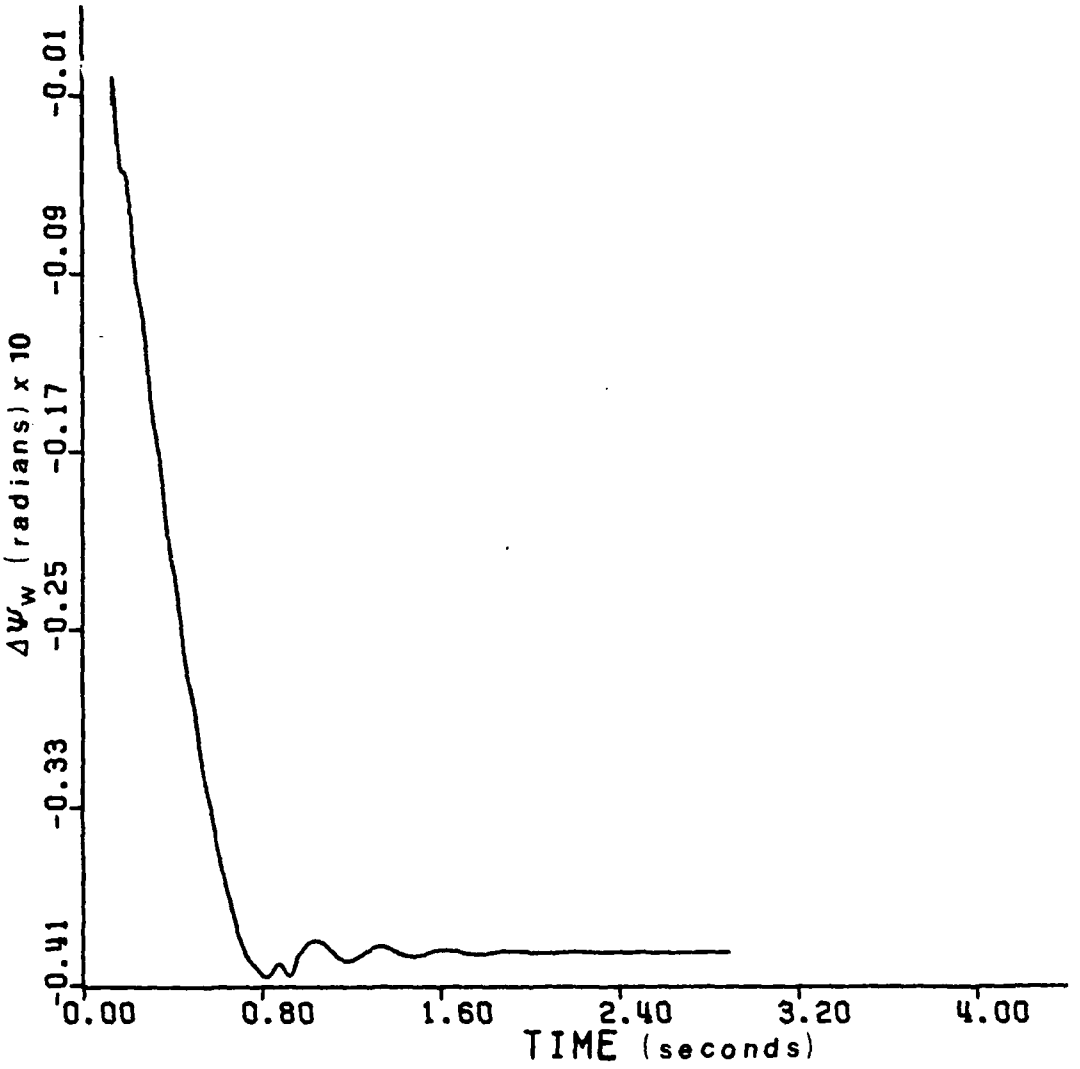

Fig. 27 Flight path angle deviation, $\Delta\psi_w$, for non-tip-off launch – ω_{Ln} = 10 Hz.

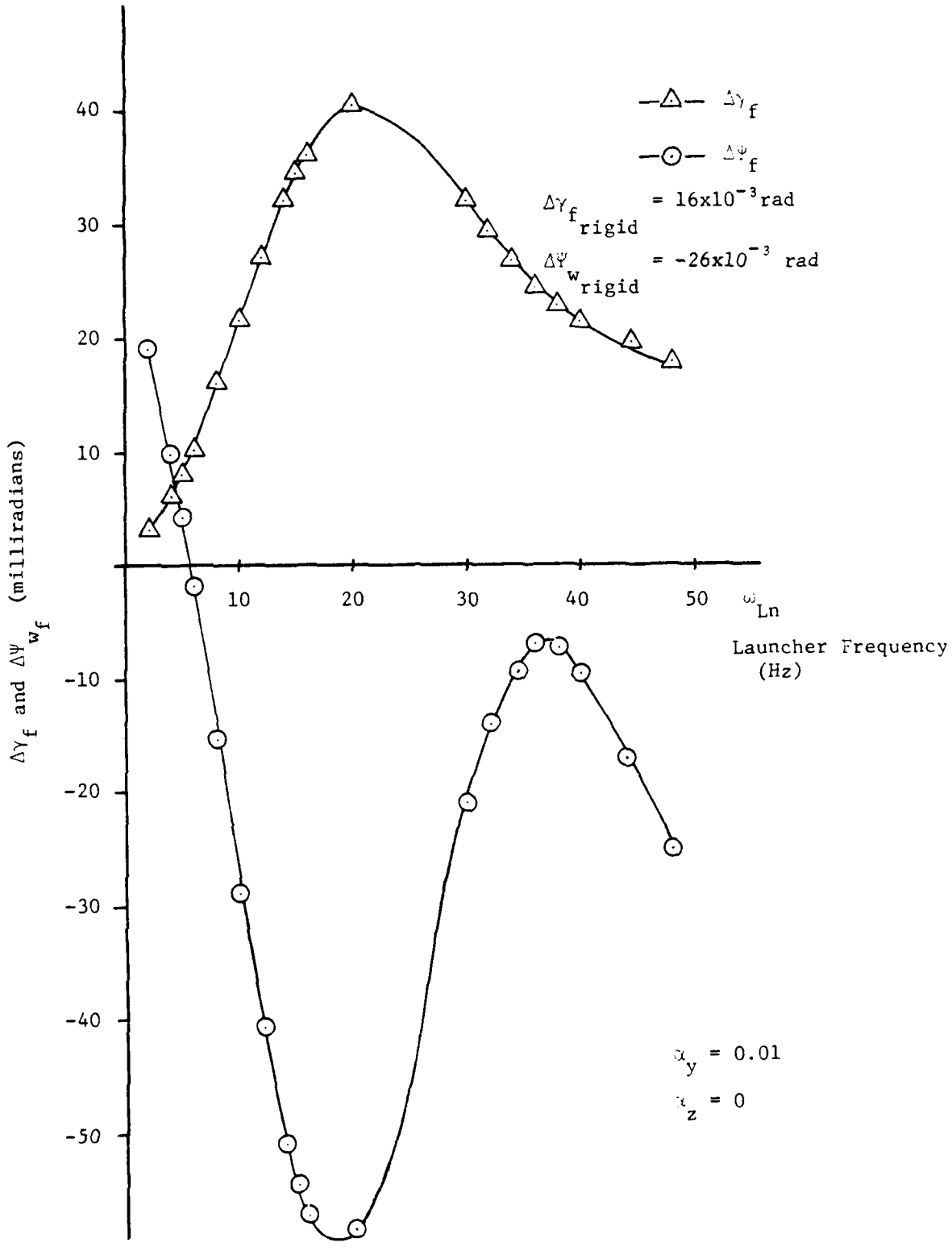

Fig. 28 Nonlinear frequency responses, $\Delta\gamma_f$ and $\Delta\Psi_f$, for tip-off launcher.

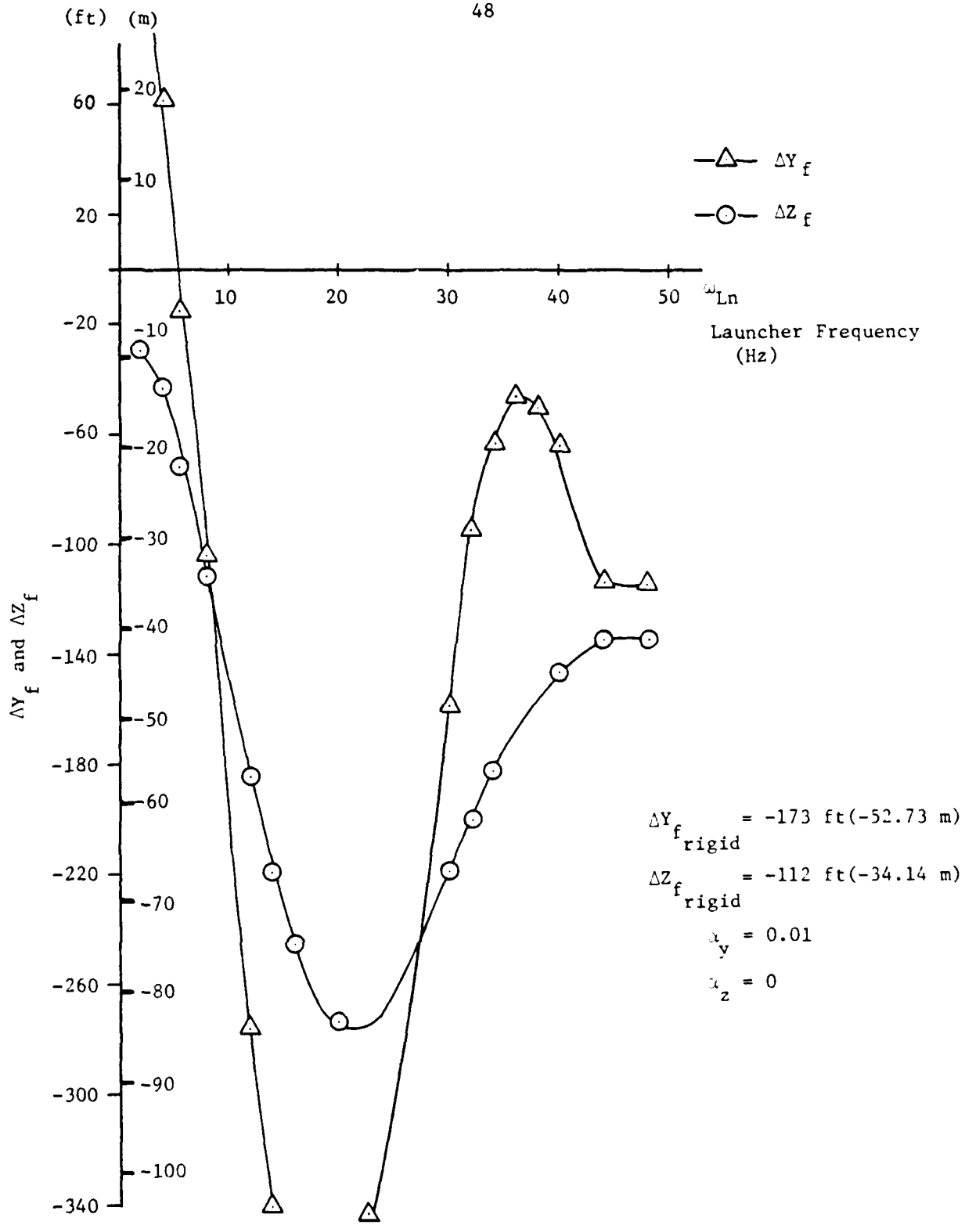

Fig. 29 Nonlinear frequency responses, ΔY_f and ΔZ_f, for tip-off launcher.

"Good" and "bad" case results analogous to those previously given for the non-tip-off launcher are presented in Figs. 30 through 31. "Good" high-frequency results for $\Delta\gamma$ and $\Delta\psi_w$ are shown in Figs. 30 and 35, respectively. "Bad" case high-frequency results follow in Figs. 32 and 33. "Good" low-frequency time histories of $\Delta\gamma$ and $\Delta\psi_w$ are presented in Figs. 34 and 35, respectively. Corresponding "bad" case results follow in Figs. 36 and 37. From these results it is apparent that the launcher can significantly decrease or increase dispersion.

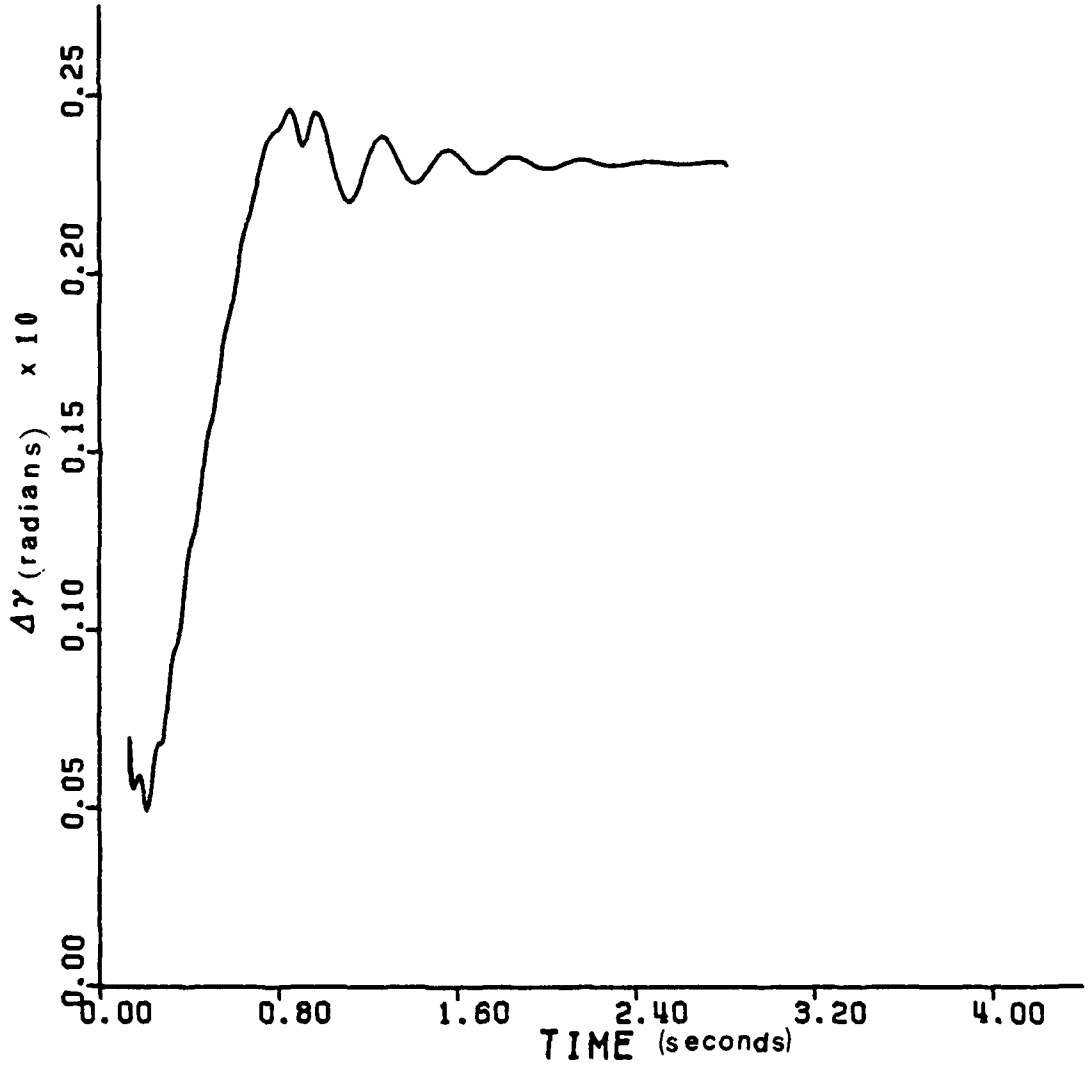

Fig. 30 Flight path angle deviation, $\Delta\gamma$, for tip-off launch $-\omega_{Ln} = 38$ Hz.

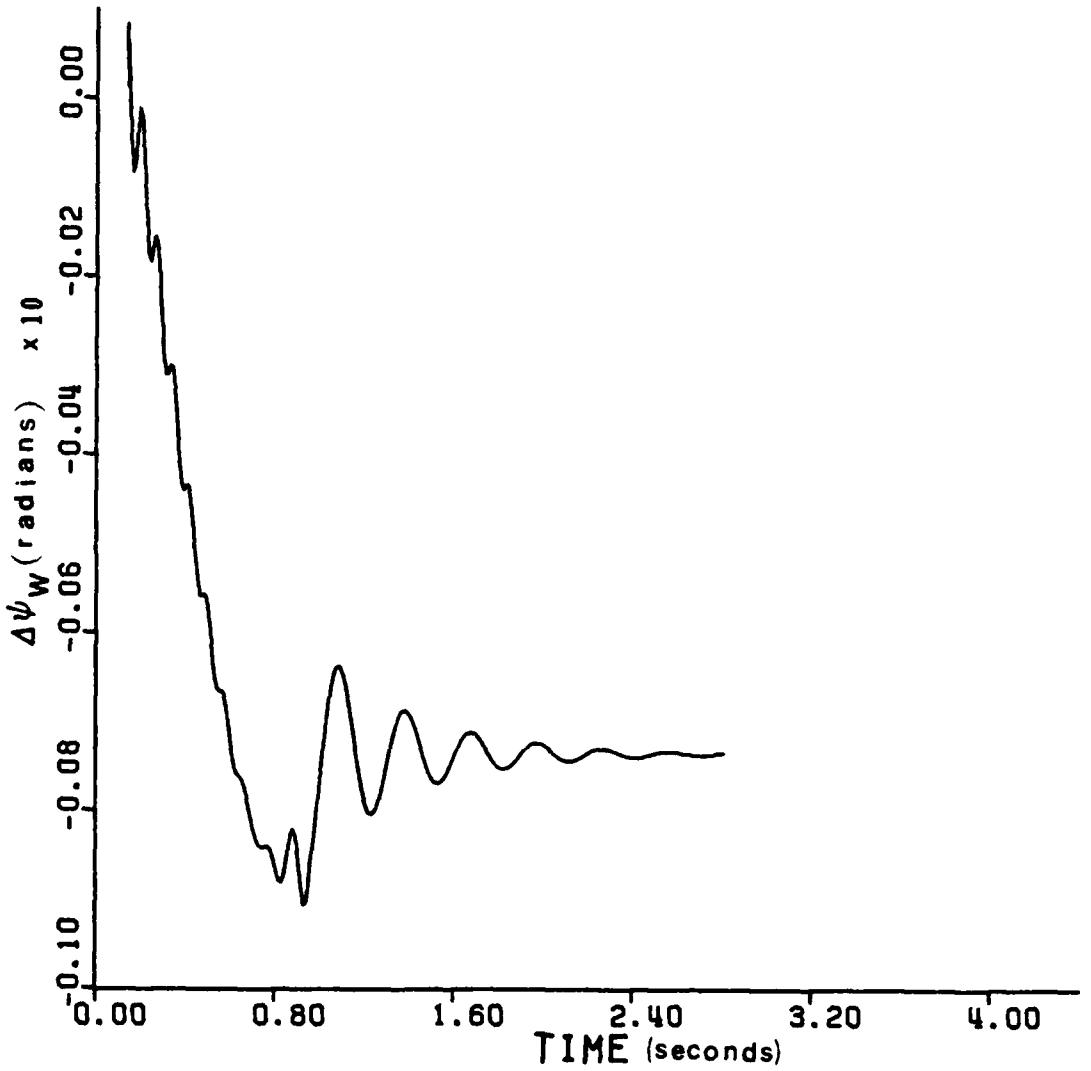

Fig. 31 Flight path angle deviation, $\Delta\psi_w$, for tip-off launch $-\omega_{Ln} = 38$ Hz.

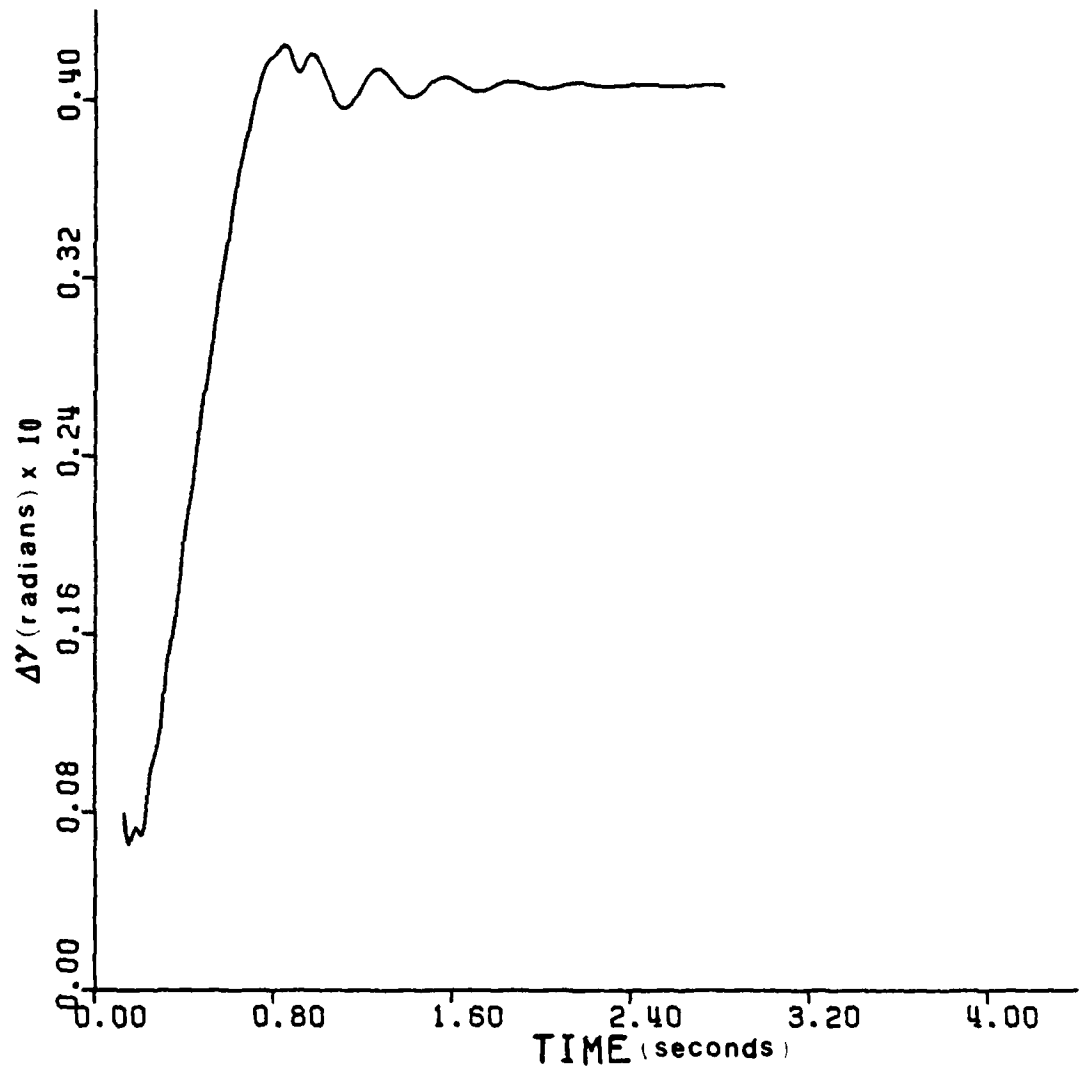

Fig. 32 Flight path deviation, $\Delta\gamma$, for tip-off launch $-\omega_{Ln} = 20$ Hz.

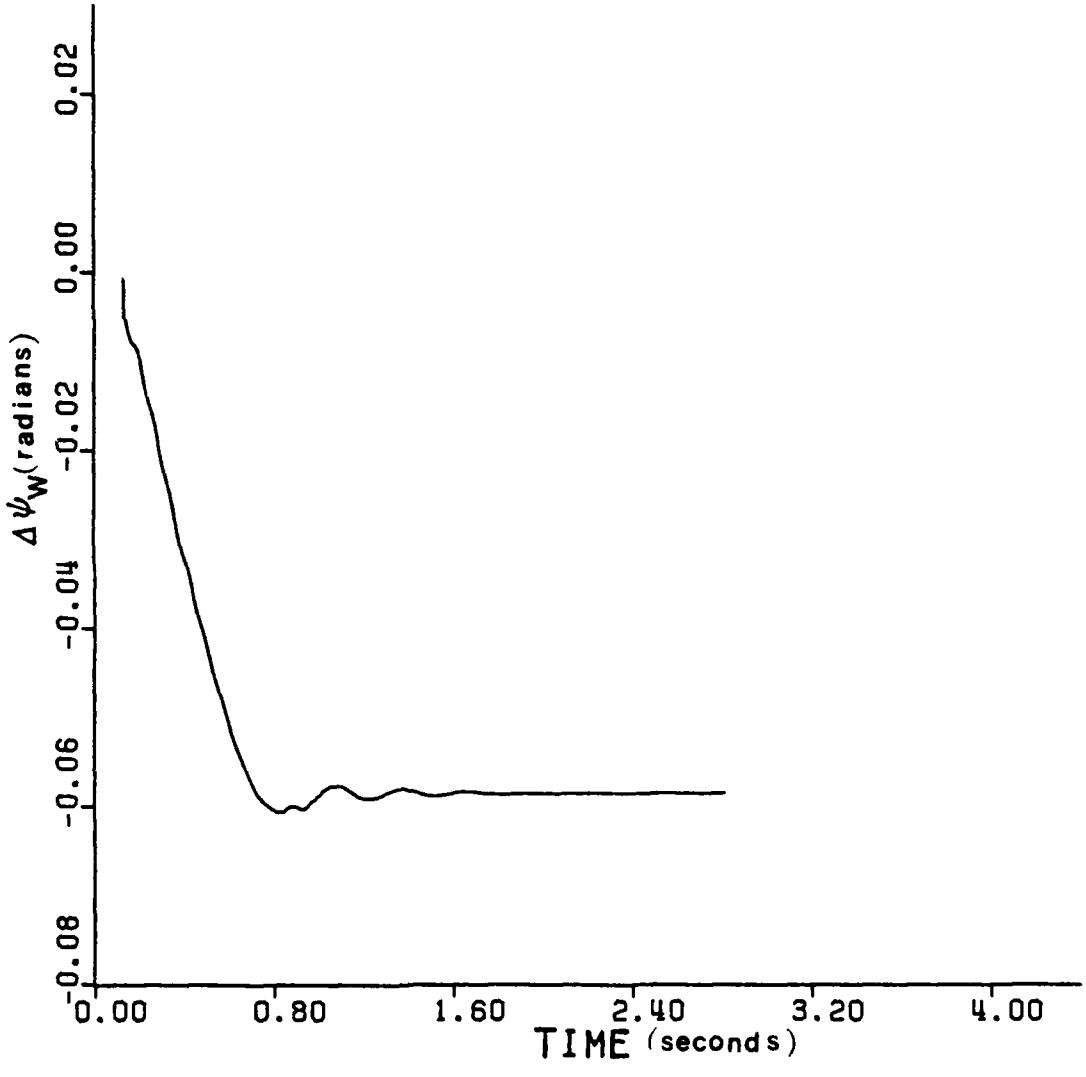

Fig. 33 Flight path deviation, $\Delta\psi_w$, for tip-off launch — ω_{Ln} = 20 Hz.

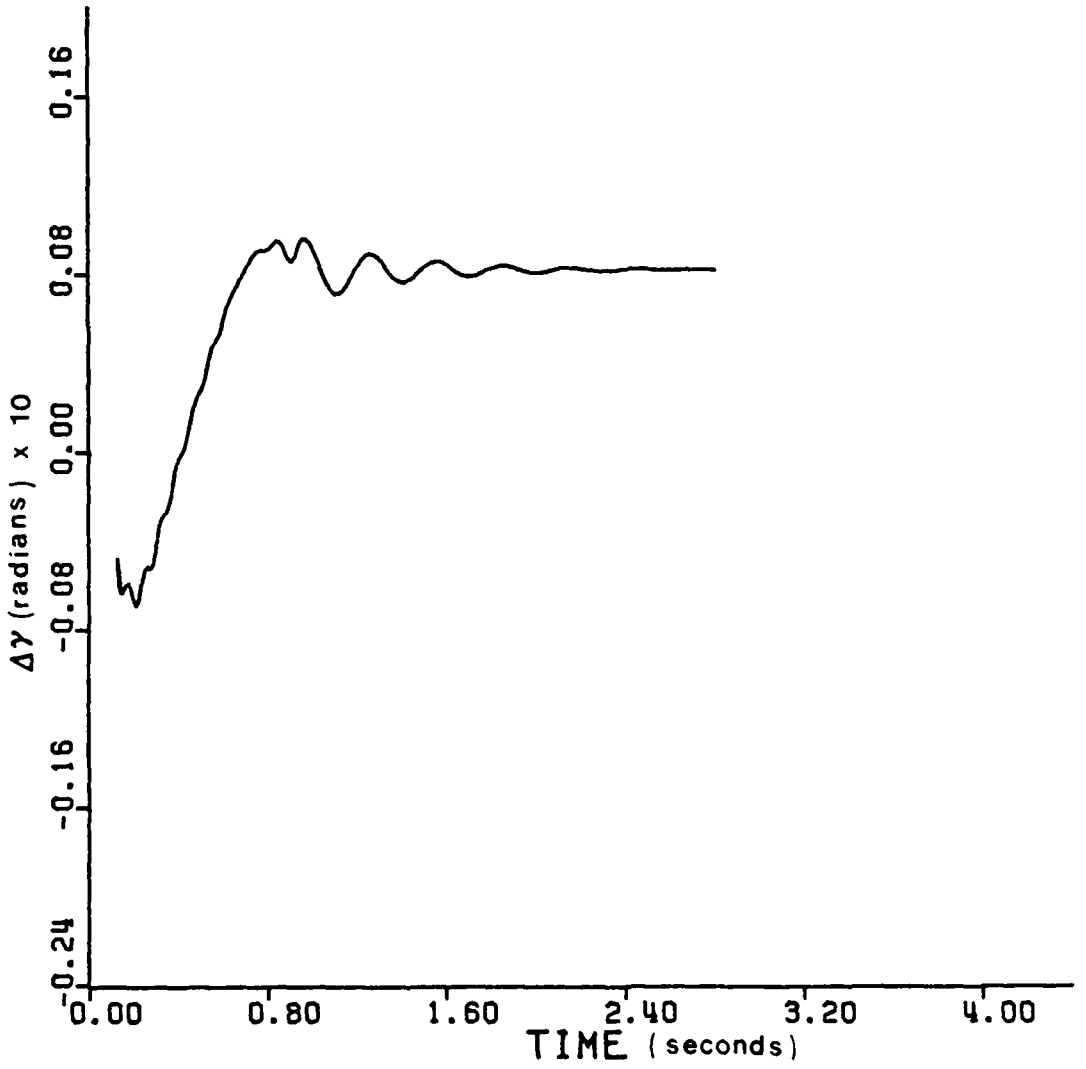

Fig. 34 Flight path angle deviation, $\Delta\gamma$, for tip-off launch — ω_{Ln} = 5 Hz.

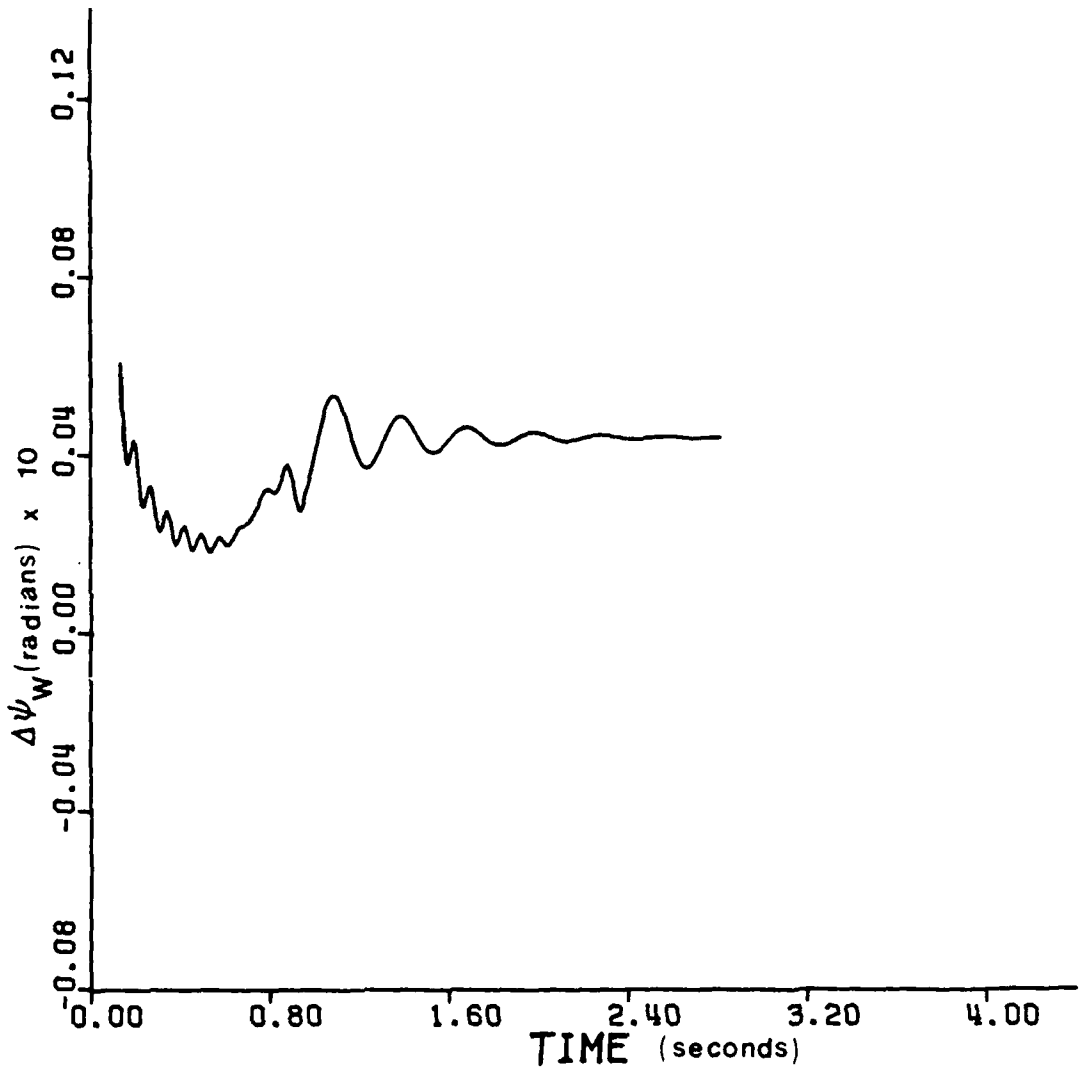

Fig. 35 Flight path angle deviation, $\Delta\psi_w$, for tip-off launch — ω_{Ln} = 5 Hz.

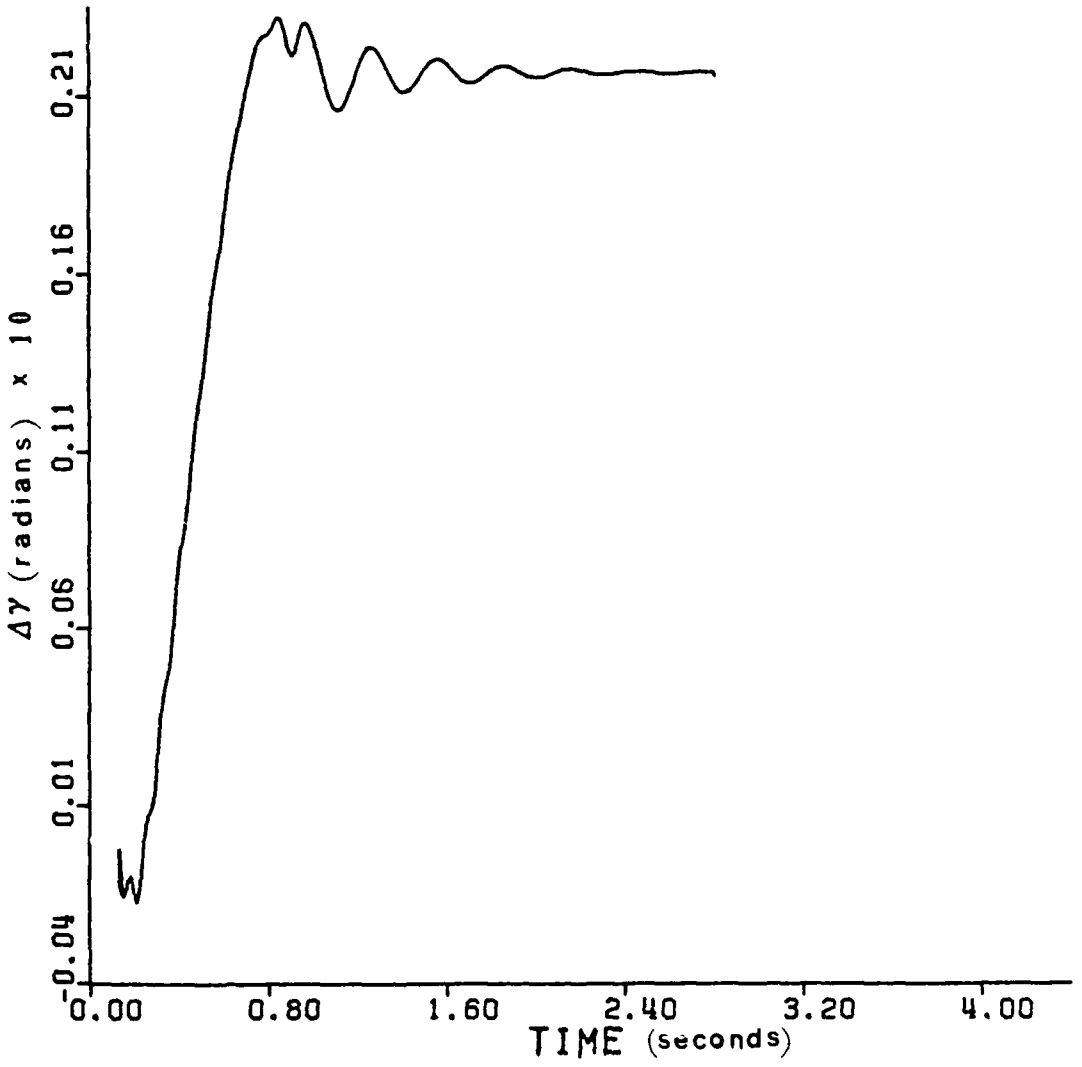

Fig. 36 Flight path angle deviation, $\Delta\gamma$, for tip-off launch — ω_{Ln} = 10 Hz.

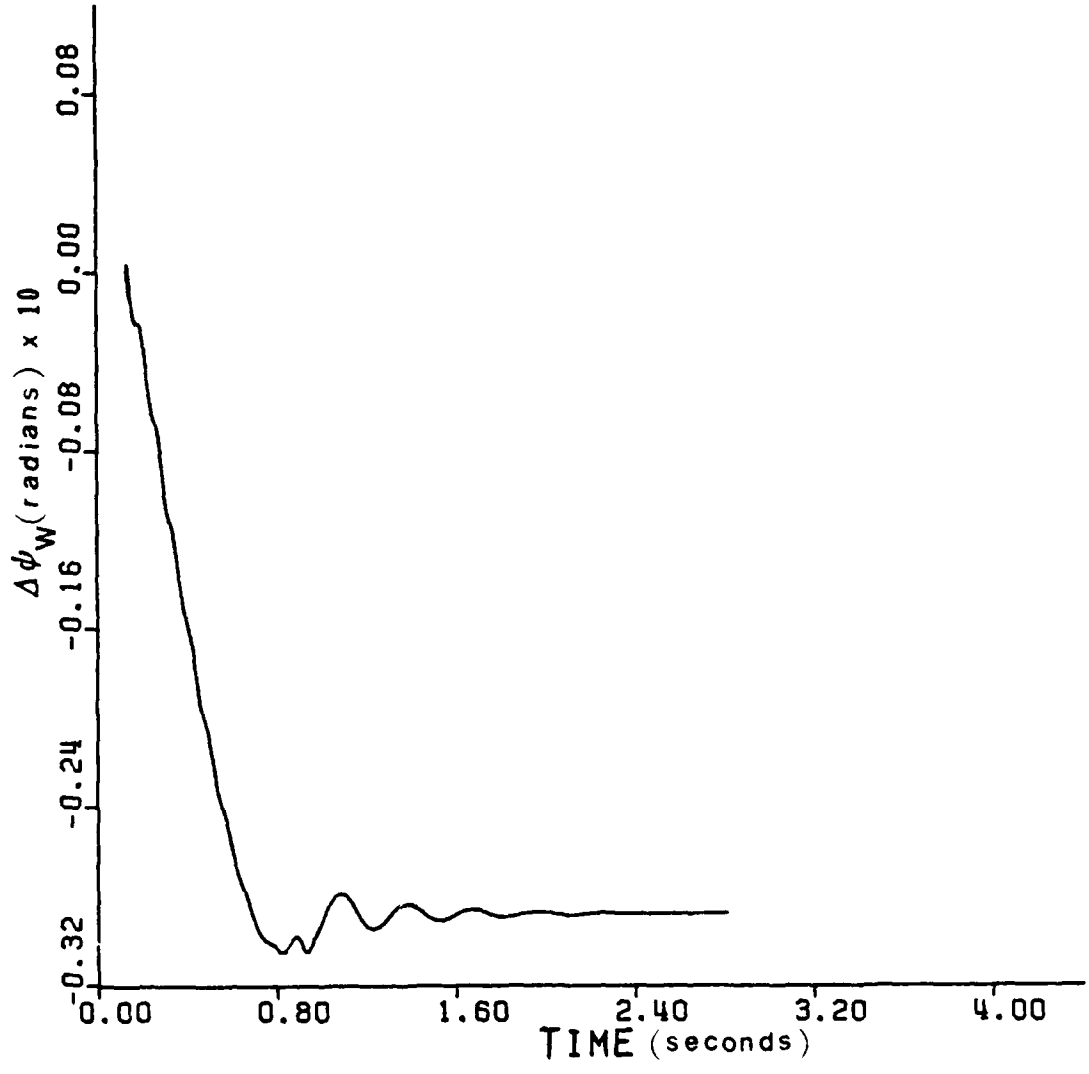

Fig. 37 Flight path angle deviation, $\Delta\psi_w$, for tip-off launch — ω_{Ln} = 10 Hz.

small at EOG. Hence, control in this frequency range is primarily "aim-change" control. At the higher frequency value of 30 Hz, the control must be achieved by imparting angular rates.

At this point, it is emphasized that if all the launcher rotation and/or angular velocity due to rocket imperfections are in the proper directions, benefit is gained from launcher motion. However, if some are in the incorrect directions, the launcher motion may be detrimental. Whether or not the launcher motion is detrimental depends upon the signs and magnitudes of the launcher motion variables at EOG.

The choice of launcher parameters which will result in launcher motion that is beneficial is not obvious. Some of the most critical parameters are the natural frequencies of the unloaded launcher. In the next section, a method is described which can be used to determine launcher natural frequencies that result in positive passive control.

SECTION 5. CONCLUSIONS

The interim character of the report makes it inappropriate to state any final conclusions. One conclusion which can be safely drawn, however, is that theoretically launcher/rocket systems can act as passive controllers which reduce dispersion by fifty percent or more from the "rigid launcher" value. The extent to which such control can be achieved in practice depends on several factors. First, the natural frequencies of launchers are usually fairly low. This is sometimes due to the massiveness of the structure of the launcher and sometimes due to the fact that it is fairly flexible (e.g., a pylon on a helicopter). The results presented in this report are evidence that launchers with relatively low natural frequencies can provide significant passive control, if a second factor, that of "massiveness," does not nulify the responsiveness of the launcher. If the launcher is much more massive than the rocket, the small forces and moments due to rocket imperfections will not produce any significant motion. This was illustrated in Section 3. Without launcher motion, there can be no passive control.

It has been shown that interaction of launchers and imperfect rockets may be favorable or unfavorable. Hence, another conclusion which is clearly valid is that the only way to predict the accuracy of a launcher/rocket system is to simulate the entire system from ignition of the rocket's motor until the effects of all errors modeled are apparent. Such simulation results would be used in designing launchers which provide passive control to the extent possible within physical constraints.

REFERENCES

1. Davis, L., Jr., Fallin, J. W., Jr., and Blitzer, L., Exterior Ballistics of Rockets, D. Van Nostrand Company, Inc., New Jersey, 1958, p. 8.

2. McCorkle, W. C., "Recent Developments in High Accuracy Free Rocket Weapons Systems (U)," Carde Report 9AXP/8, Redstone Scientific Information Center, Redstone Arsenal, Ala., April 1959.

3. Anonymous, Engineering Design Handbook - Design of Aerodynamically Stabilized Free Rockets, Headquarters, U.S. Army Material Command, Washington, D.C., July 1968.

4. James, R. F., "Free Rocket Technology Soft Shoe Launch Technique, Simulation Math Model," Technical Report RD-76-30, U.S. Army Missile Command, Redstone Arsenal, Alabama, May 1976.

5. Christensen, Dean E., "Multiple Rocket Launcher Characteristics and Simulation Technique," Technical Report RL-76-11, U.S. Army Missile Command, Redstone Arsenal, Alabama, February 1976.

6. Korovkin, A. S., "Spacecraft Control Systems," NASA TT F-774, National Aeronautics and Space Administration, Washington, D.C., May 1973, pp. 10-14.

7. Etkin, B., Dynamics of Atmospheric Flight, John Wiley & Sons, Inc., New York, 1972, Chapters 6-9.

8. Cochran, John E., Jr., "Investigation of Factors which Contribute to Mallaunch of Free Rockets," Final Report on Grant DAHC04-75-0034, Auburn University Engineering Experiment Station, Auburn University, Auburn, Alabama, January 1976.

9. Cochran, John E., Jr., "Rocket/Launcher Dynamics and Simulation," Final Report under D.O. No. 0921 for Battelle Columbus Laboratories, Durham Operations, Research Triangle Park, North Carolina, February 1979.

10. Coberly, Robert H., "Design Manual for Launchers (U), Vol. I," Report No. 33-63, Rock Island Arsenal Research & Engineering Division Development, Engineering Branch, Rock Island Arsenal, Rock Island, Illinois, December 1963.

11. Cunningham, W. J., Introduction to Nonlinear Analysis, McGraw-Hill Book Company, Inc., New York, 1958, pp. 253-257.

APPENDIX A

SIMPLE SIX-DEGREE-OF-FREEDOM FREE-FLIGHT MODEL

Purpose and Physical Description

The purpose of this model, in the context of this report, is to provide a means for determining, qualitatively, the effects of thrust misalignment, dynamic imbalance and launch conditions (angular velocity about the rocket's center of mass and linear velocity components of the rocket's center of mass at EOG) on the motion of a free-flight rocket which is also acted upon by atmospheric forces and moments and the intended thrust.

The physical model of the rocket is a "simple" one in that the following assumptions are made:

1. The rocket is rigid with constant mass and moments of inertia.
2. The thrust is either a nonzero constant value, or zero (after burnout).
3. The aerodynamic coefficients are constant with respect to Mach number.

Although the above assumptions are not necessary (indeed, they are not incorporated in the more general launcher/rocket system model described in Appendix C) the motion of the physical model based on them is mathematically modeled very easily and solutions to the equations can be obtained very rapidly via numerical integration.

Mathematical Description

The mathematical description, or mathematical model, consists of equations for the translation and rotation of a dynamically unbalanced

geometrically symmetric, rigid body which is moving under the influence of eccentric thrust, aerodynamic forces and moments, and the force due to gravity (flat earth assumed). Motion of the rocket is referred to an earth-fixed dextral, cartesian reference frame $Ox_E y_E z_E$ (see Fig. A.1). The coordinates of the center of mass C of the rocket are x_E, y_E and z_E. The reference frame Cxyz is fixed in the rocket with its x-axis collinear with the axis of geometric symmetry of the rocket. The velocity of C and the angular velocity of the Cxyz frame are expressed in the forms,

$$\underline{V} = u\hat{\underline{i}} + v\hat{\underline{j}} + w\hat{\underline{k}} \tag{A-1}$$

and

$$\underline{\omega} = p\hat{\underline{i}} + q\hat{\underline{j}} + r\hat{\underline{k}} \ , \tag{A-2}$$

respectively, where the unit vector triad $(\hat{i},\hat{j},\hat{k})$ is fixed to the Cxyz frame. The orientation of the Cxyz frame is defined by using the Euler angles ψ, θ and ϕ in the usual "flight dynamics" 3-2-1 sequence.

Required kinematical equations for translation and rotation are

$$\begin{bmatrix} \dot{x}_E \\ \dot{y}_E \\ \dot{z}_E \end{bmatrix} = \underline{\underline{C}}^T \begin{bmatrix} u \\ v \\ w \end{bmatrix} \ , \tag{A-3}$$

where[†]

$$\underline{\underline{C}} = \begin{bmatrix} 1 & 0 & 0 \\ 0 & c\phi & s\phi \\ 0 & -s\phi & c\phi \end{bmatrix} \begin{bmatrix} c\theta & 0 & -s\theta \\ 0 & 1 & 0 \\ s\theta & 0 & c\theta \end{bmatrix} \begin{bmatrix} c\psi & s\psi & 0 \\ s\psi & c\psi & 0 \\ 0 & 0 & 1 \end{bmatrix} \tag{A-4}$$

[†]For compactness, the definition c( ) = cos( ) and s( ) = sin( ) are used.

and

$$\begin{bmatrix} \dot{\phi} \\ \dot{\theta} \\ \dot{\psi} \end{bmatrix} = \begin{bmatrix} 1 & \tan\theta s\phi & \tan\theta c\phi \\ 0 & c\phi & -s\phi \\ 0 & s\phi/c\theta & c\phi/c\theta \end{bmatrix} \begin{bmatrix} p \\ q \\ r \end{bmatrix}, \tag{A-5}$$

respectively.

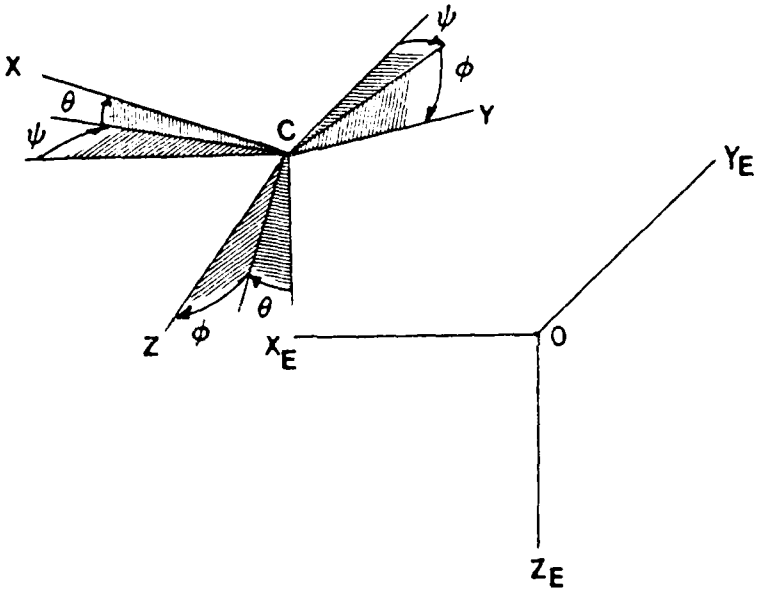

Fig. A.1 Coordinate frames and Euler angles.

The usual notation for body-fixed components of aerodynamic force is adopted to write the kinetic equations for translation in the forms,

$$m[\dot{u} + qw - rv] = X + F_T - mg \sin\theta, \tag{A-6a}$$

$$m[\dot{v} + ru - pw] = Y + F_T a_z + mg \cos\theta \cos\phi \tag{A-6b}$$

and

$$m[\dot{w} + pv - qu] = Z - F_T a_y + mg \cos\theta \cos\phi, \tag{A-6c}$$

where m is the rocket's mass, X, Y and Z are the aerodynamic force components, F_T is the thrust magnitude, α_y and α_z are thrust misalignment angles (see Fig. C.3), and g is the magnitude of the gravitational acceleration. Furthermore, the x-, y- and z-components of the aerodynamic moment about C are denoted by L, M and N, respectively; the rocket's centroidal inertia matrix is denoted by $\underline{\underline{I}}$; and $\tilde{\underline{\omega}}$ is defined as

$$\tilde{\underline{\omega}} = \begin{bmatrix} 0 & -r & q \\ r & 0 & -p \\ -q & p & 0 \end{bmatrix} ; \tag{A-7}$$

so that the kinetic equations for rotation can be written in the form,

$$\underline{\underline{I}} \begin{bmatrix} \dot{p} \\ \dot{q} \\ \dot{r} \end{bmatrix} = - \tilde{\underline{\omega}}\, \underline{\underline{I}} \begin{bmatrix} p \\ q \\ r \end{bmatrix} + \begin{bmatrix} L \\ M \\ N \end{bmatrix} + \begin{bmatrix} 0 \\ -\ell_C \alpha_y F_T \\ -\ell_C \alpha_z F_T \end{bmatrix} , \tag{A-8}$$

where ℓ_C is the distance fromC to the point of intersection of the thrust with the x-axis.

The aerodynamic force components are conventionally expressed in terms of the coefficients C_x, C_y and C_z; i.e.,

$$X = 1/2\rho SV^2 C_x, \tag{A-9a}$$

$$Y = 1/2\rho SV^2 C_y \tag{A-9b}$$

and

$$Z = 1/2\rho SV^2 C_z , \tag{A-9c}$$

where ρ is the atmospheric density, S is the reference area used in obtaining C_x, C_y and C_z and $V^2 = \underline{V}\cdot\underline{V}$ (no wind assumed). In this model,

$$C_x = \text{constant} \quad , \tag{A-10a}$$

$$C_y = C_{y_\beta}\beta + r(d/2V) \tag{A-10b}$$

and

$$C_z = -C_{N_\alpha}\alpha, \tag{A-10c}$$

where $\beta = \sin^{-1}(v/V)$; d is the characteristic distance associated with the aerodynamic coefficients; and $\alpha = \tan^{-1}(w/u)$. The stability derivatives, C_{y_β}, C_{y_r} and C_{N_α} are constants in this model.

The aerodynamic moment components can also be expressed in coefficient forms; i.e.,

$$L = 1/2\rho SV^2 dC_\ell \tag{A-11a}$$

$$M = 1/2\rho SV^2 dC_m \tag{A-11b}$$

and

$$N = 1/2\rho SV^2 dC_n \quad , \tag{A-11c}$$

where (in this model),

$$C_\ell = C_{\ell_p} p\ (d/2V) \tag{A-12a}$$

$$C_m = C_{m_\alpha}\alpha + C_{m_q} q\ (d/2V) \tag{A-12b}$$

and

$$C_n = C_{n_\beta}\beta + C_{n_r} r\ (d/2V) \tag{A-12c}$$

with C_{ℓ_p}, C_{m_α}, C_{m_q}, C_{n_β} and C_{n_r} all constant.

Flight Path Deviations

Deviations of a free-flight rocket from its intended flight path after burnout, but before impact, can be defined in terms of the location of the rocket center of mass a given time and its velocity at the same

time. Let the subscript n denote the value of a variable which is used in defining the nominal trajectory and let a variable without such a subscript be a "perturbed" variable. Then, at time t, the position deviations are

$$\Delta x_E = x_E(t) - x_{E_n}(t) , \tag{A-13a}$$

$$\Delta y_E = y_E(t) - y_{E_n}(t) \tag{A-13b}$$

and

$$\Delta z_E = z_E(t) - z_{e_n}(t) . \tag{A13c}$$

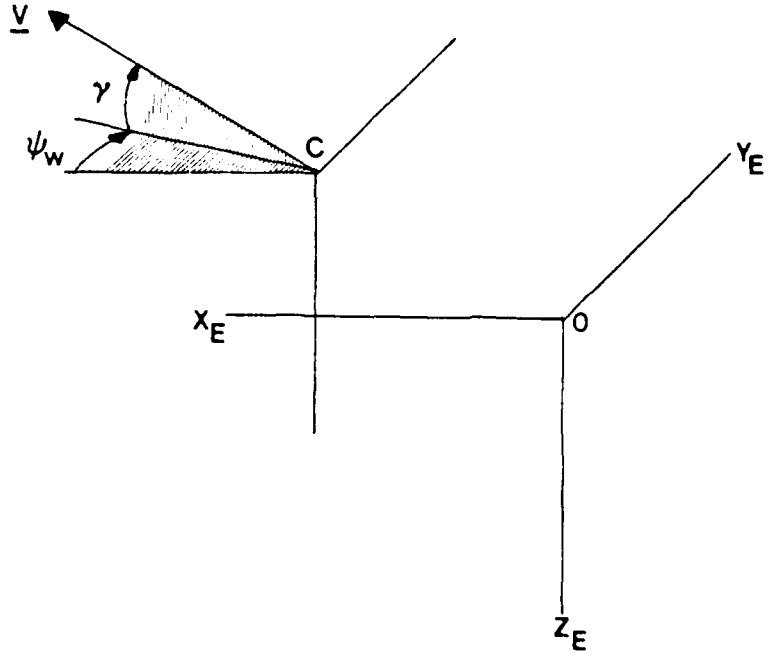

Fig. A.2 Flight path angles.

The velocity derivations are best defined by using the flight path angles γ and ψ_w illustrated in Fig. A.2. From geometry, one may write $\underline{V}$ in terms of earth-fixed unit vectors $\underline{i}_E$, $\underline{j}_E$ and $\underline{k}_E$ as follows:

$$\underline{V} = V\cos\gamma\cos\psi_w \, \hat{\underline{i}}_E + V\cos\gamma\sin\psi_w \, \hat{\underline{j}}_E - V\sin\gamma \, \hat{\underline{k}}_E \ , \tag{A-14}$$

so that (see Eq. A-4),

$$\tan\psi_w = \dot{y}_E/\dot{x}_E \ . \tag{A-15a}$$

and

$$\sin\gamma = - \dot{z}_E/V \ . \tag{A-15b}$$

The velocity error can therefore be defined in terms of the deviations,

$$\Delta V = V(t) - V_n(t) \tag{A-16a}$$

$$\Delta\gamma = \gamma(t) - \gamma_n(t) \tag{A-16b}$$

and

$$\Delta\psi_w = \psi_w(t) - \psi_{w_n}(t) \ . \tag{A-16c}$$

APPENDIX B

SIMPLE LAUNCHER/ROCKET SYSTEM

MODEL

Model Description

The simplest physical model of a launcher/rocket system which can be used to study passive control characteristics of a launcher is shown in Fig. B.1. It consists of a launcher model which is a single rigid body with one degree of freedom (rotation about the fixed point 0) and a rigid body (constant mass and moment of inertia) rocket model with one, or two, degrees of freedom with respect to the launcher. The relative degrees of freedom of the rocket are translation and, during tip-off, rotation in the $x_L y_L$-plane. Frictionless (except for launcher damping) motion in a horizontal plane above a flat earth is assumed. Motion of the launcher is restrained by a torsional spring and torsional viscous damper.

The $0x_E y_E$ coordinate frame shown in Fig. B.1 is nonrotating, while the $0x_L y_L$ frame rotates with the launcher. If there is no tip-off, the rocket is allowed to move only in the x_L-direction. Also shown in Fig. B.1 are the following: The thrust, $\underline{F}_T$; the small thrust misalignment angle, α_z; the x_L-coordinate of the center of mass, C, of the rocket, x_C; the distance from the rocket center of mass to the point of application of thrust, ℓ_C; the launcher yaw angle, ψ_L; and the launcher-fixed unit vectors, $\hat{\underline{i}}_L$ and $\hat{\underline{j}}_L$.

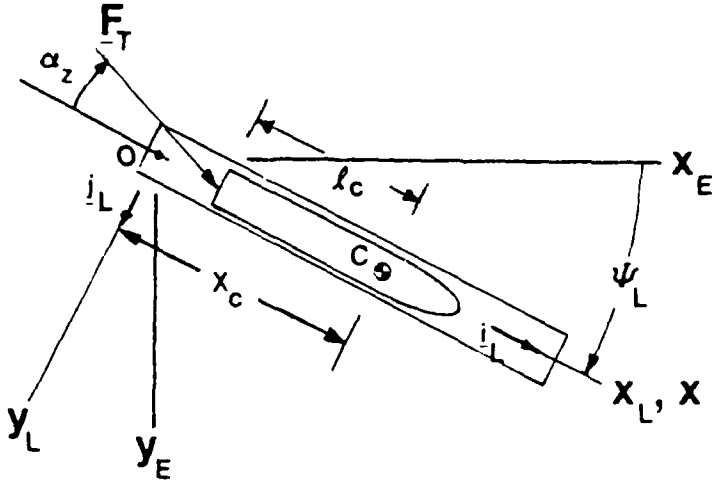

Fig. B.1 Simple launcher/rocket system model.

System Equations of Motion - Rocket on the Launcher

When there is no tip-off, translation of the rocket along the launcher is governed by the equation,

$$m\ddot{\underline{r}}_C = \underline{F} \ , \tag{B-1}$$

where m is the mass of the rocket, $\underline{r}_C = x_C \hat{\underline{i}}_L$ and $\underline{F}$ is the external force. The x_L-component of Eq. (B-1) is

$$m(\ddot{x}_C - \dot{\psi}_L^2 x_C) = F_T \text{ (if detent released)}. \tag{B-2}$$

Rotational motion of the system about 0 is governed by the equation,

$$\dot{\underline{H}}_0 = \underline{T}_0 \ , \tag{B-3}$$

where $\underline{H}_0$ is the system angular momentum and $\underline{T}_0$ is the torque, both about 0. Explicitly, when there is no tip-off,

$$\underline{H}_0 = (I_L + I_T + m\, x_C^2)\, \dot{\psi}_L \hat{\underline{k}}_L \ , \tag{B-4}$$

since $\underline{r}_C$ and $\dot{\underline{r}}_C$ are collinear. In Eq. (B-4), I_L is the moment of inertia of the launcher about 0 and I_T is the moment of inertia of the rocket about a transverse axis through C. The torque $\underline{T}_0$ is due to the launcher spring and damper and the thrust misalignment; hence,

$$\frac{d}{dt}\left[(I_L+I_T + mx_C^2)\dot{\Psi}_L\right] = \left[-K_L\Psi_L - C_L\dot{\Psi}_L + a_z(x_C-\ell_C)F_T\right] . \qquad (B-5)$$

In general, the rocket is constrained from translating along the launcher until the thrust has built up to a sufficiently high value. During this "detent phase," Eq. (B-5) holds with x_C constant.

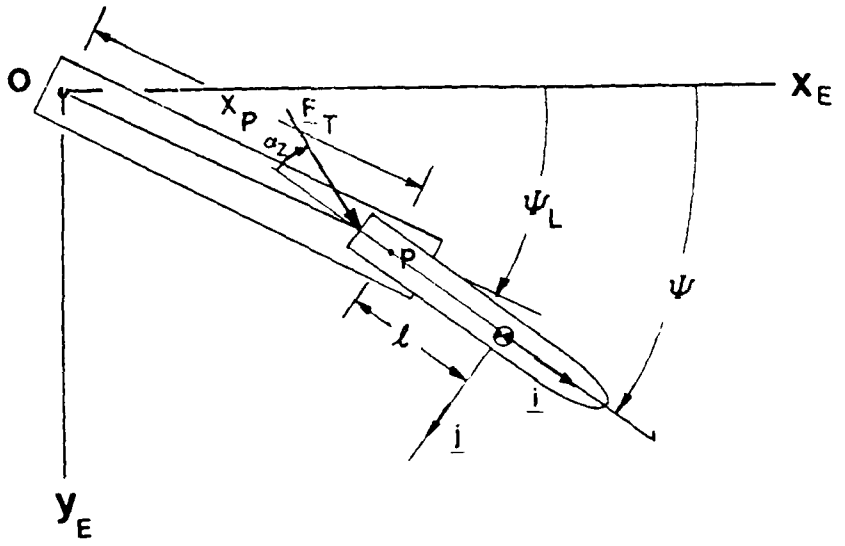

Fig. B.2 Tip-off geometry.

If tip-off of the rocket as it leaves the launcher is to be modeled, rotation of the rocket relative to the launcher must be allowed. In this case, during tip-off,

$$\underline{r}_C = x_P \underline{i}_L + \ell \underline{i} , \qquad (B-6)$$

where x_p is the x_L-coordinate of the point about which relative rotation occurs, ℓ is the distance from P to C and $\hat{i}$ is a unit vector along the longitudinal axis (x-axis) of the rocket. Let ψ denote the total yaw angle of the rocket (see Fig. B.2) and $\Delta\psi = \psi - \psi_L$ and assume that ψ_L and ψ are small angles. Then,

$$\ddot{\underline{r}}_C = a_{x_L}\hat{\underline{i}}_L + a_{y_L}\hat{\underline{j}}_L \ , \tag{B-7}$$

where

$$a_{x_L} = \ddot{x}_p - \dot{\psi}_L^2 x_p - \dot{\psi}^2 \ell - \Delta\psi\ddot{\psi}\ell \tag{B-8a}$$

and

$$a_{y_L} = \ddot{\psi}_L x_p + \ddot{\psi}\ell + 2\dot{\psi}_L \dot{x}_p - \dot{\psi}^2 \ell\Delta\psi \ . \tag{B-8b}$$

By equating components of $m\ddot{\underline{r}}_C$ to corresponding components of the force which acts on the rocket, the following two equations can be obtained:

$$m\, a_{x_L} = F_T \tag{B-9a}$$

and

$$m\, a_{y_L} = (\alpha_z + \Delta\psi)F_T - F_C \ , \tag{B-9b}$$

where F_C is the y_L-component (and the only component) of the constraint force which causes point P to remain on the x_L-axis.

The rotational motion of the rocket is governed by the equation,

$$I_T\ddot{\psi} = -F_C\ell - \ell_C F_T \alpha_z \ , \tag{B-10}$$

while the launcher equation of motion is

$$I_L\ddot{\psi}_L = F_C x_p - K_L\psi_L - C_L\dot{\psi}_L \ . \tag{B-11}$$

From Eq. (B-9),

$$F_C = - ma_{y_L} + (\alpha_z + \Delta\Psi)F_T \ . \tag{B-12}$$

Equation (B-12) can be used to eliminate F_C from Eqs. (B-10) and (B-11) and thereby obtain the results,

$$I_T\ddot{\Psi} = -m\ell a_{y_L} + [(\alpha_z + \Delta\Psi)\ell - \ell_C\alpha_z]F_T \tag{B-13}$$

and

$$I_L\ddot{\Psi}_L = -K_L\Psi_L - C_L\dot{\Psi}_L + x_p[-a_{y_L}m + (\alpha_z + \Delta\Psi)F_T] \ . \tag{B-14}$$

From Eqs. (B-13) and (B-14) it follows that

$$(I_T + \ell^2 m)\ddot{\Psi} + mx_p\ell\ddot{\Psi}_L = -2m\ell\dot{x}_p\dot{\Psi}_L + \ell^2 m\,\Delta\dot{\Psi}\dot{\Psi}_L + [(\alpha_z + \Delta\Psi)\ell - \ell_C\alpha_z]F_T \tag{B-15}$$

and

$$(I_L + mx_p^2)\ddot{\Psi}_L + mx_p\ell\ddot{\Psi} = -2mx_p\dot{x}_p\dot{\Psi}_L + mx_p\ell\dot{\Psi}_L^2\Delta\Psi - K_L\Psi_L - C_L\dot{\Psi}_L + (\alpha_z + \Delta\Psi)x_p F_T \ . \tag{B-16}$$

The required equations of motion are (B-9a), (B-15) and (B-16). Obviously, Eqs. (B-15) and (B-16) must be solved for $\ddot{\Psi}_L$ for use in Eqs. (B-8a) and (B-9a) to get $\ddot{x}_p$.

System Equations of Motion - Free Flight

For the purposes of this report, the motion of the launcher after the rocket leaves it is not of principal importance. Thus, only equations of motion for a very simple rocket model are given here for the free-flight phase. The rocket is assumed to move in a horizontal plane and to

rotate only in yaw. It is also assumed that burnout occurs very soon after the beginning of free flight so that the rocket's mass and transverse moment of inertia can be considered constant. Furthermore, the sideslip angle β (see Fig. B.3) is assumed to be small.

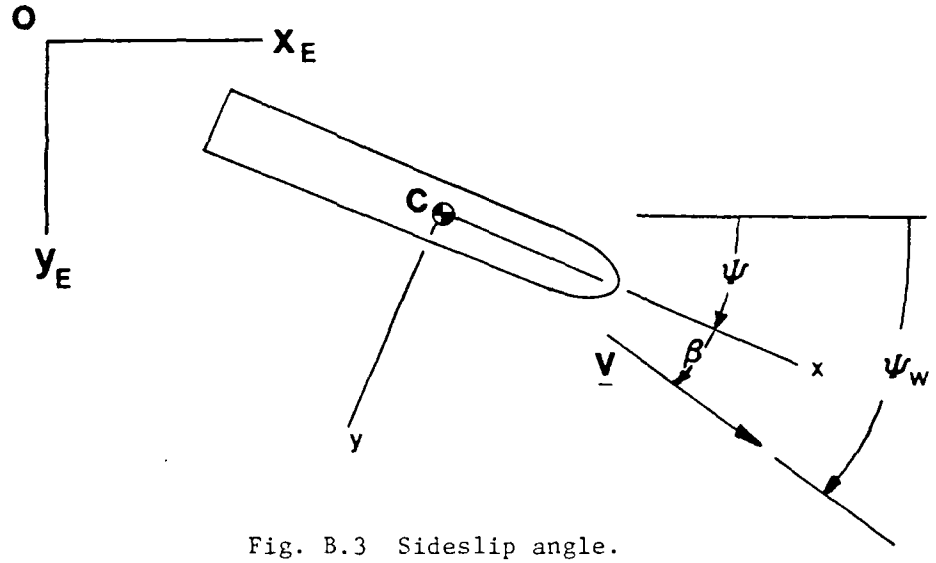

Fig. B.3 Sideslip angle.

The velocity of the rocket's center of mass C is

$$\underline{V} = u\hat{\underline{i}} + v\hat{\underline{j}} \ , \tag{B-17}$$

where $\hat{\underline{i}}$ and $\hat{\underline{j}}$ are body-fixed (with regard to rotation) unit vectors. The angular velocity component of the rocket about its z-axis is r and the x- and y-components of the aerodynamic force are X and Y, respectively.

The translational equations of motion of the rocket are

$$m(\dot{u} - vr) = X + F_T \tag{B-18a}$$

and

$$m(\dot{v} + ur) = Y + \alpha_z F_T . \tag{B-18b}$$

The rotational equation of motion is

$$\dot{r} = N/I_T - \alpha_z \ell_C F_T/I_T \ , \tag{B-19}$$

where N is the z-component of the aerodynamic yawing moment.

In addition to Eqs. (B18) and (B-19), the three kinematic equations are needed. These are, if Ψ is small,

$$\dot{x}_E = u, \tag{B-20a}$$

$$\dot{y}_E = v + \Psi u \tag{B-20b}$$

and

$$\dot{\Psi} = r \ . \tag{B-20c}$$

Both the sideslip angle and Ψ_w, the lateral flight path angle, are needed. The former to determine aerodynamic forces and moment and the latter to determine the angular derivation of the velocity vector of the rocket. Since it is defined by the equation, $\beta = \sin^{-1}(v/|\underline{V}|)$, $\beta \simeq v/u$ and

$$\dot{\beta} \simeq \dot{v}/u - \dot{u}v/u^2 \ . \tag{B-21}$$

Hence β can be used in place of v. It can be shown using Eqs. (B-18), the definition of β and Eq. (B-22) that, for $\beta^2 << 1$,

$$\dot{\beta} = - r - (X + F_T)\beta/(mu) + Y/(mu) + \alpha_z F_T/(mu) \ . \tag{B-22}$$

The angle Ψ_w is given by the equation,

$$\Psi_w = \Psi + \beta \ . \tag{B-23}$$

The aerodynamic force components are given by

$$X = 1/2 \rho S V^2 C_x \tag{B-24a}$$

and

$$Y = 1/2\ \rho S V^2 C_y\ , \tag{B-24b}$$

where ρ is the atmospheric density, S is the aerodynamic reference area and C_x and C_y are aerodynamic coefficients. In this model it is assumed that C_x is constant and that

$$C_y = C_{y_\beta}\beta + C_{y_r} r[d/(2V)] \tag{B-25}$$

where C_{y_β} and C_{y_r} are constant and d is the characteristic distance associated with the aerodynamic coefficients.

The aerodynamic yawing moment is

$$N = 1/2\ \rho S V^2 d\ C_n\ , \tag{B-26}$$

where the yawing moment coefficient C_n is assumed to be given by the equation,

$$C_n = C_{n_\beta}\beta + C_{n_r} r[d/(2V)]. \tag{B-27}$$

In this model, C_{n_β} and C_{n_r} are assumed to be constant even though in actuality they vary due to center of mass and center of pressure motion within the rocket.

Nondimensional Equations - Rocket on the Launcher

Because a solution to nondimensional equations represents a family of solutions to dimensional ones, nondimensional equations are desirable. If the nonlinear terms involving $\dot{\psi}_L$ and, in the tip-off equations, those involving products and squares of ψ_L, ψ, $\dot{\psi}_L$ and $\dot{\psi}$ are neglected, equations which do not contain α_z may be obtained by defining

$$\bar{\Psi}_L = \Psi_L/\alpha_z \tag{B-28a}$$

and

$$\bar{\Psi} = \Psi/\alpha_z \ . \tag{B-28b}$$

The nondimensional time,

$$\tau = t/t^* \ . \tag{B-29}$$

Here,

$$t^* = \sqrt{2mL/F_{T_{max}}} \ , \tag{B-30}$$

where $F_{T_{max}}$ is the maximum thrust magnitude and L is the guidance length. The independent variable, τ, may be introduced along with the dimensionless variables given in Table B.1 to obtain nondimensional equations. Table B.2 contains definitions of nondimensional parameters.

For the guidance phase,

$$\bar{I}(\tau)\bar{\Psi}_L'' + (c + \bar{x}\bar{u})\,\bar{\Psi}_L' + k\bar{\Psi}_L = (\bar{x} - \bar{\ell}_C)f(\tau) \ , \tag{B-31a}$$

$$\bar{u}' = 2f(\tau) \quad \text{(if detent released)} \tag{B-31b}$$

and

$$\bar{x}' = \bar{u} \ , \tag{B-31c}$$

where $\bar{I}(\tau) = \bar{I}_T + \bar{I}_L + \bar{x}^2/2$.

for the tip-off phase, if present, the nondimensional equations are

$$(\bar{I}_T + \bar{\ell}^2/2)\bar{\Psi}'' + (\bar{x}_P\bar{\ell}/2)\bar{\Psi}_L'' = -\bar{x}_P'\bar{\ell}\bar{\Psi}_L'$$
$$+ [(1 + \Delta\bar{\Psi})\bar{\ell} - \bar{\ell}_C]f(\tau) \ , \tag{B-32a}$$

Table B.1 Nondimensional Variables and Functions

Dimensional Variable or Function	Divisor	Nondimensional Variable or Function
$F_T(t)$	$F_{T_{max}}$	$f(\tau)$
$I(t)$	$2mL^2$	$\bar{I}(\tau)$
r	α_z/t^*	$\bar{r}$
u, u_c, u_p	L/t^*	$\bar{u}, \bar{u}_C, \bar{u}_p$
v	L/t^*	$\bar{v}$
$x_C - x_C(0)$	L	ξ
x_E, y_E	L	$\bar{x}_E, \bar{y}_E$
x_P	L	$\bar{x}_P$
β	α_z	$\bar{\beta}$
$\dot{\psi}_L, \dot{\psi}, \dot{\psi}_w$	α_z	$\bar{\dot{\psi}}_L, \bar{\dot{\psi}}, \bar{\dot{\psi}}_w$
$d(\ )/dt$	$1/t^*$	$d(\ )/d\tau = (\ )'$

Table B.2 Nondimensional Parameters

Dimensional Parameter	Divisor	Nondimensional Parameter
C_L	$2mL^2/t^*$	c
d	L	$\bar{d}$
I_L, I_T	$2mL^2$	$\bar{I}_L, \bar{I}_T$
K_L	$F_{T_{max}} L$	k
ℓ, ℓ_C	L	$\bar{\ell}, \bar{\ell}_C$
m	ρSL	μ

$$(\bar{I}_L + \bar{x}_P^2/2)\bar{\psi}_L'' + (\bar{x}_P\bar{z}/?)\bar{\psi}'' = -\bar{x}_P\bar{x}_P'\bar{\psi}_L' - k\bar{\psi}_L - c\bar{\psi}' \ , \qquad \text{((B-32b)}$$

$$\bar{u}_P' = 2\ f(\tau) \qquad \text{(B-32c)}$$

and

$$\bar{x}_P' = \bar{u}_P \ . \qquad \text{(B-32d)}$$

Nondimensional Equations - Free Flight

For the free-flight phase, it is assumed that the thrust is equal to $F_{T_{max}}$ (i.e., $f(\tau) = 1$) until burnout, after which it is, of course, zero. Until burnout, the nondimensional equations are

$$\bar{u}' = 2 + (1/2\mu)C_x\bar{u}^2, \qquad \text{(B-33a)}$$

$$\bar{\beta}' = -\bar{r} - [2/\bar{u} + 1/(2\mu)C_x\bar{u}]\bar{\beta} + 1/\bar{u} + 1/(2\mu)[C_y\bar{\beta} + C_{y_r}\bar{r}(\bar{d}/2)/\bar{u}]\bar{u} \ , \qquad \text{(B-33b)}$$

$$\bar{\psi}' = \bar{r} \ , \qquad \text{(B-33d)}$$

$$\bar{x}_E' = \bar{u} \qquad \text{(B-33e)}$$

and

$$\bar{y}_E' = \bar{u}(\bar{\psi} + \bar{\beta}) = \bar{u}\,\bar{\psi}_w \ . \qquad \text{(B-33f)}$$

After burnout,

$$\bar{u}' = (1/2\mu)C_x\bar{u}^2 \ , \qquad \text{(B-34a)}$$

$$\bar{\beta}' = -\bar{r} - 1/(2\mu)C_x\bar{u}\bar{\beta} + 1/(2\mu)[C_{y_\beta}\bar{\beta} + C_{y_r}\bar{r}(\bar{d}/2)/\bar{u}]\bar{u} \ , \qquad \text{(B-34b)}$$

$$\bar{r}' = \bar{d}/(2\mu\bar{I}_T)[C_{n_\beta}\bar{\beta} + C_{n_r}(\bar{r}/\bar{u})\bar{d}/2]\bar{u}^2 \qquad \text{(B-34c)}$$

and Eqs. (B-33d) through (B-33f) are still valid.

Comments on the Equations of Motion

The dimensional equations are nonlinear and no exact closed-form solution to them has been obtained. If one chooses $f(\tau)$ to be a simple function of time, such that the nondimensional equations for $\bar{u}$ and $\bar{x}$ are integrable prior to the tip-off phase, the nondimensional equation for $\bar{\Psi}_L$ is a linear differential equation with variable coefficients subsequent to detent. No exact, closed-form solution to the variable coefficient equation has been found. However, approximate analytical solutions are given in Appendix E.

During free-flight, the equations for $\bar{u}$ can be integrated exactly for C_x constant. Then the equations for $\bar{\beta}$ and $\bar{r}$ become linear equations with variable coefficients. Approximate analytical solutions to such equations can probably be obtained,but were not attempted during this study.

APPENDIX C

MORE GENERAL LAUNCHER/ROCKET SYSTEM MODEL

Purpose and Physical Description

A more general launcher/rocket system model than that discussed in Appendix B is needed to determine, more or less quantitatively, the effects of rocket imperfections on launcher motion and passive control characteristics of different launcher configurations. The launcher model must be general enough to account for dynamic coupling between launcher degrees of freedom. The system should include models of spin-producing mechanisms, such as helical rails. The rocket model should account for the variation in mass and inertia of the rocket and for the variations in aerodynamic coefficients due to compressibility.

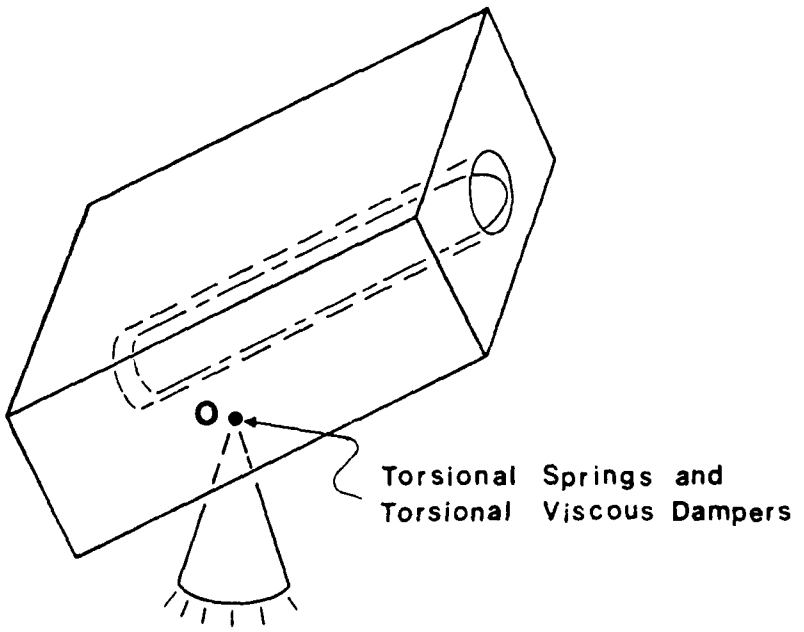

Fig. C.1 More general launcher/rocket system model.

All of the above requirements are incorporated into the "more general" model described herein. It is basically that described in Refs. 8 and 9. The launcher physical model is that of a rigid body with up to three degrees of freedom in rotation about a fixed point (labeled 0 in Fig. C.1). Rotation of the launcher is constrained by torsional springs and torsional viscous dampers. While the rocket is on the launcher, its motion is rigidly constrained. During various periods of time, the rocket may have zero to four degrees of relative degrees of freedom.

The rocket is modeled at each instant of time as a "system" consisting of a rigid solid body within which gaseous fluid is flowing and from which such fluid is being expelled through a nozzle (see Fig. C.2). The rigid solid body represents the always solid parts of a free rocket and also the unburned portion of the solid propellant used to propell the rocket. The gaseous fluid represents the propellant that has been burned but which has not been expelled.

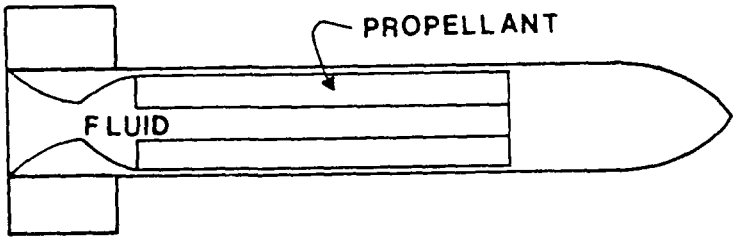

Fig. C.2 Rocket physical model.

The environment of the rocket, after it has left the launcher, is composed of a constant density and temperature atmosphere which may be

in steady motion; i.e., steady winds may be present. A "flat" earth gravitational model is also part of the environment.

Verbal Description of the Mathematical Model

The equations which mathematically define the system of launcher plus rocket are rather lengthy. For the most part, they are documented in Refs. 8 and 9. The full equations including modifications which have been made, and will be made, during this contractual effort will be documented in the final report. Hence, a verbal description of the mathematical model as it now exists is considered sufficient at this time.

The total flight of the rocket is divided into five phases: spin detent, guidance, tip-off and free-flight. Such a division is necessary because the equations governing each phase are different. There is a spin phase only if spin is imparted to the rocket by using a spin motor. If such is the case, the rocket has one degree of freedom with respect to the launcher during the spin and detent phases. During the latter phase, the thrust builds up to a specified value. The motion of the rocket relative to the launcher during guidance is restricted to spin and translation along the "launch axis." The mathematical model includes provisions for imparting spin during the guidance phase via eroding spin turbines or helical rails.

The guidance phase ends at the beginning of either the tip-off phase or the free-flight phase. However, although there is some danger of ambiguity, the time of end of guidance (EOG) is taken as the instant of last physical contact between the launcher and the rocket. During the tip-off phase the rocket may rotate with respect to the launcher about a point on the axis of geometric symmetry of the rocket.

The expulsion of mass from the rocket is modeled during all but the spin phase, since it is the principal contributor to the total thrust. The actual modeling of the thrust is accomplished by specifying a thrust profile. Effects of flow within the rocket are not modeled except during free-flight. Even then, only "jet damping" is considered significant. By ignoring the thrust due to exit pressure differential, computing an exit mass flow rate based on a specified exit velocity, and assuming a hollow cylindrical propellant charge and a linear variation of mass flow rate within the rocket, a jet damping moment is determined (see Ref. 8).

The aerodynamic reactions are modeled using tabulated data for aerodynamic coefficients and the center of pressure location. The coefficients are, in general, functions of Mach number and total angle of attack.

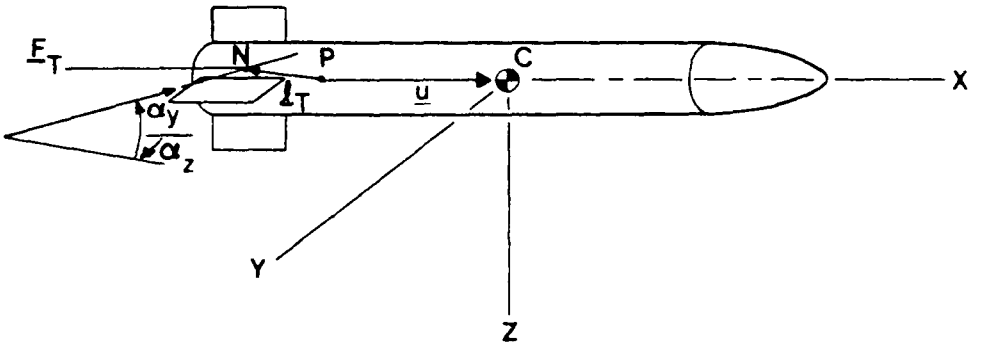

Fig. C.3 Thrust misalignment angles.

Throughout the various phases, the effects of thrust misalignment are modeled by specifying misalignment angles α_y and α_z (see Fig. C.3) and the vector $\underline{l}_T$. The angles α_y and α_z define the angular misalignment and the transverse components of $\underline{l}_T$ define the linear thrust misalignment.

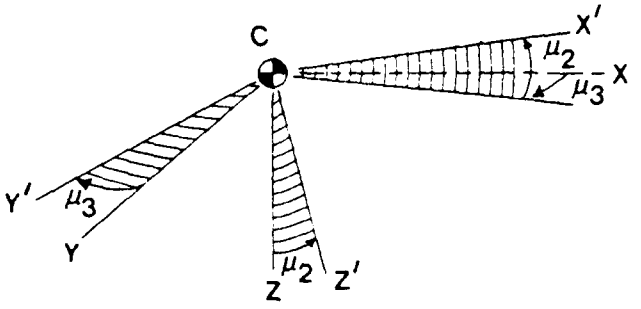

Fig. C.4 Dynamic mass imbalance angles

Dynamic imbalance of the rocket is modeled by specifying two small angles μ_2 and μ_3. As shown in Fig. C.4, these angles define the initial orientation of the centroidal principal axes of the rocket relative to the centroidal "geometric" reference frame Cxyz and hence define products of inertia. Although the moments of inertia of the rocket are time varying, the products of inertia are assumed to be constant. The rocket is assumed to be statically balanced.

Solution of the Equations of Motion

Solutions to the equations of motion are obtained by numerically integrating the equations of motion using a fourth-order Runge-Kutta algorithm. Until the rocket starts to move with respect to the launcher and also during free-flight, integration is with respect to time. To obtain precise guidance lengths, integration is with respect to displacement along the launcher after the rocket begins to translate until the end of the tip-off phase.

Calculation of Trajectory Deviations due to Imperfections

To determine trajectory deviations due to rocket imperfections, nominal and "perturbed" trajectories are generated. The nominal trajectory is that for a perfect rocket; i.e., one with no thrust misalignment and no dynamic imbalance. Deviation in the position of the rocket's center of mass and its velocity well after burnout are obtained as indicated in Appendix A.

AD-A096 881 AUBURN UNIV ALA ENGINEERING EXPERIMENT STATION F/G 19/7
LAUNCHERS AS PASSIVE CONTROLLERS.(U)
DEC 80 J E COCHRAN DAAH01-80-C-0523
UNCLASSIFIED DRSMI/RL-CR-81-2 NL

END
DATE FILMED
4-81
DTIC

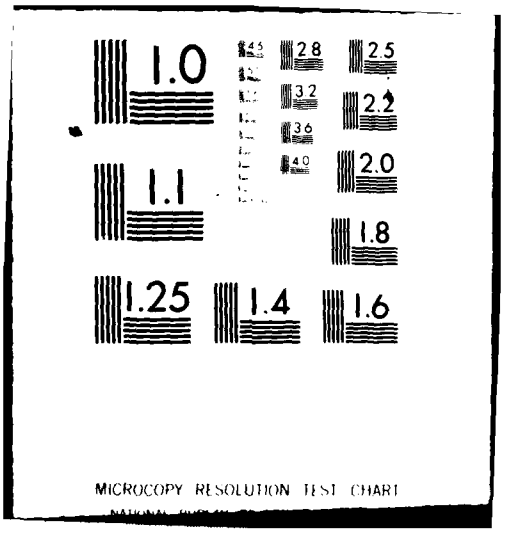
1.0
1.1
1.25
1.4
1.6
1.8
2.0
2.2
2.5
2.8
3.2
3.6
4.0
MICROCOPY RESOLUTION TEST CHART

APPENDIX D

"SECULAR" RATES DUE TO THRUST MISALIGNMENT AND DYNAMIC IMBALANCE

Most Elementary Model of a Free Rocket with Imperfections

The most elementary model of a free rocket that is imperfect because its thrust vector is misaligned and/or it is dynamically imbalanced is a rigid body which is acted upon by a constant magnitude thrust force and no other forces or moments. Such a model is obviously not a valid one for the entire free flight of a rocket; however, it provides remarkably good results[9,10] for a short period of time after end-of-guidance (EOG). The attitude motion of such a model is composed of an essentially constant spin about its longitudinal axis, a periodic nutation of the longitudinal axis at a frequency almost equal to the spin frequency, and a very low frequency periodic precession of the longitudinal axis about a fixed axis which is not collinear with the longitudinal axis at EOG. The precessional frequency is so low for slender rockets that the precessional motion appears secular; i.e., monotonic in time.

Because in actual flight a free rocket is acted upon by stabilizing (in most cases) aerodynamic moments and because the speed required to give significant magnitude to these moments is achieved shortly after EOG, the "secular" precessional motion is rather quickly replaced by a shorter period oscillatory motion. It appears that the majority of the total flight error is caused by this "secular" precessional motion during the period of time before the aerodynamic moments become significant.

Generation of the "Secular" Rate

If the launcher is perfectly rigid, there is, of course, no transverse component of the angular velocity of the rocket at EOG. However, the precessional rate which appears as essentially constant transverse angular velocity components of a non-rolling coordinate frame with origin at the rocket center of mass is generated during one-quarter of a revolution of the spinning rocket. This fact can be shown by considering the solution to the equations of motion of the elementary model.

Let the longitudinal, or axial, moment of inertia of the rocket (model) be I_x and let its transverse moment of inertia be I_T. Also, let the spin rate of the model be p. Let the angular velocity of the rocket be

$$\underline{\omega} = p\hat{\underline{i}} + q\hat{\underline{j}} + r\hat{\underline{k}} \ , \qquad \text{(D-1)}$$

where the unit vector triad ($\hat{\underline{i}}$, $\hat{\underline{j}}$, $\hat{\underline{k}}$) is associated with the rocket-fixed reference frame Cxyz (see Fig. A.1).

Consider now the case of thrust misalignment (similar results exist for the case of dynamic imbalance) wherein the torque on the rocket about C is

$$\underline{T} = F_T \ (-\ell_C \alpha_y \hat{\underline{j}} - \ell_C \alpha_z \hat{\underline{k}}) \ , \qquad \text{(D-2)}$$

where ℓ_C is the distance from C to the point of intersection of the thrust, $\underline{F}_T$, with the x-axis and α_y and α_z are thrust misalignment angles. The equations of rotational motion are

$$\dot{p} = 0 \qquad \text{(D-3a)}$$

$$\dot{q} = nr - \ell_C \alpha_y F_T / I_T \qquad \text{(D-3b)}$$

and

$$\dot{r} = -nq - \ell_C \alpha_z F_T / I_T \tag{D-3c}$$

where $n = [(I_T - I_x)/I_x]p$.

The angular velocity components, p, q, and r, are related to the time rates of change of Euler angles ψ, θ and ϕ (see Fig. A.1) by the equations,

$$\dot{\phi} = p + (q \sin\phi + r \cos\phi) \tan\theta \tag{D-4a}$$

$$\dot{\theta} = q \cos\phi - r \sin\phi \tag{D-4b}$$

and

$$\dot{\psi} = (q \sin\phi + r \cos\phi)/\cos\theta. \tag{D-4c}$$

Let the non-rotating reference frame $Ox_E y_E z_E$ shown in Fig. A.1 be oriented such that the x_E-axis is collinear with the launch direction. Then θ will be small, so that,

$$\dot{\phi} \simeq p \tag{D-5a}$$

and

$$\begin{bmatrix} \dot{\theta} \\ \dot{\psi} \end{bmatrix} \simeq \begin{bmatrix} \cos\phi & -\sin\phi \\ \sin\phi & \cos\phi \end{bmatrix} \begin{bmatrix} q \\ r \end{bmatrix} . \tag{D-5b}$$

The solution to Eqs. (D-3) with q and r initially zero is

$$p = \text{constant}, \tag{D-6a}$$

$$q = -\ell_C F_T [\alpha_z (1-\cos nt) + \alpha_y \sin nt]/(nI_T) \tag{D-6b}$$

and

$$r = -\ell_C F_T [\alpha_z \sin nt - \alpha_y (1-\cos nt)]/(nI_T). \tag{D-6c}$$

The approximate pitch and yaw rates, $\dot{\theta}$ and $\dot{\psi}$, which may be obtained from Eqs. (D-4) and (D-5) are (ϕ=0 initially),

$$\dot{\theta} \simeq [\ell_C F_T/(nI_T)]\{\alpha_z[\cos\lambda t - \cos\phi] + \alpha_y[\sin\lambda t - \sin\phi]\} \qquad \text{(D-7a)}$$

and

$$\dot{\psi} \simeq [\ell_C F_T/(nI_T)]\{\alpha_z[\sin\lambda t - \sin\phi] - \alpha_y[\cos\lambda t - \cos\phi]\}\ , \qquad \text{(D-7b)}$$

where $\lambda = (I_x/I_T)p$. The angular rates $\dot{\theta}$ and $\dot{\psi}$ are the transverse anglular velocity components of a non-rolling (non-spinning) coordinate frame otherwise fixed in the rocket. Since for the range of values of the inertia ratio, I_x/I_T, corresponding to free rockets $\lambda \ll p$, the solutions for $\dot{\theta}$ and $\dot{\psi}$ can be further simplified to obtain

$$\dot{\theta} \simeq \dot{\theta}_s(1-\cos\phi) + [\ell_C F_T/(nI_T)]\alpha_y(\lambda t - \sin\phi] \qquad \text{(D-8a)}$$

and

$$\dot{\psi} \simeq \dot{\psi}_s(1-\cos\phi) + [\ell_C F_T/(nI_T)]\alpha_z[\lambda t - \sin\phi], \qquad \text{(D-8b)}$$

where

$$\dot{\theta}_s = \alpha_z \ell_C F_T/(nI_T) \qquad \text{(D-9a)}$$

and

$$\dot{\psi}_s = -\alpha_y \ell_C F_T/(nI_T) \qquad \text{(D-9b)}$$

are the "secular" rates alluded to above. Without loss of generality, one can assume that the rocket-fixed axes are oriented so that $\alpha_y=0$, or $\alpha_z=0$. Then, it is evident that $\dot{\theta}\simeq\dot{\theta}_s$ or $\dot{\psi}\simeq\dot{\psi}_s$ for the first time when $\phi=\pi/2$. Also, it is clear that, since $\lambda t \ll 1$ for several spin revolutions $\dot{\theta}_s$ and $\dot{\psi}_s$ are the average values of $\dot{\theta}$ and $\dot{\psi}$, respectively.

It is of interest also to see how the "secular" rate of a spinning rocket compares to the truly secular rate generated by the same torque acting on a non-spinning rocket. From Eqs. (D-9) it is clear that if a torque $\alpha_z \ell_C F_T \hat{j}$ acted on a non-spinning rocket for a time period 1/n, a pitch rate equal to $\dot{\theta}_s$ would be generated. This time period is less than

that required for a quarter revolution of the spinning rocket; i.e., $\pi/2p \approx \pi/2n$.

APPENDIX E

APPROXIMATE ANALYTICAL SOLUTIONS FOR LAUNCHER MOTION

Comments on the Equations of Motion

The equations of motion for even the simple launcher/rocket system model described in Appendix B are fairly complicated nonlinear, ordinary differential equations. No exact general solution to these equations have been found. However, an approximate analytical solution for the angular rate of a single-degree-of-freedom launcher before tip-off has been obtained. This solution appears to be more accurate than that given in Ref. 10 (pp. 57-59).

Simplification of the Equations of Motion

To remove the complications presented by nonlinear equations, it is assumed that $|\dot{\Psi}_L|$ is small so that Eqs. (B-31) describe the launcher motion. Also, $f(\tau)$ is assumed to be the explicit function of τ defined as

$$f(\tau) = \begin{cases} \tau/\tau_1 & \text{for } \tau<\tau_1 \ , \\ 1 & \text{for } \tau\geq\tau_1 \ , \end{cases} \tag{E-1}$$

where τ_1 is a constant. Equations (B-31b) and (B-31c) can easily be integrated exactly if $f(\tau)$ has this simple form.

A further simplification is acheived by setting the damping coefficient equal to zero. Finally, the form of Eq. (B-31a) is modified somewhat by introducing the definitions,

$$J(\tau) = 1 + \varepsilon[\bar{x}_0 + \frac{1}{2}\xi(\tau)]\xi(\tau) \tag{E2a}$$

$$\varepsilon = 2mL^2/I_0 \tag{E-2b}$$

$$I_0 = I_T + I_L + mx_C^2(0) \tag{E-2c}$$

$$\omega_0^2 = (k/I_0)\varepsilon \tag{E-2d}$$

and, as in Appendix B,

$$\xi(\tau) = [x_C(\tau)\ x_C(0)]/L\ . \tag{E-2e}$$

Then, one has

$$\frac{d}{d\tau}[J(\tau)\ \bar{\Psi}_L'] + \omega_0^2\bar{\Psi}_L = \varepsilon(\bar{x}_0 + \xi - \bar{\ell}_C)f(\tau)\ . \tag{E-3}$$

Let

$$h(\tau) = J(\tau)\ \bar{\Psi}_L'\ . \tag{E-4}$$

Then,

$$h' + \omega_0^2 \int_0^\tau h/J(\tau)\ d\tau = \varepsilon(\bar{x}_0 + \xi - \bar{\ell}_C)f(\tau)\ . \tag{E-5}$$

or

$$h'' + [\omega_0^2/J(\tau)]h = \varepsilon(\bar{x}_0 + \xi - \bar{\ell}_C)f'(\tau) + \varepsilon\ \bar{u}(\tau)f(\tau)\ . \tag{E-6}$$

Equation (E-6) is the basic equation of motion considered in this appendix. During the detent phase, Eq. (E-6) is a nonhomogeneous, linear, constant-coefficient, ordinary differential equation and can easily be solved exactly. However, after detent release, its coefficients are time varying and its exact, analytical, general solution probably cannot be found.

Solution During the Detent Phase

Before the detent mechanism releases, $\xi \equiv 0$, $\bar{u} \equiv 0$ and $J(\tau)=1$. Also, $f'(\tau) = 1/\tau_1$. Thus, for $0 \leq \tau < \tau_D$,

$$h'' + \omega_0^2 h = \varepsilon(\bar{x}_0 - \bar{\ell}_C)/\tau_1 \qquad \text{(E-7)}$$

The general solution to Eq. (E-7) can be found by standard methods and is

$$h(\tau) = \varepsilon(\bar{x}_0 - \bar{\ell}_C)/(\omega_0^2 \tau_1)(1 - \cos \omega_0 \tau) \ . \qquad \text{(E-8)}$$

Furthermore, since $J(\tau) = 1$, $\bar{\Psi}_L' = h(\tau)$ for $0 \leq \tau < \tau_D$.

Approximate Solution During the Interval (τ_D, τ_1)

After the rocket starts to translate, $\xi(\tau)$ and $\bar{u}(\tau)$ must be determined. Since [see Eq. (B-31b)]

$$\bar{u}' = 2\tau/\tau_1 \ , \qquad \tau_D \leq \tau < \tau_1 \ , \qquad \text{(E-9)}$$

and $\bar{u}(\tau_D) = 0$,

$$\bar{u}(\tau) = \tau^2/\tau_1 - \tau_D^2/\tau_1, \quad \tau_D < \tau < \tau_1 \ . \qquad \text{(E-10)}$$

Also, since

$$\xi' = \bar{u} \ , \qquad \text{(E-11)}$$

it follows that

$$\xi(\tau) = \tau^3/(3\tau_1) - \tau_D^3/(3\tau_1) - (\tau_D^2/\tau_1)(\tau - \tau_D) \ . \qquad \text{(E-12)}$$

Let $z = \tau - \tau_D$. Then, Eq. (E-6) can be written as

$$h'' + G^2(z)\, h = g(z) \ , \qquad \text{(E-13)}$$

where now $(\ )' = d(\ )/dz$,

$$G^2(z) = \omega_0^2/[1 + \varepsilon(\bar{x}_0 + \frac{1}{2}\varepsilon)\varepsilon] \qquad \text{(E-14a)}$$

and

$$g(z) = a_0 + a_1 z + a_2 z^2 + a_3 z^2 \qquad \text{(E-14b)}$$

with

$$a_0 = [\bar{x}_0 - \bar{\ell}_c]/\tau_1 \ , \qquad \text{(E-15a)}$$

$$a_1 = 4\varepsilon\tau_D{}^2/\tau_1{}^2, \qquad \text{(E-15b)}$$

$$a_2 = 4\varepsilon\tau_D/\tau_1{}^2 \qquad \text{(E-15c)}$$

and

$$a_3 = 4\varepsilon/(3\tau_1{}^2) \ . \qquad \text{(E-15d)}$$

An approximate solution to Eq. (E-13) can be obtained by treating ε as a small parameter and letting

$$h = h_0 + \varepsilon h_1 + \ldots \qquad \text{(E-16)}$$

where $h_0, h_1, \ldots$ are functions of time to be determined.

First, $G^2(z)$ can be rewritten (for ε suitably small) as

$$G^2(z) = \omega_0{}^2[1-\varepsilon(\bar{x}_0 + \frac{1}{2}\xi)\xi+\ldots] \qquad \text{(E-17)}$$

By substituting Eq. (E-16) into Eq. (E-13) and equating the coefficients of various powers of ε to zero, one gets, for ε°

$$h_0'' + \omega_0{}^2 h_0 = 0 \ , \qquad \text{(E-18a)}$$

and for ε,

$$h_1'' + \omega_0{}^2 h_1 = \frac{1}{2}\omega_0{}^2[2\bar{x}_0 + \xi]\xi\, h_0 + g(z)/\varepsilon \ . \qquad \text{(E-18b)}$$

Because the term $\frac{1}{2}\omega_0{}^2\xi^2 h_0$ should be very small, it is neglected.

Standard methods may be used to first solve Eq. (E-18a) and next Eq. (E-18b), so that the first-order solution for h can be expressed as

$$
\begin{aligned}
h(z) = {} & [h(\tau_D) - a_0/\omega_0^2 + a_2/\omega_0^4]\cos\omega_0 z \\
& + [h'(\tau_D)/\omega_0^3 = a_1/\omega_0^3 + a_3/\omega_0^5]\sin\omega_0 z \\
& + a_0/\omega_0^2 - a_2/\omega_0^4 + [(a_1/\omega_0^2) - a_3/\omega_0^4]z \\
& + [a_2/(2\omega_0^3)]z^2 + [a_3/(6\omega_0^2)]z^3 \\
& + \varepsilon \bar{x}_0 \omega_0/\tau_1\{[\tau_D z^3/6 + z^4/24][h(\tau_D)\sin\omega_0 z - h'(\tau_D)/\omega_0\cos\omega_0 z] \\
& + \int_0^z [\tau_D\tau^2/2 + \tau^3/6]\cos 2\omega_0\tau\, d\tau[h'(\tau_D)/\omega_0\cos\omega_0 z + h(\tau_D)\sin\omega_0 z] \\
& + \int_0^z [\tau_D\tau^2/2 + \tau^3/6]\sin 2\omega_0\tau d\tau[h(\tau_D)\cos\omega_0 z - h'(\tau_D)/\omega_0\sin\omega_0\tau]\}
\end{aligned}
\tag{E-19}
$$

where the integrals are available in standard tables.

Approximate Solution when $\tau > \tau_1$

The function $G^2(z)$ will differ a good deal from ω_0^2 for $\tau > \tau_1$ and a solution for this time period which has the form of Eq. (E-19) is not very accurate. An alternative is to use the WBKJ approximation.[11] The approximate solution obtained has the form, (here $z = \tau - \tau_1$)

$$
h_h(z) = [G(z)]^{-1/2}\{C_1\cos\phi(z) + C_2\sin\phi(z)\}\ , \tag{E-20}
$$

where C_1 and C_2 are arbitrary constants and

$$
\phi(z) = \int_0^z G(z)\, dz\ .
$$

Thus, one may consider

$$h_1(z) = p(z)\sin\phi(z) \tag{E-22a}$$

and

$$h_2(z) = p(z)\sin\phi(z) \tag{E-22b}$$

where

$$p(z) = [1 + \varepsilon(\bar{x}_0 + \frac{1}{2}\xi)\xi]^{-1/4} \tag{E-23}$$

to be approximate, linearly independent solutions to (E-13) with $g(z) = 0$. Then, by the method of variation of parameters, one may get an approximate solution to the nonhomogeneous equations in the form,

$$h = p(z)\{(A_1\cos\phi + B_1\sin\phi] + \int_0^z \frac{g(z)\cos\phi}{p(z)\phi'}\,dz \quad \sin\phi - \int_0^z \frac{g(z)\sin\phi}{p(z)\phi'}\,dz \quad \cos\phi \ . \tag{E-24}$$

It is obvious that the integrals in Eqs. (E-23) and (E-24) are complicated; and, apparently, no closed-form evaluations of them can be obtained. However, if one assumes that ε is small, then neglecting terms which are second-order in ε

$$G(z) \simeq \omega_0[1-\varepsilon(2\bar{x}_0\,\xi + \xi^2)/4] \ , \tag{E-25}$$

and

$$p(z) \simeq [1+\varepsilon(2\bar{x}_0\,\xi + \xi^2)/8] \ . \tag{E-26}$$

Furthermore, since g(z) is of order ϵ, it appears reasonable to replace p(z) in the integrands by 1, ϕ' by ω_0 and ϕ by $\omega_0 z$ for the purpose of evaluation. The approximate solution thereby obtained is

$$h(\tau) = p(z)\ \{(A_1\cos\phi + B_1\sin\phi] + r_1(z)\cos\phi + r_2(z)\sin\phi\}\ , \qquad \text{(E-27)}$$

where

$$A_1 = h(\tau_1)\ , \qquad \text{(E-28a)}$$

$$B_1 = h'(\tau_1) - p'(\tau_1)h(\tau_1)/\omega_0\ , \qquad \text{(E-28b)}$$

$$r_1(z) = -\epsilon/\omega_0{}^2[\xi(\tau_1) - \xi\cos\omega_0 z + 2/\omega_0\sin\omega_0 z] \qquad \text{(E-29a)}$$

and

$$r_2(z) = -\epsilon/\omega_0{}^2[-\xi'\sin\omega_0 z + 2(1-\cos\omega_0 z)] \qquad \text{(E-29b)}$$

In Eqs. (E-29),

$$\xi = z^2 + \xi'(\tau_1)z + \xi(\tau_1)\ . \qquad \text{(E-30)}$$

Comments on the Approximate Solution

The solution given above should be fairly good approximations to the actual solution for $h(\tau)$ when $G(\tau)$ does not vary too much. Results obtained from the solutions and hopefully other approximate solutions for more detailed launcher models will be given in the final report.

DISTRIBUTION

	No. of Copies
Defense Technical Information Center Cameron Station Alexandria, VA 22314	2
Commander US Army Missile Command Attn: DRSMI-C	3
DRSMI-RLH, Mr. Christensen	5
ACO	1
PCO	1
DRSMI-TI	1
DRSMI-TBD	1
DRSMI-LP	1
Redstone Arsenal, AL 35809	
Office of Naval Research Atlanta Area Office Attn: Mr. Henry Cassall Georgia Institute of Technology 325 Hinman Research Bldg. Atlanta, GA 30332	1
US Army Material Systems Analysis Activity Attn: DRXSY-MP Aberdeen Proving Ground, MD 21005	1
IIT Research Institute Attn: GACIAC 10 West 35th Street Chicago, IL 60616	1


DATE
ILME